EUROPEAN ORGANIZATION FOR NUCLEAR RESEARCH

CERN/PS 93-03 (AR)

EXPERIMENTAL INVESTIGATION OF AN ELECTRON BEAM IN COMPENSATED STATE

A.V. Burov, V.I. Kudelainen, V.A. Lebedev, V.V. Parkhomchuk,
A.A. Sery, V.D. Shiltsev

Institute of Nuclear Physics
Siberian Division of the Russian Academy of Sciences

Translated from Russian by Bernard Meares

Abstract

The present paper suggests the results of experimental and analytical study of an electron beam space charge when compensated by residual gas ions. The main factor hampering stable compensation when the density of an electron current is increased is excitation of the transverse electron-ion oscillations, leading to a decrease in the compensation ratio. The instability threshold is strongly dependent on the system's parameters. The experimental techniques developed have provided fairly complete information on the state of ions (density, temperature, mass and charge composition), that are needed if we are to understand the mechanism of instability development and ways to suppress it.

CERN, Geneva, Switzerland
January 1993

INTRODUCTION

High-intensity electron beams are a major instrument in both research and applied physics. The natural desire of an experimental researcher to use the strongest possible electron currents is usually hindered by the presence of strong proper fields of the beam. The space charge of electrons rises so high that the charge-induced potential becomes equal to the energy of electrons and repels the 'superfluous' current [1]. It would seem to have been from a desire to overcome this disadvantage by compensating the electric field of an electron beam with fields of positive ions that the old-established idea of the compensated electron beam was born.

One example in the development of this method is the Budker relativistic stabilized electron beam [2], in which even a small quantity of ions should be enough to transform Coulomb repulsion into strong shrinking. Although the method was never put into practice, Budker's idea was a spur to the development of physics. Another example of work on the compensated beam were the experiments by Nezlin et al. [3], which showed that the maximum current of a compensated electron beam could be limited not only by the Pierce aperiodic instability [4], but also (in the case of a long enough beam) by the emergence of beam-drift instability in the electron-ion plasma with a threshold current density [8]:

$$j_{th} = \frac{v_0^2 B}{8Lc}\left(1 + \frac{1}{\ln\sqrt{\frac{b}{a}}}\right), \quad \frac{a^2}{L} \ll \frac{mcv_0}{eB}, \tag{1}$$

which was in fairly good agreement with the experiment. Here v_0 and m are the velocity and mass of electrons respectively, B is the magnetic field, L is the electron beam length, c is the velocity of light, and a, b are the radii of the beam and the vacuum chamber.

Electron beams for electron cooling are an important field for applying the compensated beam idea [5]. This is explained by the fact that an increase in the electron cooling decrement with an increase in electron current is limited by the perturbative effect of the space charge field on the motion of cooled particles. Compensation of the electron space charge by ions helps to overcome this limitation. The electron beams utilized in electron cooling facilities usually have a high current density and tend to be long (ranging from one to several metres). In this case the main limitation on obtaining a stable compensated state is the emergence of beam-drift instability. But unlike the operating conditions in [3] for facilities with electron cooling, one feature is a high vacuum and a low coefficient of electron reflection from the collector, so one could expect an increase in the threshold current density in the development of instability. In fact, experiments carried out on the NAP-M facility [6] showed a noticeable growth in threshold currents. Thus, at an electron energy of 35 keV there was no instability below the maximum current density attainable by the collector perveance, of 3 A/cm^2, which was some four times greater than the instability threshold given in (1). The high degree of compensation attained was controlled by electron cooling. At a low electron energy of 550 eV the threshold current density was exceeded by two orders of magnitude. But no direct measurements of the degree of compensation were made, and a lack of instability does not in itself necessarily mean good compensation.

In the studies performed on the 'Solenoid Model' facility, the subject of the present paper, the threshold factor was not exceeded to such an extent, which may be accounted for by different configurations of the accompanying magnetic field in the installations. The electron beam set-up of the NAP-M storage ring was Π-shaped, i.e. it consisted of three interlinked straight solenoids of approximately equal length (~1 m). Thus, the electrons in movement along the magnetic field from the cathode to the collector had to turn twice at an angle of approximately $2 \times 45°$, where a drift of secondary electrons to the chamber wall took place, while the 'Solenoid Model' consisted of one ~3 m long straight section.

The difficulties of obtaining a high compensation ratio on the 'Solenoid Model' gave rise to more thoroughgoing both experimental and theoretical investigations. Various methods of measuring compensation ratio and other important parameters, such as temperature, mass distribution of compensating ions, etc., were used. The analytical estimation [9] predicted threshold currents which were in good agreement with experimental data (except those obtained at NAP-M at an energy of 550 eV, where the instability was not observed, but where the existence of a high compensation state was also not proven).

The length of the compensation section of the 'Solenoid Model' could be varied from 40 to 270 cm in steps of 40 cm. But even on a short section, to obtain a close to 100% compensation was fairly complicated, judging by the fact that it took some six months of intense experimentation from obtaining compensation in a short section to doing so in a long one. A good compensation state turned out to exist in a fairly narrow range of residual gas pressures, and for the total length equal pressure on both ends of the compensation section was also needed. Another condition required was also a smooth switching on of the electron beam current, otherwise a stable state could not be obtained. The experiments showed that a stable compensated state exists up to certain current values. We termed the maximum possible currents of this state threshold currents (under certain conditions besides these 'upper' thresholds there were also observed 'lower' thresholds, i.e. with no compensation at currents below certain values). With currents above (or below) the threshold currents in the electron beam transverse electron-ion oscillations were excited, i.e. beam-drift instability occurred, which was accompanied by excitation of longitudinal oscillations of the ion column.

Although at currents higher than threshold there were transverse oscillations, their amplitude was as a rule not very high (about 0.1 of the electron beam radius) and the compensation ratio was still 50–70%, which might be enough for certain experiments. For example experiments to measure longitudinal friction force [7] were conducted at a compensation ratio of $\simeq$ 50%, as high as currents of $\sim$ 10 mA, one order of magnitude higher than the instability excitation threshold. Nevertheless, at that time we were not able to attain stability over the whole length at any current strength.

It should be noted that if there is no feedback, beam-drift instability is convective (drawn-down), i.e. any perturbation at the start of the beam grows exponentially with length but is limited in time at the given point. Instability can become absolute only if there is high enough feedback. Feedback can be defined as the effect of ion oscillations at the beam end on the degree of oscillation at the start.

The feedback can be brought about, for example, by electrons being reflected from the collector or being ionized, and it is the number of such electrons that in turn determines the instability threshold. One should therefore be very cautious in comparing threshold currents obtained in our experiments with those described by other authors such as Nezlin [3], as in the latter the experiments were carried out under much different conditions, in a different range of residual gas pressure, and with more electrons being reflected from the collector.

This paper gives the results of experimental investigation into the compensated state and describes various experimental techniques used. The analytical section of the paper interprets the results of the experiments.

The basic experimental results were obtained in 1984–1987 on the 'Solenoid Model'.

1. EXPERIMENTAL SET-UP, GENERAL

A diagram of the 'Solenoid Model' as used for the study of electron cooling in a single-flight mode [7] is given in Figure 1. The electron beam is generated in an electron gun [15] set in the solenoid's magnetic field [16] and transported along the magnetic field to the electron collector. To provide local changes in the magnetic field in the vicinity of the gun a short auxiliary solenoid is placed inside the main one, so the size of the electron beam can be regulated at its cooling section. The electrode of the electron gun closest to the cathode (4 in Fig. 2) is insulated from the cathode 3. This permits the current density distribution to be regulated over the beam cross-section by varying the voltage between the cathode and electrode. Unless otherwise specified, we shall henceforth assume this difference in voltage to be zero, which corresponds to the constant current density over the beam cross-section (the measurements showed that the non-homogeneity of the current density over the beam cross-section in this case is only a few per cent). After acceleration in an electrostatic accelerator, H^- ions are sent to the solenoid, where they are brought together (spatially, in direction and velocity) with the electron beam. After leaving the solenoid the ions are sent to the electrostatic spectrometer for the longitudinal friction force to be measured, or to a two-coordinate H^- beam position detector for measuring the transverse friction force. The following are the basic parameters of the set-up:

Energy of H^- ions	850 keV
Ion current	$\approx$ 1 nA
Electron energy	450 eV
Electron beam current	0–15 mA
Electron beam radius	1 mm
Magnetic field of solenoid	1–4 kG
Magnetic field of auxiliary solenoid	-2 - $+2$ kG
Solenoid length	2.88 m
Length of electron beam section from cathode to collector	2.50 m
Residual gas pressure	10^{-8}–10^{-6} Pa

The effect of cooled ions on the state of compensation could always be ignored in view of the low value of the ion current. When studying compensation without electron cooling, electron energy was varied from 100 to 1 000 eV.

The positively charged compensating ions were generated when atoms of the residual gas were ionized by the beam electrons. The electric field of the electron beam and the strong longitudinal magnetic field hampered motion of the ions from the electron beam in a transverse direction to the walls of the vacuum chamber. Electrostatic mirrors at the edges of the compensation region hampered motion of the ions along the beam. At the same time the ions between the mirrors accumulated and compensated the electron beam space charge.

The electrostatic mirrors used for confining the ions (6, 7, 12, 13, 17, 18 in Fig. 2) were similar to those described in [6], i.e. they consisted of two arcs with semiconducting glass inserts between them. One arc was usually earthed while a cut-off voltage was applied to the other. The cut-off technique of confinement ensured both the accumulation of ions in the beam and effective cleaning of the mirrors from the ionization electrons generated and building up in the mirror potential well (ionization electrons drifting in the crossed electric field of the mirror and magnetic field onto the semiconducting inserts, thus removing them from the mirror). The mirrors were also cleansed of ionization electrons by an 'electron wind', i.e. by the ionization electrons becoming heated through collisions with electrons of the beam. It should be noted that the latter mechanism was of key importance for us in our circumstances, since the electron energy in the main beam was on the low side ($\simeq$ 450 eV). On the other hand, in the NAP-M experiments it did not provide a sufficiently high rate of electron removal because of high electron energy in the main beam, of $\simeq$ 30 keV).

Besides the mirrors described above, mirrors of another type, shown in Fig. 2b, were also used. In an earthed cylindrical copper pipe (internal diameter 2 cm) in which the axis coincided with that of the beam, two holes, each $\sim 1 \times 1$ cm, were cut, opposite one another and with a 2 cm difference in alignment. On the outside, a pipe-section of slightly larger diameter, insulated from the earthed pipe, was placed over it. On applying voltage, the electric field penetrated inside through the cuts, creating the ion cut-off. The various mirrors could be used not only for storing but also for cleansing the beam of ions by applying to them voltage of a different polarity.

Three different pick-up electrodes were used for observing longitudinal or transverse beam oscillations. Two of them (8 and 15) were cut in the horizontal plane, while the third 16 was cut in the vertical plane, permitting the observation of transverse oscillations in the two planes. The ion mass distribution was measured by an analyser 14 (see section 5.2 below). The electron collector 19 was placed at the edge of the solenoid and had an additional magnetic screen, such that the magnetic field in it fell almost to zero, creating a magnetic mirror preventing the electrons elastically reflected from the reflecting (radiation accepting) collector surface from returning to the beam. All the experiments, unless described otherwise, were carried out with a collector potential of +600 V with respect to the earth, the ring electrode close to the collector 20 being earthed, thereby allowing the ionization electrons to escape freely from the beam. To aim the electron

beam more accurately at the collector, the angle between the magnetic field line and the geometrical axis of the solenoid was slightly altered ($\sim 2 \times 10^{-2}$ rad). This was done by two magnetic correcting systems setting up a transverse magnetic field both vertically and horizontally.

The earthed copper pipe enclosing the beam and the various electrodes (cutoffs, pick-ups, etc.) had the same internal diameter (2 cm), providing a constant potential over the whole beam length. In addition internal surfaces of the pipes and the electrodes (i.e. those facing the beam) were gilded to ensure against poorly conductive oxide films.

It should be kept in mind that different kinds of compensation ratio can be considered, in relation to various parameters, e.g. an electric field compensation ratio inside the electron beam, or a potential compensation ratio between the beam centre and the chamber wall. Similarly, the compensation ratio can be measured by the charge, i.e. the difference between the aggregate ion charge and the electron charge in the beam. The key characteristic is of course the electric field compensation ratio inside the electron beam, as this directly affects the dynamics of cooled particles.

2. LONGITUDINAL WAVES

The conventional way of investigating electron beam states and beam-compensating ions is through a study of the propagation of small perturbations in the beam. The most simple case both theoretically through analytical calculations, and experimentally, is by studying the propagation of axisymmetric (longitudinal) waves in the beam.

2.1 Dispersion equation in the hydrodynamic approximation

Let an electron beam with a radius a and a homogeneous electron density distribution n_0 over the beam cross-section be propagated along a vacuum chamber axis with radius b. The electron space charge is compensated by 'cold' ions, whose charge density coincides with that of the electrons:

$$\sum_i e n_i Z_i = e n_e \ . \tag{2.1}$$

To produce transverse stability the electron beam is placed in a longitudinal magnetic field B. Then, in the hydrodynamic approximation, the equation of motion for the ions and electrons will take the form:

$$\frac{\partial n_i}{\partial t} + \mathrm{div}\ n_i \vec{v}_i = 0 \ , \qquad \frac{\partial n_e}{\partial t} + \mathrm{div}\ n_e \vec{v}_e = 0 \ ;$$

$$\frac{\partial \vec{v}_i}{\partial t} = \frac{e Z_i}{M_i}\left(- \bigtriangledown \Phi + \frac{\vec{v}_i \times \vec{B}}{c} \right) , \quad \frac{\partial \vec{v}_e}{\partial t} = -\frac{e}{m}\left(- \bigtriangledown \Phi + \frac{\vec{v}_e \times \vec{B}}{c} \right) ; \tag{2.2}$$

$$\triangle \Phi = 4\pi \left(e n_e - \sum_i Z_i e n_i \right) \ .$$

Here we assume that the velocity of electrons v_0 is low compared to the velocity of light c, and the natural magnetic field of the beam can be ignored. In Ref. [13] a solution to

the equations in (2.2) was given in linear approximation, and the small deviations from the equilibrium state can be written down as follows:

$$f(r)\ \exp\left[i(kz + l\varphi - \omega t)\right], \tag{2.3}$$

where l and k are the azimuthal and longitudinal wave numbers respectively. For axisymmetric ($l = 0$) perturbations a solution to the equations results in the following dispersion equation:

$$\sqrt{-\frac{\varepsilon_\parallel}{\varepsilon_\perp}}\ ka\ \frac{J_1\left(\sqrt{-\frac{\varepsilon_\parallel}{\varepsilon_\perp}}\ ka\right)}{J_0\left(\sqrt{-\frac{\varepsilon_\parallel}{\varepsilon_\perp}}\ ka\right)} - \frac{ka}{\varepsilon_\perp}\ \frac{K_0(kb)\ I_1(ka) + K_1(ka)\ I_0(kb)}{K_0(ka)\ I_0(kb) - K_0(kb)\ I_0(ka)}\ , \tag{2.4}$$

where

$$\varepsilon_\parallel = 1 - \sum_i \frac{\omega_{pi}^2}{\omega^2} - \frac{\omega_{pe}^2}{(\omega - kv_0)^2}\ ; \qquad \omega_{pi}^2 = \frac{4\pi n_i e^2 Z_i^2}{M_i}\ ; \qquad \omega_{pe}^2 = \frac{4\pi n_e e^2}{m}\ ; \tag{2.5}$$

$$\varepsilon_\perp = 1 - \sum_i \frac{\omega_{pi}^2}{\omega^2 - \Omega_i^2} - \frac{\omega_{pe}^2}{(\omega - kv_0)^2 - \Omega_e^2}\ ; \qquad \Omega_i = \frac{Z_i eB}{M_i c}\ ; \qquad \Omega_e = -\frac{eB}{mc}\ ; \tag{2.6}$$

J, K, I are the Bessel functions of the real and imaginary arguments; n_i, eZ_i, M_i are the density, charge and mass of i-ions; and n_e is the density of electrons. In a strong magnetic field the last addend in the expression for $\varepsilon_\perp$ can be ignored.

For longer waves ka, $kb \ll 1$ and $b \gg a$, the Bessel functions can be expanded in the vicinity of zero. As a result we obtain a dispersion equation for longitudinal waves:

$$\varepsilon_\parallel + \frac{2}{k^2 a^2 \ln\left(\frac{b}{a}\right)} = 0$$

or

$$1 - \frac{\omega_p^2}{\omega^2} - \frac{\omega_{pe}^2}{(\omega - kv_0)^2} + \frac{2}{k^2 a^2 \ln\left(\frac{b}{a}\right)} = 0\ , \qquad \omega_p^2 = \sum_i \omega_{pi}^2\ . \tag{2.7}$$

Here we have used the condition $\varepsilon_\perp \ln(b/a) \gg 1$, which means a rather high detuning from the resonance ion frequencies, where $\varepsilon_\perp$ turns into zero. If the electron current is much less than the limiting current in the pipe, i.e.:

$$\omega_{pe}^2 \ll \frac{2v_0^2}{a^2 \ln\left(\frac{b}{a}\right)}\ , \qquad \omega_{pe}^2 \gg \omega_p^2\ ,$$

then the waves in electrons and ions become separated, i.e. they can be considered individually. Thus, we obtain a dispersion equation for the waves related to ions:

$$u = \frac{\omega}{k} = \pm\omega_p a \sqrt{\frac{\ln\left(\frac{b}{a}\right)}{2}}\ , \qquad \omega \ll \omega_p\ , \tag{2.8}$$

and for the waves related to electrons:

$$\left(\frac{\omega}{k} - v_e\right) = \pm\omega_{pe} a \sqrt{\frac{\ln\left(\frac{b}{a}\right)}{2}}\ , \qquad \omega \ll \omega_{pe}\ . \tag{2.9}$$

2.2 Damping of ion-related longitudinal waves

In the above calculation the dissipation of wave energy was ignored. In the parameter region characteristic for our experiments two main mechanisms contribute to damping: Landau damping and the damping that results from ion–ion collisions of various types. Since we are more interested in fairly long waves, the transverse motion of ions can be ignored, which considerables simplifies the calculation.

Let us first consider the dissipation mechanism due to Landau damping. For $a \ll b$; ka, $kb \ll 1$, the perturbation of the beam potential by the wave may be expressed:

$$\Phi = 2\pi(Z_i n_i - n_e)a^2 e \ \ln(b/a) \ . \tag{2.10}$$

The longitudinal electric field can therefore be presented as follows:

$$E_z = -2\pi a^2 e \ \ln(b/a) \ \frac{\partial n_i}{\partial z} \ Z_i \ . \tag{2.11}$$

Substituting this equation for the field in the linearized Vlasov equation for a distribution function f:

$$\frac{\partial f}{\partial t} + v\frac{\partial f}{\partial z} + \frac{ZeE_z}{M} \ \frac{\partial f_0}{\partial v} = 0 \ , \tag{2.12}$$

bearing in mind that $n = \int f \ dv$, then, provided the equation has the form $f \sim e^{ikz - i\omega t}$, we will obtain the following dispersion equation:

$$D(\omega, k) = 1 + \frac{2\pi a^2 e^2 \ln(b/a) Z^2}{M} \int \frac{\partial f_0}{\partial v} \ \frac{k}{(\omega - kv + i\delta)} \ dv = 0 \ , \qquad \delta \to 0 \ . \tag{2.13}$$

For the Maxwellian distribution function f_0 at $\omega/kv_T \gg 1$ the integral is easily calculated:

$$D(k,\omega) = 1 + \frac{2\pi a^2 e^2 \ln(b/a) Z^2}{M} \int \frac{\partial}{\partial v}\left(n_i \sqrt{\frac{M}{2\pi T}} \ \exp\left\{-\frac{Mv^2}{2T}\right\}\right) \ \frac{k \ dv}{\omega - kv + i\delta} \simeq$$

$$\simeq 1 - \frac{u^2}{v_T^2}\left[\frac{v_T^2 k^2}{\omega^2} + 3\frac{v_T^4 k^4}{\omega^4} - i\frac{\omega}{kv_T}\sqrt{\frac{\pi}{2}} \ \exp\left(-\frac{\omega^2}{2k^2 v_T^2}\right)\right] = 0 \ , \tag{2.14}$$

where $v_T = (T/M)^{1/2}$ is the thermal ion velocity, and $u = (2\pi a^2 Z_i^2 e^2 n_i \ln(b/a)/M)^{1/2}$ is the velocity of the longitudinal wave if there is no damping. When solving the equation for ω/k where $\omega/kv_T \gg 1$, in approximation we get:

$$\frac{\omega}{k} \simeq u\left(1 + \frac{3}{2}\frac{v_T^2}{u^2} - i\sqrt{\frac{\pi}{8}}\frac{u^3}{v_T^3} \ \exp\left\{-\frac{u^2}{2v_T^2}\right\}\right) \ . \tag{2.15}$$

If the beam contains ions of different charges and mass (Z_i, M_i), their contribution must be summed up both in phase velocity and in Landau damping:

$$\frac{\omega}{k} \simeq u\left(1 + \frac{3}{2u^4}\sum_i u_i^2 \ v_{T_i}^2 - i\sqrt{\frac{\pi}{8}} \ u \sum_i \frac{u_i^2}{v_{T_i}^3} \ \exp\left\{-\frac{u_i^2}{2v_{T_i}^2}\right\}\right) \ . \tag{2.16}$$

Here

$$u_i^2 = \frac{2\pi a^2 \epsilon^2 n_i Z_i^2}{M_i} \ln\left(\frac{b}{a}\right) , \qquad u^2 = \sum_i u_i^2 , \qquad v_{T_i}^2 = \frac{T}{M_i}$$

and it is supposed that the temperatures of all types of the ions are the same.

Besides the Landau damping, collision damping is also essential for longitudinal waves (especially at low ion temperatures), due to friction between various types of particles. To find the decrement of such damping let us calculate the dielectric penetrability of the plasma, consisting as it does of ions of different types at an identical temperature. For the condition $r_L \gg r_D$ (the Larmor radius is greater than the Debye radius) the Landau collision integral can be used [12] with logarithmic accuracy. For a system of ions of two different types of charges e_1 and e_2, the masses M_1 and M_2, and the collision logarithm L_{12} can be written as follows:

$$\frac{\partial f_i}{\partial t} = -St\ f_i \equiv \frac{\partial S_{i\alpha}}{\partial p_\alpha} , \qquad i = 1, 2,$$

where

$$S_{1\alpha} = 2\pi (e_1 e_2)^2 L_{12} \int d^3 p_2 \left(f_1(p_1) \frac{\partial f_2(p_2)}{\partial p_{2\beta}} - f_2(p_2) \frac{\partial f_1(p_1)}{\partial p_{1\beta}} \right) \times$$

$$\times \frac{(\vec{v}_1 - \vec{v}_2)^2 \delta_{\alpha\beta} - (v_1 - v_2)_\alpha (v_1 - v_2)_\beta}{|\vec{v}_1 - \vec{v}_2|^3} .$$

Multiplying this by $v_{1\alpha}$ and integrating it over $d^3 p_1$ will give us:

$$\frac{dw_{1k}}{dt} = \frac{1}{M_1} \int S_{1_k} d^3 p_1 , \qquad w_{1k} = \langle v_{1_k} \rangle .$$

Let us choose the velocity distribution functions as being Maxwellian:

$$f_i = c_i \exp\left\{ -\frac{M_i (v_i - v_i)^2}{2T} \right\} .$$

Then

$$S_{1\alpha} = 2\pi (\epsilon_1 \epsilon_2)^2 L_{12} \int d^3 p_2 f_1 f_2 \frac{1}{T} \frac{1}{|v_1 - v_2|^3} \times$$

$$\times \left[(v_1 - v_2)^2 \delta_{\alpha\beta} - (v_1 - v_2)_\alpha (v_1 - v_2)_\beta \right] \left[(v_1 - v_2)_\beta \right] .$$

If we take the vector $\frac{u_1 - u_2}{|u_1 - u_2|}$ as being the axis z, we will obtain

$$M_1 \frac{dw_{1z}}{dt} = -(w_{1z} - w_{2z}) \frac{2\pi (\epsilon_1 \epsilon_2)^2}{T} L_{12} \int d^3 p_1 d^3 p_2 f_1 f_2 \frac{(v_1 - v_2)_\perp^2}{|\vec{v}_1 - \vec{v}_2|^3} .$$

In linear approximation (where $w_i \ll \sqrt{T/M_i}$) f_i as a function of w_i can be ignored, and then:

$$\frac{dw_{1z}}{dt} = -(w_1 - w_2)_z \frac{2\pi (\epsilon_1 \epsilon_2)^2}{T} n_2 L_{12} \left(\frac{M_1 M_2}{2\pi T} \right)^{3/2} \times$$

$$\times \int d^3 v_1 d^3 v_2 \exp\left\{ -\frac{M_1 v_1^2 + M_2 v_2^2}{2T} \right\} \cdot \frac{(v_1 - v_2)_\perp^2}{|\vec{v}_1 - \vec{v}_2|^3} .$$

The integral in the right-hand part is calculated at the transition to the variables $v_1 + v_2$ and $v_1 - v_2$ and is equal to:

$$I = \frac{16}{3}\sqrt{2\pi^5}\,\frac{T^{5/2}}{M_1 M_2 (M_1 + M_2)^{1/2}} .$$

Thus,

$$\frac{dw_{1z}}{dt} = -(w_{1z} - w_{2z})\,\frac{4\sqrt{2\pi}}{3}\,\frac{n_2 (e_1 e_2)^2 L_{12}}{T^{3/2}}\,\mu_{12}^{1/2} = -c_{12}(w_{1z} - w_{2z}) ,$$

where $\mu_{12} = \frac{M_1 M_2}{(M_1 + M_2)}$. In this case the equation of motion for ions of type i in the wave $E_z e^{-i(\omega t - kz)}$:

$$-i\omega v_i = \frac{e_i}{M_i}\,E_z - \sum_{j \neq i} \gamma_{ij}(v_i - v_j) , \qquad \gamma_{ij} = \frac{c_{ij}}{M_i}$$

provided $\gamma_{ij} \ll \omega$, yields:

$$v_i = i\,\frac{E_z}{\omega}\left[\frac{e_i}{M_i} - \frac{i}{\omega}\sum_{j \neq i}\left(\frac{e_i}{M_i} - \frac{e_j}{M_j}\right)^2 \gamma_{ij}\right] .$$

From this can be determined the conductivity

$$\sigma = i \sum_i \frac{e_i n_i}{\omega}\left[\frac{e_i}{M_i} - \frac{i}{\omega}\sum_{j \neq i}\left(\frac{e_i}{M_i} - \frac{e_j}{M_j}\right)^2 \gamma_{ij}\right]$$

and dielectric penetrability

$$\varepsilon_\epsilon = 1 + i\frac{4\pi\sigma}{\omega} = 1 - \frac{\omega_p^2}{\omega^2}\left(1 - i\frac{\nu_{ii}}{\omega}\right) , \tag{2.17}$$

$$\nu_{ii} = \frac{8(2\pi)^{3/2}}{3\omega_p^2 T^{3/2}} \sum_{j>i} n_i n_j \epsilon_i^2 \epsilon_j^2 L_{ij}\mu_{ij}\left(\frac{e_i}{M_i} - \frac{e_j}{M_j}\right)^2 , \tag{2.18}$$

$$\omega_p^2 = \sum_i \frac{4\pi n_i \epsilon_i^2}{M_i} .$$

Using this expression in place of that for dielectric penetrability (2.17) in (2.7), we can obtain the dispersion equation with the friction between ions of various types being taken into account:

$$\frac{\omega}{k} \simeq u\left(1 - i\frac{\nu_{ii}}{2\omega}\right) .$$

Now, summing the contributions of the Landau damping and the ion–ion friction, we can finally obtain the dispersion equation for longitudinal waves:

$$\frac{\omega}{k} \simeq u\left(1 + \frac{\delta u}{u} - i\gamma_{\|} - i\frac{\nu_{ii}}{2\omega}\right) , \qquad \frac{\delta u}{u} = \frac{3}{2u^4}\sum u_i^2\, v_{T_i}^2 ,$$

where

$$\gamma_{\|} = \sqrt{\frac{\pi}{8}}\,u \sum \frac{u_i^2}{v_T^3}\exp\left(-\frac{u^2}{2v_T^2}\right) \tag{2.19}$$

and ν_{ii} is obtained from expression (2.18). The contribution of ion damping is clearly seen to decrease with frequency increase as against the contribution of Landau damping.

2.3 Excitation of a standing longitudinal wave in an ion column of finite length

Now we consider the process of excitation in a standing longitudinal wave in an ion column of length L. In the experiments the excitation was induced by an electrode that was short compared to the wavelength and was placed at the very beginning of the compensation section; the technique used was to apply to it a harmonic voltage at constant amplitude. The equations describing the excitation process are similar to system (2.2). In the case of low frequencies ($\omega \ll \omega_p, \Omega_i$), the transverse ion motion can be ignored but wave damping and the external excitation field have to be taken into account. For simplicity's sake, we shall write the equation for only one kind of ion, without any sacrifice of generality:

$$\frac{\partial n}{\partial t} + n_0 \frac{\partial v}{\partial z} = 0, \qquad \frac{\partial v}{\partial t} = -v\delta + \frac{e}{M}\,(-\nabla\,\Phi + E_{int}), \qquad \Phi = 2\pi n a_e^2\,\ln\left(\frac{b}{a}\right)\,,$$

here δ is the decrement of damping.
For the harmonic perturbation $e^{-i\omega t}E_{int}(z)$, whence it follows that the ion density equation:

$$\omega(\omega + i\delta)n + u^2\frac{d^2n}{dz^2} = \frac{en_0}{M}\,\frac{dE_{int}}{dz} \tag{2.20}$$

If there is no external field, we obtain a dispersion equation:

$$\omega/k = u(1 - i\delta/2\omega).$$

Comparing it with (2.19), for the damping decrement we obtain $\delta/2\omega = \gamma_{||} + \nu_{ii}/\omega \equiv \gamma$. The general solution to equation (2.20) for $z > 0$ can be written as follows:

$$n(z) = Ae^{ikz} + Be^{-ikz} + \frac{en_0}{kMu^2}\int_0^z \frac{dE_{int}}{dx}\,\sin[k(z-x)]\,dx\,, \tag{2.21}$$

where $k = k' + ik'' \simeq \omega(1 - i\gamma)/u$. The constants A and B are determined by the boundary conditions at the column extremities:

$$\left.\frac{dn}{dz}\right|_{z=0} = \left.\frac{dn}{dz}\right|_{z=L} = 0\,.$$

If the length of the excitation plate and the distance between the plate and the beginning of the column $z = 0$ are small compared to the wavelength, the integral in the right-hand part of (2.21) is easy to calculate:

$$\int_0^z \frac{dE_{int}}{dx}\sin(k(z-x))\,dx = +k^2\int_0^z \sin[k(z-x)]\,\Phi_{int}(x)dx$$

$$= +k^2\int_0^z (\sin\,kz\,\cos\,kx - \sin\,kx\,\cos\,kz)\,\Phi_{int}(x)dx$$

$$\simeq k^2\,\sin\,kz\int_0^z \Phi_{int}(x)dx = k^2 u_p l_p \sin\,kz, \qquad z > l_p\,.$$

Here, u_p, l_p are the voltage at the excitation plate and its effective length. This addend, like the first two terms in (2.21), also has a harmonic appearance along the whole length

of the ion column except for the origin of the coordinates, where the excitation plate is located, while at the origin of the coordinates it produces an abrupt change

$$\left.\frac{dn}{dz}\right|_{z=0} = \frac{ek^2 n_0}{Mu^2}\, l_p u_p \equiv n' \ .$$

This makes it evident that the account of the excitation field can be reduced to one where, if the solution to Eq. (2.21) does not have the last addend it should be added to by the boundary conditions for the density variable over the coordinate $dn/dz = n'$ for $z = 0$ and $dn/dz = 0$ for $z = L$. Thus, the solution will have the form:

$$n(z) = \frac{n'}{k}\ \mathrm{Re}\left[\frac{\cos\left((z-L)k\right)}{\sin Lk}\right] \ ,$$

where $k = k' + ik''$. If the measurements are performed by a pick-up electrode, in which z_p is the coordinate of the mid-point, and L_p is the length, then it will be necessary to average the density perturbation along the pick-up electrode, and the module of the complex amplitude of the total (full) charge inside the pick-up electrode will be:

$$q(k) = \frac{u_p L_p}{\sqrt{2\pi}\ \ln(b/a)} \times \tag{2.22}$$

$$\times \left(\frac{(\mathrm{ch}\ (k''L) - \cos\ (k'L))(\mathrm{ch}\ [2k''(z_p - L_p/2)] + \cos\ [2k'(z_p - L_p/2)])}{(\mathrm{ch}\ (L_p k'') - \cos\ (L_p k'))}\right)^{1/2}$$

From this expression it follows that the spectrum of longitudinal oscillations contains information both on the phase velocity and on the decrements of longitudinal wave damping in the ion column. The difference in the dependences of collision damping and the Landau damping of the frequency makes it possible to calculate both the decrements from the spectra. The temperature of compensating ions, which is an important characteristic of the beam, can in its turn be calculated from the decrements.

2.4 Experimental study of longitudinal wave propagation

The longitudinal oscillations were excited by applying a.c. voltage to one of the plates of the split locking electrode at the beginning or end of the ion column. Another plate was used for locking the ions. In this case the excitation affects only the very end of the ion column, which considerably simplifies interpretation of the results at a high excitation voltage frequency (when the wavelength becomes comparable with the length of the locking plate).

To measure the spectrum of the forced longitudinal oscillations the voltage from the generator of a controlled frequency was applied to the excitation plate. The response was measured from the summing output of one of the pick-up electrodes using two synchronous detectors, whose comparison voltages were shifted in phase by 90°. This provided information on both amplitude and response phase. The scanning was mainly performed in the range 10 Hz to 200 kHz, and the amplitude of the excitation voltage did not exceed 10 mV. When the results of measurements by the r.m.s. method were processed,

the parameters for (2.22) were chosen. As a result, we obtained three basic parameters: wave velocity, dimensionless Landau damping decrement $\gamma_{||}$, and ion–ion collision frequency $f_{st} = \nu_{ii}/2\pi$, as well as length of the ion column and the position of the pick-up electrode—values determined by the system geometry but not known accurately enough.

In Fig. 3 a longitudinal oscillation spectrum obtained by the method described above method is given as an example (L = 40 cm, I_e = 0.9 mA, B = 3 kG), where the adjustment, obtained via (2.21), is also presented. The measurements were performed with a pick-up electrode placed in the centre of the ion column, and the odd harmonics in the spectrum are therefore suppressed. Calculation using this approach yields the following results:

$$u = 0.605 \times 10^6 \text{ cm/s}, \quad \gamma_{||} = 0.0163, \quad f_{st} = 0.0367 \text{ kHz} .$$

Assuming that the mass distribution of compensating ions is close to the one shown in Fig. 21, we can calculate the ion temperature from the decrement of the Landau damping T = 0.1 eV and the collision damping T = 0.19 eV.

It should be noted that formula (2.21) is in good agreement with experimental data only up to frequencies of the order of 100 kHz, since at higher frequencies the wavelength $\lambda = 2\pi u/\omega$ becomes comparable with the size of the vacuum chamber and the linear dispersion law (2.19), and the method of calculating the longitudinal oscillation excitation (A 2.3) is also violated. The parameters were therefore adjusted in relation to the χ-square only in the frequency range 0–100 kHz, which corresponds to the wavelengths $\lambda > 10$ cm.

2.5 Nonlinear dispersion

Let us calculate the first correction to the linear dispersion law (2.8), describing longitudinal wave propagation in ions. For this purpose, let us expand the Bessel functions in accordance with the approximated formulae:

$$I_0(x) = 1 + \frac{x^2}{4} , \qquad I_1(x) = \frac{x}{2}\left(1 + \frac{x^2}{8}\right), \qquad x \ll 1 , \qquad \gamma = 1.78107 ,$$

$$K_0(x) = \ln\left(\frac{2}{\gamma x}\right)\left(1 + \frac{x^2}{4}\right) + \frac{x^2}{4} , \qquad K_1(x) = \frac{1}{x} + \frac{x}{2}\left(\ln\left(\frac{\gamma x}{2}\right) - \frac{1}{2}\right) ,$$

and retain the next term of expansion. The dispersion equation can then be written down as follows:

$$\frac{\omega_p^2}{\omega^2} - 1 = \frac{2}{k^2 a^2} \frac{1}{\ln\frac{b}{a} - \frac{k^2 b^2}{4} + \frac{1}{4\varepsilon_\perp}} .$$

Since for characteristic parameters of the machine the value $\varepsilon_\perp$ exceeds unity, then the addend $2/4\varepsilon_\perp$ in the denominator can be ignored and for the nonlinear dispersion law the following expression can be written:

$$\omega^2 = \frac{\omega_p^2 k^2 a^2 \ln(b/a)}{2} \frac{1}{1 + \frac{k^2 b^2}{4\ln(b/a)}\left(1 + 2\frac{a^2}{b^2}\ln^2(b/a)\right)} ,$$

$$a \ll b , \qquad kb \leq 1 . \tag{2.23}$$

So it is evident that with a decrease in wavelength phase velocity also falls. Figure 4 gives a comparison of experimentally measured phase velocity of the reverse wavelength $\lambda^{-1} = k/2\pi$ with expression (2.23) ($b/a = 10$, $2\pi/k \gg b$). Qualitatively, the experimental and the analytical curves behave similarly, but for quantitative comparison the accuracy of the experiment seems insufficient.

2.6 Nonlinear large amplitude waves

For a large amplitude wave the dispersion non-linearity, as defined above, can be compensated by non-linearity of waves, which provides for the existence of solitary nonlinear waves (solitons). For fairly high wavelengths the transverse motion of ions can be ignored. In this case the equations of motion will have the form:

$$\frac{\partial v}{\partial t} + v\frac{\partial v}{\partial z} = -\frac{Ze}{M}\frac{\partial \Phi}{\partial z}\,, \qquad \frac{\partial n}{\partial t} + \frac{\partial}{\partial z}(nv) = 0\,,$$

$$\Phi = 2\pi e a^2\, Z \ln\left(\frac{b}{a}\right)\,(n - n_0) + \kappa e \frac{\partial^2 n}{\partial z^2}\, Z\,. \tag{2.24}$$

Here the coefficient κ is responsible for nonlinear dispersion and will be determined by a comparison with (2.23). Let us seek a solution in the form of a solitary wave:

$$n = n(z - wt)\,, \qquad v = v(z - wt)\,, \qquad \Phi = \Phi(z - wt)\,.$$

In this case the first two equations are easy to integrate:

$$\left\{w^2 - \frac{2eZ}{M}\Phi(x)\right\}\, n^2(x) = w^2 n_0^2\,,$$

$$\Phi = 2\pi e a^2\, Z \ln\left(\frac{b}{a}\right)\,(n(x) - n_0) + Ze\kappa n^4(x)\,, \qquad x = z - wt$$

Expanding the first equation while preserving only the terms up to the second order of smallness

$$\tilde{n}(x) \equiv n(x) - n_0 \simeq n_0\left(\frac{e\Phi}{Mw^2} + \frac{3}{2}\,\frac{Z^2e^2\Phi^2}{M^2w^4}\right)$$

and substituting it in the second one, in a quasi-linear approximation we obtain:

$$\Phi \cdot (w^2 - u^2) = \frac{3}{2}\,\frac{Zeu^2}{Mw^2}\,\Phi^2 + \frac{b^2u^2}{4\ln(b/a)}\Phi''\,.$$

Here $u = (2\pi n_0 e^2 a^2 Z^2 \ln(b/a)/M)^{1/2}$ is the velocity of the small-amplitude wave, and $\kappa = (\pi/2)a^2b^2$ is determined by comparison with (2.23). The solution to this equation describes a solitary wave with a positive density perturbation

$$n(z - wt) = \frac{n_{\max}}{\mathrm{ch}^2\left(\frac{z-wt}{b}\sqrt{\frac{n_{\max}}{n}\ln\left(\frac{b}{a}\right)}\right)} + n_0\,, \tag{2.25}$$

propagating at a velocity higher than that of sound:

$$w = u\left(1 + \frac{1}{2}\frac{n_{\max}}{n_0}\right) \tag{2.26}$$

From (2.25) it is evident that the length of the solitary wave is related to the amplitude as:

$$\triangle = b\sqrt{\frac{n_0}{n_{\max}\ln(b/a)}} \tag{2.27}$$

In our experiments waves with a high amplitude were excited by applying a pulse of regulated value to one of the plates in the locking electrode. The other plate of this electrode was used for locking ions. The character of the excited signal was closely dependent on the time of pulse excitation. For example, at a short pulse ($\sim 1\mu$s) only waves with a negative density perturbation ('density well') were excited when applying a pulse of negative polarity. When applying a positive pulse the excitation of a solitary wave was strongly suppressed. This can apparently be accounted for by the fact that with short-pulse excitation the dependence of the density perturbation on the coordinate is a sign-variable value, and the propagation of the $(+\ -)$ type differs from that of $(-\ +)$. Since this way of excitation yielded results that were hard to interpret, another method of excitation was used. The initial rise time of the excitation pulse was short (less than 0.5 μs), while its duration was long enough—more than the characteristic wave lifetime. This method caused excitation both of positive and negative waves. The space structure of these waves was not sign-variable, which made their interpretation easier. Wave propagation in the beam was controlled by the summed signal of pick-up electrodes (i.e. the signal proportional to the charge in the pick-up electrode). Shown in Fig. 5 are signals from the pick-up electrode that are dependent on time if waves of different polarity are excited. The pick-up electrode was placed in the middle of the compensation section (the section was 40 cm long), so the distance between the pick-up electrodes corresponds to 40 cm of the wave motion (20 cm from the pick-up electrode to the mirror and back). The positive wave is seen to have a clearer structure than the negative one and closer correspondence to a solitary wave. The general decrease in the level shown in Fig. 5c for wave excitation of a negative pulse is accounted for by partial decompensation of the beam at a potential appearing on the excitation plate. The density excitation amplitude $\triangle n/n$ of the initial pulses shown in Fig. 5, amounts to 5–6%. The pulse width, as shown in Fig. 5, makes it possible to judge the excitation length propagating in the beam.

Figure 6 shows the signal from the pick-up electrode read at the moment of first pass by a perturbation with a higher time resolution. From the signal derivative versus time given in the same figure the perturbation length can be calculated, which in our case was approximately 3.5 cm. From the previous figure the perturbation length is seen to grow with damping to reach 15–20 cm. Identical behaviour of the perturbation length was observed for perturbations at any amplitude in the $\delta n/n$ range from 20 to 0.05%.

Such a difference in wave behaviour from that predicted is apparently bound up with the presence of fairly strong damping. Figure 7 shows the decrement of longitudinal wave damping versus their amplitudes. In a fairly broad range the decrement is shown to be independent of the perturbation amplitude, which may either indicate that the

decrement is predominantly the result of collision damping, or that the boundary has not yet been reached where the Landau damping is reduced through non-linearity (i.e. nonlinear Landau damping).

2.7 Decompensation wave

Another example of a high amplitude non-linear wave is the decompensation wave that appears when ion extraction is commenced at any point in the ion column. The ions are extracted by applying a negative pulse to one of the electrodes surrounding the electron beam. In this case compensating ions will leave the electron beam over a period of approximately $2L/u_i$. The ion motion in this case is described by equation (2.24). And since the characteristic size of the longitudinal wave is great, the dispersion non-linearity can be ignored. Let us move in these equations to the dimensionless variables $n = n/n_0$, $v = v/u$ and search for the solution in the self-similar form $v(\xi)$, $n(\xi)$, where $\xi = (z/ut)$. Then equation (2.24) can be written down in the form;

$$v' = \frac{n'}{\xi - v} \; ; \quad n' = \frac{nv'}{\xi - v} \; ,$$

from which we get:

$$n = \frac{(\zeta_0 - \zeta)^2}{9} \; , \quad v = \frac{(\zeta_0 + 2\zeta)}{3} \tag{2.28}$$

The constant ζ_0 is determined from the condition, whereby the leading edge of the perturbation moves along the ion column at the velocity of sound, giving $\zeta_0 = 2$. The form of the solution obtained by the formulae (2.28) and corresponding to beam expansion in a vacuum, is shown in Fig. 8. After the decompensation wave reaches the end of the compensated section (where the condition $v = 0$, i.e. $\partial n/\partial z = 0$ must be satisfied) the wave, whose density is independent of the z-coordinate (see Fig. 9), is reflected from it. From (2.24) we obtain the equation describing the change in velocity:

$$\frac{\partial v}{\partial t} + v\frac{\partial v}{\partial z} = 0 \; .$$

Its self-similar solution will take the form:

$$v = \frac{z - L}{ut} \; ,$$

yielding the density dependence on time of:

$$n = \frac{L}{ut}, \quad t > L/u \; .$$

Figure 9 shows ion densities in the beam as functions of coordinates for various moments in time. The results were obtained from numerical solutions to the equations in (2.24) with a boundary condition at the right-hand boundary $n(z = 0) = 0$. Despite another boundary condition the numerical calculation results was observed to fit closely to the solution theoretically predicted above.

The decompensation wave we have described was excited so as to measure the degree of the charge compensation (i.e. values Q_i/Q_e, where Q_i, Q_e are the electron and the ion charges per unit length) by ion extraction, as follows. The plates of the pick-up electrode, located in the compensated section of the electron beam, were connected up with one another and to the integrating amplifier input (the equivalent capacity is 100 pF, and maximum integration time 6 ms). The signal from this amplifier was applied to a digital oscillograph input (ADC). The measurements were performed as follows: a pulse (-200 V, duration 2 ms) was applied to one of the free plates from the boundary of the compensated region. All compensating ions were extracted from the beam, and at the integrator output a signal appeared that was proportional to the ion charge inside the pick-up electrode. 1.5 ms after the first pulse another pulse was applied to the gun anode, shutting down the electron current (-600 V, duration 1 ms), and the signal at the integrator output was changed to a value proportional to the electron charge in the pick-up electrode. While running these various procedures the signal from the integrator was detected by a digital oscillograph. After processing the signal the relationship of the electron and ion charges located in the pick-up electrode was easily obtained, i.e. the compensation ratio to the charge. An example of such a signal, detected by the ADC, is given in Fig. 10. Besides the compensation ratio, it is also useful in visualizing the dynamics of the ion charge located in the pick-up electrode after the extraction pulse start as a function of time. Figure 11 shows the ion charge value in the pick-up electrode as a function of time, obtained by means of numerical simulation. The reflection of the decompensation wave is clearly seen. Good agreement between the experimental and theoretically calculated data was observed.

2.8 Longitudinal waves connected with electrons—beam potential measurement by time of flight

The method described in the previous section makes it possible to determine the compensation ratio by the ion charge per unit of length. Nevertheless a close to 100% charge compensation in no way proves the presence of real compensation in the space charge, since in the case of a high ion temperature the radius of the ion column can noticeably exceed that of the electron beam. To prove good compensation the electric field or potential in the beam has to be measured.

A simple way of measuring potential is to measure the velocity of electrons. From the energy of electrons $\mathcal{E}$ and their velocity v_0 the beam potential can easily be calculated:

$$e\Phi = \mathcal{E} - \frac{mv_0^2}{2} . \tag{2.29}$$

Electron velocity was measured by means of electron cooling (see below). But this method is fairly labour-intensive and time-consuming. For measuring the potential, therefore, a 'time of flight' method of measuring electron velocity was worked out. To this end a density perturbation is set up in the electron beam at the point of entry into the drift chamber and the time taken by the perturbation to propagate through to the system's end-point $\tau_0 = l/v_0$ is measured. But if the electron current is increased the wave propagation in the electron beam itself seriously affects the perturbation pattern, which considerably hampers interpretation of results.

Let us consider the process of creating a perturbation in the electron beam by means of a pick-up electrode, to both halves of which alternating voltage $U_p \cos(\omega t)$ is applied. In this case the analysis is simplified, since we can single out for separate consideration the perturbations generated by the input and the output sections of the pick-up electrode, and then simply add them together.

At the input to the pick-up electrode a velocity perturbation δv almost immediately appears in the electron beam ($\tau_p \sim R_p/v_0$, R_p is the pick-up radius) and since the current density at this point must be maintained, the density perturbation will be δn. After passing through a short section at the input with a noticeable electric field $E_z = -\partial\Phi/\partial Z$, all the electrons inside the pick-up electrode move at constant velocity. What happens to the density and velocity perturbations? If we now switch to a system where the beam is motionless, then, by ignoring the influence of ions for longitudinal waves we will obtain [see (2.9)]:

$$\left(\frac{\omega}{k}\right)^2 = u_e^2 = \frac{2\pi n_e e^2 a^2 \ln(b/a)}{m} . \tag{2.30}$$

This means that the perturbation that arises is divided into two density (or velocity) perturbations, which will travel in opposite directions at a velocity of $\pm u_e$. In the laboratory system the two perturbation waves will travel at velocities of $v_0 - u_e$ and $v_0 + u_e$:

$$\begin{aligned} v &= v_0 + \delta v_+ \cos(\omega t - k_+ z) + \delta v_- \cos(\omega t - k_- z) , \\ n &= n_0 + \delta n_+ \cos(\omega t - k_+ z) + \delta n_- \cos(\omega t - k_- z) , \end{aligned} \tag{2.31}$$

where $k_\pm = \frac{\omega}{v_0 \pm u_e}$, and the symbols '+' and '−' are referred to as the fast and slow waves respectively.

If we assume that the coordinate of the pick-up electrode input is $z = 0$, and that of its end-point is $z = L_p$, then through the continuity equation (2.2), we will obtain at $z = 0$ the velocity-density relationship in the wave:

$$\delta n_\pm = \pm \frac{\delta v_\pm}{u_e} n_0 . \tag{2.32}$$

It can easily be seen that when $eU_p \ll \mathcal{E}_k$ ($\mathcal{E}_k$ being the kinetic energy of beam electrons) the full velocity perturbation at $z = 0$ will be:

$$\delta v = \delta v_+ + \delta v_- = \frac{1}{2} \frac{eU_p}{\mathcal{E}_k} v_0 . \tag{2.33}$$

Since at $z = 0$ the current density is maintained $nv = \text{const}$, then $\delta n/n_0 = -\delta v/v_0$, and from (2.32) and (2.33) we will obtain:

$$\frac{\delta v_+}{u_e} - \frac{\delta v_-}{u_e} = -\frac{1}{2} \frac{eU_p}{\mathcal{E}_k} . \tag{2.34}$$

By solving the system of equations (2.33), (2.34), we find the velocity perturbation amplitudes for the fast and slow waves:

$$\delta v_+ = \frac{1}{4}\frac{eU_p}{\mathcal{E}_k}(v_0 - u_e),$$
$$\delta v_- = \frac{1}{4}\frac{eU_p}{\mathcal{E}_k}(v_0 + u_e), \qquad (2.35)$$

Thus,

$$n(z,t) = n_0\left(1 + \frac{1}{4}\frac{eU_p}{\mathcal{E}_k}\left[\left(\frac{v_0 - u_e}{u_e}\right)\cos(\omega t - k_+ z) - \left(\frac{v_0 + u_e}{u_e}\right)\cos(\omega t - k_- z)\right]\right)$$
$$v(z,t) = v_0\left(1 + \frac{1}{4}\frac{eU_p}{\mathcal{E}_k}\left[\left(\frac{v_0 - u_e}{v_0}\right)\cos(\omega t - k_+ z) + \right.\right.$$
$$\left.\left. + \left(\frac{v_0 + u_e}{v_0}\right)\cos(\omega t - k_- z)\right]\right) \qquad (2.36)$$

and $j_e = j_{e0} + j_\sim$, where the current density perturbation

$$j_\sim(z,t) = j_{e0}\frac{eU_p}{2\mathcal{E}_k}\frac{v_0^2 - u_e^2}{v_0 u_e}\sin\left(\omega t - \frac{z v_0 \omega}{v_0^2 - u_e^2}\right)\sin\left(\frac{\omega z u_e}{v_0^2 - u_e^2}\right) \qquad (2.37)$$

It is worth noting that the perturbation amplitudes of density and velocity differ in fast and slow waves, while the amplitudes of the two waves in the current density are similar. This characteristic is a feature of perturbation excitation by a pick-up electrode (drift tube).

It is easy to determine the waves excited at the other end of the pick-up electrode. All formulae (2.36), (2.37) remain unchanged apart from exchanging z for $z - L_p$ and since the field E_z has different signs at the points $z = 0$ and $z = L_p$ (at an identical moment in time t), the density and velocity perturbations will have a sign opposite to the one used in (2.36), (2.37). Finally, we will have the sum of the four above-mentioned waves:

$$j_\sim = j_{e0}\frac{eU_p}{2\mathcal{E}_k}\frac{v_0^2 - u_e^2}{v_0 u_e}\left[\sin\left(\omega t - \frac{z v_0 \omega}{v_0^2 - u_e^2}\right)\sin\left(\frac{\omega z u_e}{v_0^2 - u_e^2}\right) - \right.$$
$$\left. - \sin\left(\omega t - \frac{(z - L_p)v_0\omega}{v_0^2 - u_e^2}\right)\sin\left(\frac{\omega(z - L_p)u_e}{v_0^2 - u_e^2}\right)\right] \qquad (2.38)$$

Formulae (2.36) - (2.38) are obtained on the supposition that longitudinal wave damping in the electron beam is low. Let us estimate it. According to (2.18) the collision portion is:

$$\gamma_{st} \sim \frac{\nu_{ei}}{\omega} = \frac{4\pi n_e e^4 L_{ei}}{\mathcal{E}_k^{3/2} m^{1/2}\omega} \sim 10^{-6}\, j_e(\mathrm{mA})/f(\mathrm{MHz}).$$

If $I_e = 5$ mA and $f = 5$ MHz then γ_{st} is about 10^{-6}. Since the wavelength at this frequency is about one fourth of the installation length, then total damping is no greater than 10^{-5}

The Landau damping is much smaller since:

$$\gamma_L \simeq p^{-3} \exp(-p^2) ,$$

where $p = v_T/u_e$ is about 50 if $I_e = 5$ mA and the temperature of electrons $T = 0.1$ eV.

Compensated ions also have little influence on the phase velocity of longitudinal waves in an electron beam. From (2.7) the deviation of this velocity in the presence of ions can be estimated as:

$$\frac{\delta u_e}{u_e} \simeq \frac{m\, u_e^2}{M_i (v_0 - u_e)^2} ,$$

and it is less than 10^{-6} for $I_e \leq 10$ mA.

Experiments confirmed the picture described above. We applied to ring electrode 6 (see Fig. 2) a short (10 nsec) pulse of amplitude 10 V and observed an initial disturbance of density $g(t)$ being divided by two parts with velocities $v_0 + u_e$ and $v_0 - u_e$. As described in (2.36) the density perturbation in this case must be:

$$\delta n(z,t) = A \left[\frac{v_0 - u_e}{u_e} g\left(t - \frac{z}{v_+}\right) - \frac{v_0 + u_e}{u_e} g\left(t - \frac{z}{v_-}\right) \right] . \qquad (2.39)$$

The difference between times of travel for slow and fast waves $\Delta\tau$ the point z_p contains information on the phase velocity of longitudinal waves:

$$u_e = \sqrt{\left(\frac{z_p}{\Delta\tau}\right)^2 + v_0^2} - \frac{z_p}{\Delta\tau}$$

The estimated phase velocity u_e as a function of electron current are shown in Fig. 12. The solid line corresponds to (2.30). There is rather good agreement between theory and experiment.

Simultaneously measured amplitudes of slow and fast waves are presented in Fig. 13. The shortcomings of this technique are in poor accuracy and it is hard to automate the process. For this reason we usually used another method of measurement.

The idea of the method is to detect synchronously the signal from a collector current when pick-up electrodes near the electron gun are driven by alternating voltage (similarly to the way described for ions in chapter 2.4). The measured frequency spectrum of longitudinal waves was fitted using (2.38) to parameters v_0 and u_e.

For a value v_0 the degree of compensation on the potential was determined using (2.29). For example in the measurement shown in Fig. 14 when ions were specially removed from the beam we obtained $v_0 = 1.27$ cm/nsec and the degree of potential compensation $k_\varphi = 0.05$.

The accuracy of time-of-flight method is about 0.2 eV for potential or 5% in respect of the degree of compensation.

3. TRANSVERSE ELECTRON–ION OSCILLATIONS

As we said above the main limitation on increasing the compensated beam current is the generation of drift instability. In this section, the stability of a system of ions and

electrons and the linking of charge compensation to transverse electron–ion oscillations are discussed. The low ion temperatures which simplify the task of calculation, are features of a well-compensated state, the most interesting case for us.

3.1 The main equations

If the temperature of ions is significantly less than the potential well in an uncompensated electron beam:

$$T \ll \pi n_e e^2 a^2 \bar{Z}_i = U \ , \tag{3.1}$$

then electrically the system is generally close to the neutral state. The highest compensation ratio is obtained in the centre of an electron beam:

$$1 - \frac{\overline{Z_i n_i}}{n_e}|_{r=0} \simeq \exp(-a/r_D) \ , \qquad r_D = \left(\sqrt{\frac{T_i}{4\pi e^2 \Sigma n_i Z_i^2}}\right) \tag{3.2}$$

here a is the electron beam radius, and r_D the Debye radius. There is no high compensation in the region close to the boundary of an electron beam only. The width of the zone is about that of the Debye radius and smaller than the beam radius because the inequality $r_D \ll a$ proceeds from (3.1).

Therefore in the case under consideration the ion density profile is somewhat similar to the stepped profile of electron beam density.

The only condition for the validity of the previous conclusion is the requirement for thermodynamic equilibrium of the ions in the electron beam:

$$\nu_{ii} \tau \frac{r_L^2}{a^2} \gg 1 \ , \qquad r_L < a \tag{3.3}$$

here ν_{ii} is the ion–ion collision frequency, τ is the ion lifetime in the electron beam, and r_L is the Larmor radius of an ion. The inequality (3.3) expresses not only local equilibrium at a given point inside the beam but also thermodynamic equilibrum along the beam's entire cross-section due to the random movement of the ions after collision. $D = \nu_{ii} r_L^2$ is really the coefficient of diffusion and the average pass of an ion is $\sqrt{D\tau}$, i.e. greater than a (see 3.3).

In satisfying (3.1) the system can be described in a hydrodynamic approximation. In the most important case, that of dipole oscillations at fairly long wavelengths ($ka \ll 1$), both ion and electron clusters move coherently in a transverse direction [13].This makes it possible to describe the system not in terms of individual particles but rather as whole units. In this case, the equations of motion describing the mid-points of the ion column and electron beam will be:

$$\begin{aligned} \ddot{\xi}_i &= -i\Omega_i \dot{\xi}_i + \frac{\epsilon Z_i}{M_i} E - \gamma_\perp \dot{\xi}_i \ , \\ \dot{\xi}_e &+ v \frac{\partial \xi_e}{\partial l} = -i\Omega_d \frac{E}{2\pi n_e \epsilon} \ , \\ E &= 2\pi n e (\xi_e - \sum_i Z_i q_i \xi_i) \ . \end{aligned} \tag{3.4}$$

In (3.4) the indexes e, i correspond to electrons and ions of type i respectively; $\xi = x + iy (i = \sqrt{-1})$ is the overall deviation of a mid-point; $\Omega_i = Z_i eH/M_i c$ is the

Larmor frequency; z is the longitudinal coordinate; $E = E_x + iE_y$ is the complex electric field; $q_i = n_i/n_e$ is the relative concentration of ions of type i; $\Omega_d = 2\pi nec/B$ is electron drift frequency in the field formed by the compensating ions; $\gamma_\perp$ damping decrement for the transverse motion of the ions. This system of equations leads to the same dispersion equation as the precise hydrodynamics equation system in the long wavelength limit described in [13]. Here we also take into account a damping of the transverse oscillations, however. The value of the decrement $\gamma_\perp$ will be defined below.

3.2 Solution of the boundary problem

The system of equations in (3.4) must be supplemented by an initial condition for a positioning of ions $\xi_i(z)|_{t=0}$ and a boundary condition for electron deviations $\xi_e(t)|_{z=0}$. The resultant solution will be the sum of the two solutions connected with the initial and boundary conditions. Let us consider a problem with initial conditions, i.e. ions of a single type i at time $t = 0$ with the same deviation in length $\xi_i(z) = \xi_{i0}$. The problem is solved in Appendix 1 and for time $t \gg z/v$ its asymptotic behaviour is:

$$\xi_e \sim \xi_{i0} \exp\left(-\frac{\gamma_\perp t}{2}\left(1 - \frac{\Omega_i}{2\sqrt{\frac{\Omega_i^2}{4} + \frac{\omega_T^2}{2}}}\right) + 2\sqrt{\kappa_3 z t}\right) ,$$

where κ_3 is defined in A1-5. We can see that the amplitude of oscillations rises, reaching a peak after $t' \simeq (z\omega_\perp\Omega_d)/(v\gamma_\perp^2)$, before being damped in time $\sim 1/\gamma_\perp$. The maximum oscillation amplitude is:

$$\xi_{i\,\max} \sim \xi_{i0} \exp\left(\frac{\Omega_d z \omega_\perp}{v\gamma_\perp}\right) ,$$

where $\omega_\perp$ is defined in A1-3. The system (3.4) is stable because after some considerable time, any solution with an initial deflection is damped.

3.3 Dispersion equation and estimation of threshold current density

For obtaining a solution produced by initial deflection of an electron beam let us show the latter in the form $\xi_e(t)|_{z=0} = \xi_0 e^{-i\omega t}$, and we will then find that all unknown quantities will be proportional to $\sim e^{ik(\omega)z - i\omega t}$ The result will be:

$$\begin{aligned}
\xi_e(z,t) &= \xi_0 e^{i(k(\omega)z - \omega t)} \qquad E(z,t) = \frac{2\pi n_e e}{\varepsilon_\perp(\omega)}\xi_e(z,t) , \\
\xi_i(z,t) &= -\frac{2\pi n_e e^2 Z_i}{M_i\omega(\omega + \Omega + i\gamma_\perp)}\xi_e(z,t)\frac{1}{\varepsilon_\perp(\omega)} , \\
\xi(z,t) &\equiv \xi_e(z,t) - \sum \frac{Z_i n_i}{n_e}\xi_i = \frac{\xi_0 e^{ik(\omega)z - i\omega t}}{\varepsilon_\perp(\omega)} ,
\end{aligned} \tag{3.6}$$

here:

$$k(\omega) = \frac{\omega}{v} - \frac{\Omega_d}{v\varepsilon_\perp(\omega)} , \tag{3.7}$$

$$\varepsilon_\perp(\omega) = \varepsilon'_\perp(\omega) + i\varepsilon''_\perp(\omega) = 1 - \sum \frac{\omega_{pi}^2}{2\omega(\omega - \Omega_i + i\gamma_\perp)} , \tag{3.8}$$

$$\omega_{pi}^2 = \frac{4\pi n_i Z_i^2 e^2}{M_i} , \qquad \Omega_i = \frac{eZ_i B}{M_i c} , \qquad \Omega_e = \frac{eB}{mc} , \qquad \Omega_d = \frac{\omega_{pe}^2}{2\Omega_e} = \frac{2\pi n_e ec}{B}$$

Allowance for dissipation $\gamma_\perp$ leads to the appearance of the imaginary part $i\varepsilon''_\perp(\omega)$. The imaginary part of the wave number $k''(\omega)$ is bound up with the perturbation amplification coefficient down the beam length:

$$K(\omega) = \exp\{k''(\omega)L\} = \left|\exp\left\{\frac{i\Omega_d L}{v[\varepsilon'_\perp(\omega) + i\varepsilon''_\perp(\omega)]}\right\}\right| \tag{3.9}$$

The coefficient of amplification achieves its greatest value when the real part $\varepsilon_\perp(\omega)$ is made equal to zero. For one type of ion the resonant frequency is :

$$\omega_\perp = \frac{\Omega_i}{2} - \sqrt{\frac{\omega_p^2}{2} + \frac{\Omega_i^2}{4}} , \tag{3.10}$$

and the maximum amplification coefficient is:

$$K_{\max} = K(\omega_\perp) = \exp\left\{\frac{\Omega_d L}{v\varepsilon''_\perp(\omega_\perp)}\right\} \tag{3.11}$$

Reference [9] shows that coherent oscillations possessing multipolarity higher than 2 (quadrupole, etc.) are degenerate in terms of frequencies and, where there is rectangular electron density distribution, have coefficients of amplification that are less than (3.11). Here only dipole oscillations will be taken into consideration.

Therefore we reached the conclusion that the amplitude of oscillations increases exponentially along the beam axis z but remains limited in time.

Let us make very simple estimates of maximum electron current in a state of good compensation. In this case, the limitations follow from the low oscillations at the beam end. If a maximum possible amplification $K_{\max}$ is taken then from (3.11):

$$j < j_{th} = \frac{v^2 B}{Lc}\varepsilon''(\omega_\perp)\frac{\ln K_{\max}}{2\pi} \tag{3.12}$$

Maximum experimental amplification values (see below) correspond to $\ln K_{\max} \leq 6$ and the upper limit of $\varepsilon''_\perp(\omega_\perp)$ is about 1, giving a logarithmic precision of:

$$j_{th} \simeq \frac{v^2 B}{2Lc} \tag{3.13}$$

The damping decrement γ and its mechanism need to be taken better account of, if a more precise value of threshold current density is to be obtained.

3.4 Influence of secondary electrons

One of the most significant limitations on the maximum amplification coefficient is the ever-present phenomenon of feedback, i.e. the influence by oscillations at the end of the beam on those at its beginning.

Let us denote the feedback by the coefficient η, equal to the ratio of the field at the beam's beginning to the field at its end. Then the criterion of transverse oscillation stability will limit the maximum value of amplification as follows:

$$|K_{\max}\eta| < 1 \ . \tag{3.14}$$

Feedback can occur through secondary electrons, both those due to ionization and those repelled from the collector.

The bulk of electrons repelled from the collector have energies close to the initial energy of beam electrons. In this case a simple estimate of the feedback coefficient can be made:

$$\eta_r \simeq \frac{n_{e_2}}{n_e} \ . \tag{3.15}$$

If electrons from residual gas ionization can be stored, they have quite long lifetimes in the beam and their velocity distribution is close to the Maxwell equivalent. Thus, electrons moving at different velocities take differing times to travel from the end of beam back to the beginning and their effect is mutually compensatory. The feedback coefficient can be estimated, by making an average for each phase:

$$\eta_{\text{ion}} \simeq \left| \frac{n_{e_2}}{n_e} \left[\int_0^\infty f(v) \exp\left\{ i \frac{\Omega_d L}{v} \right\} dv \right] \right| , \tag{3.16}$$

which when $\Omega_d L / \sqrt{2} v_{T_2} \gg 1$:

$$\eta_{\text{ion}} = \frac{n_{e_2}}{n_e} \frac{1}{\sqrt{3}} \exp\left\{ -\frac{3}{4} \left(\frac{\Omega_d L}{v_{T_2}} \right)^{2/3} \right\} \qquad v_{T_2} = \sqrt{\frac{T_{e_2}}{m}} \tag{3.16a}$$

Here the integral for the Maxwell function distribution is calculated using the pass method. More accurate estimates taking into account the dynamics of secondary electron movement are given in [9]. We should note that in asymptotic $\Omega_d L / v_{T_2} \gg 1$ care must be taken over estimates because changing an upper limit in an integral from infinite to finite value (for example due to voltage on a collector) gives power, i.e. non-exponential behaviour of η. With positive voltage on the collector, ionization electrons pass along the beam only once and, with a strong vacuum in the device, this type of feedback is so small that it can be ignored in relation to the contribution of electrons repelled from the collector.

3.5 Transverse oscillation damping

As can be seen from (3.11) the maximum amplification coefficient depends heavily on a decrement in transverse oscillation damping, in other words, on the imaginary part of dielectric permittivity $\varepsilon''_\perp(\omega_\perp)$ at the resonance frequency.

For ion–ion collisions $\varepsilon''_\perp(\omega_\perp)$ can be easily estimated from (2.18):

$$\varepsilon''_\perp \simeq \frac{\nu_{ii}}{\omega}\frac{\omega_p^2}{\omega^2} \simeq \frac{\nu_{ii}}{\omega_{pi}} \simeq \left(\frac{2}{\pi}\right)^{3/2} \frac{L_{ii}\bar{Z}}{3a^3 n_e}\left(\frac{eU}{T}\right)^{3/2} , \tag{3.17}$$

where: n_e is electron density, U is the 'potential well' in the electron beam [see (3.1)], T is the ion temperature, L_{ii} is Coulomb's logarithm, a is beam radius, and

$$\bar{Z} = \frac{\Sigma_{i>j}\chi_i\chi_j Z_i Z_j \mu_{ij}(Z_i/M_i - Z_j/M_j)^2}{\Sigma_i \chi_i Z_i/M_i} , \qquad \mu_{ij} = \frac{M_i M_j}{M_i + M_j}$$

is the mean ion charge, where $\chi_i = n_i Z_i/n_e$ is the relative ion charge density of type $i(\Sigma\chi_i = 1)$, M_i is the mass of the ion in atomic units. Ion–ion collisions are significant at low temperatures only (for example at $n_e = 10^9$ cm^{-3}, $\bar{Z}_i = 2$, $a = 0.1$ cm and $T = 10$ K is needed to obtain $\varepsilon'' \simeq 0.1$) and in real conditions this damping may be ignored.

Another dissipation mechanism is Landau damping. The finite temperature of ions causes them to move over the beam across its section. Energy exchange from wave to particles is possible when the wave is at a frequency in the spectrum of the ion's thermal motion. The shape of this spectrum depends on the plasma frequency ω_p and Larmor frequency Ω_i.

In the case of $\Omega_i > \omega_{pi}$ the movement of the ions is a drift in crossed electric and magnetic fields. The electric field is concentrated in the Debye boundary layer and can be estimated by:

$$E_T = \frac{T}{e r_D} . \tag{3.18}$$

which determines the maximum frequency of ion drift:

$$\omega_d = c\frac{E_T}{Ba} = \Omega_d \frac{r_D}{a} . \tag{3.19}$$

But from (3.10) the frequency of the transverse wave will be $\omega_\perp \simeq \Omega_d$ in this example. Landau damping is therefore absent in the compensated state of $r_D \ll a$ in the case of magnetized ions.

With unmagnetized ions the wave frequency is $\omega_\perp \simeq \Omega_d$, and ions inside the beam move freely during time $\simeq a/v_T$ but are then quickly repelled from the boundary ($\Delta t \simeq \omega_{pi}^{-1}$). Let us estimate the damping decrement in simplified form.

An ion has a velocity v_{T_i} and is repelled elastically from the walls of the beam in the presence of an electric field with a transverse wave $E_0 \exp(i\omega t)$. At times when the directions of its velocity and wave force are the same, the ion travels further along $Z_i e E_0/M_i\omega_{pi}^2$ than when such directions are opposite. And the probability of a phase being broken between a particle and a wave after collision with a boundary wall is therefore higher at $[(Z_i e E_0)/(M_i\omega_{pi}^2)]/(v_{T_i}/\omega_{pi})$ during acceleration than deceleration. On average the ion is accelerating, thereby damping the wave. For a period of motion $2a/v_{T_i}$ on average an ion develops an energy of:

$$\Delta\varepsilon \simeq 2e E_0 \frac{v_{T_i}}{\omega_{pi}} \frac{e E_0 Z_i^2}{m\omega_{pi}^2}\left(\frac{v_{T_i}}{\omega_{pi}}\right)^{-1} = \frac{2e^2 E_0^2}{m\omega_{pi}^2} Z_i^2 .$$

If we consider that the energy of the wave per unit length of the beam, taking account of the kinetic energy of particles in the wave and the fields outside the beam, is:

$$W = 2\frac{E_e^2}{8\pi}(\pi a^2 + \pi a^2) = \frac{E_0^2}{2\pi}\,\pi a^2 ,$$

then we obtain the damping decrement:

$$\gamma_\perp \simeq \frac{\pi a^2 n_i}{2}\frac{\Delta\varepsilon/\Delta t}{W} = \frac{\pi a^2 n_i}{2}\left(\frac{2e^2E_0^2}{m\omega_{pi}^2}Z_i^2\right)\left(\frac{2a_i^2}{v_{T_i}}\frac{E_0^2}{4\pi}\pi a^2\right)^{-1} = \frac{v_{T_i}}{4a} .$$

More accurate estimates (see Appendix 2) give:

$$\gamma_\perp = \sqrt{\frac{2}{\pi}}\frac{v_{T_i}}{a} , \qquad r_D \equiv \left(\frac{T}{4\pi n_e e^2}\right)^{1/2} \ll r_L \ll a , \tag{3.20}$$

governing the contribution to dielectric permeability:

$$\varepsilon_\perp'' = \frac{2\gamma_\perp}{\omega_\perp} = \frac{4}{\sqrt{\pi}}\frac{r_D}{a} = \sqrt{\frac{4T}{\pi eU}} \tag{3.21}$$

As usual, here U is the potential difference between the centre and boundary of an uncompensated electron beam. The result obtained is significantly different from the known result in the case of infinite plasma where the damping decrement depends exponentially on temperature. The reason is the wider spectrum of particle motion. The spectrum covers frequencies ranging from v_{T_i}/a (the frequency of ion movement inside the beam) to ω_{pi} (reflection from a boundary takes the low time of about ω_{pi}^{-1}). It leads to a power (non-exponential) dependence on temperature.

To sum up: the main mechanism for dissipating transverse oscillations is Landau damping; a fairly high ion temperature is necessary for system stability, which breaks down compensation at the boundaries of a beam (thickness of the layer is about r_D); in a strong external magnetic field or at low currents when $\Omega_i > \omega_{pi}$ Landau damping disappears and this, if the beam is long, leads to instability (i.e. there can be a lower instability threshold in terms of current).

3.6 Experimental investigation of induced transverse oscillations

An experimental investigation of transverse oscillations was carried out by exciting the electron beam in the transverse direction before entry to the compensated region. This was done by applying paraphase alternating voltage to different parts of pick-up electrodes (see Fig. 2, 6 or 7), causing electrons in crossed electric and magnetic fields to drift and the beam to be displaced downstream from the electrodes. The output signal was measured by differential pick-up electrodes. The general pattern of measurements is the same as during the investigation of induced longitudinal oscillations. Sometimes we used a computer controlled SK4-59 spectrum analyser instead of synchronous detectors.

Measurements showed that the amplitude of perturbation rises quickly along the beam. The value of the signal $\xi(z,t)$, corresponding to (3.6), depends not only on its

amplification in the electron beam but also on the resonance multiplier $1/\varepsilon_\perp(\omega)$ bound up with excitation of ions. Measurements from pick-up electrodes placed at different points along the beam can help in defining the imaginary part of dielectric permeability at resonance frequency (quality of ion oscillation).

The spectrum of induced transverse oscillations in a well compensated state is shown in Fig. 15, by way of example. The smoothed curve corresponds to formulas (3.6), (3.9) with parameters $\varepsilon''_\perp = 0.179$, $\langle M_i/Z_i \rangle = 4.3$.

4. THERMAL NOISE

One of the best ways of studying compensating ion states is through the analysis of noise signals, induced on pick-up electrode. Measurements of noise make it possible to determine the temperature of compensating ions, a key characteristic. In this section, transverse and longitudinal thermal oscillations are described.

4.1 The spectral strength of noise from longitudinal oscillations in the beam and determination of ion temperatures

Let us consider an ion beam in thermodynamic equilibrium, with temperature T_i. All possible longitudinal thermal oscillations can be presented as a sum of harmonics:

$$\delta\rho = \rho_n \cos(\pi n x/L) \tag{4.1}$$

where L is the length of the ion beam, n the number of the harmonic, $\delta\rho$ the deviation of ion density from mean value (per unit of length) and ρ_n the amplitude deviation in density of the n-th harmonic. Due to cos-like dependence, the boundary conditions (ion velocity and thus $d\rho/dx$) should be zero at the beam boundaries, will be satisfied automatically. Let us investigate the probability of the n-th harmonic having amplitude ρ_n. Obviously, the probability is equal to:

$$P_n(\rho_n) = \prod_{m=0}^{L/dx} \mathcal{P}(\delta\rho(x_m)) = \mathcal{P}(\delta\rho(x_1)) * \mathcal{P}(\delta\rho(x_2)) \ldots \mathcal{P}(\delta\rho(L)) \,, \tag{4.2}$$

where $\mathcal{P}(\delta\rho(x_m))$ is the probability of finding in the range $x_m - x_{m+1}$ a deviation in the number of ions $\delta\rho(x) * dx$, $x_m = m * dx$, and step dx is relatively large, so the condition $\delta\rho(x) * dx \gg 1$ is satisfied. The function $\mathcal{P}(\delta\rho(x))$ is determined by a Gaussian distribution multiplied by a Boltzmann distribution. The latter takes into account interaction between particles $\exp(-\phi/T)$:

$$\mathcal{P}(\delta\rho(x_m)) = \exp\left(-\frac{\delta\rho^2(x_m)}{\rho_0}dx - \frac{e^2\delta\rho^2(x_m)dx(\ln b/a + 1/2)}{T}\right) \,,$$

where $\rho(x) = \rho_0 + \delta\rho$, $\rho_0 = N/L$, $\delta\rho/\rho_0 \ll 1$. In this case, the probability P_n will be

$$P_n(\rho_n) = \exp\left\{-\int_0^L \left(\frac{\delta\rho^2}{\rho_0} + \frac{e^2\delta\rho^2(\ln b/a + 1/2)}{T}\right) dx\right\}$$

or, for $\delta\rho$ from (4.1):

$$P_n(\rho_n) = \exp\left\{-\frac{\rho_n^2 L}{2\rho_0}\left(1 + \frac{e^2\rho_0}{T}\left(\ln\frac{b}{a} + \frac{1}{2}\right)\right)\right\} . \tag{4.3}$$

The noise strength in this case will be determined by dispersion of the magnitude ρ_n:

$$\langle\delta\rho_n^2\rangle = \frac{\rho_0}{L(1 + e^2\rho_0(\ln b/a + 1/2)/T)} = \begin{cases} \frac{T}{e^2L(\ln b/a+1/2)} , & T \ll T_{cr} , \\ \frac{N}{L^2} , & T \gg T_{cr} . \end{cases} \tag{4.4}$$

where the value of:

$$T_{cr} = \pi n e^2 a^2\left(\ln\frac{b}{a} + \frac{1}{2}\right) = U\left(\ln\frac{b}{a} + \frac{1}{2}\right)$$

determines the characteristic energy of particle interaction. The asymptotics written in (4.4) correspond to two well-known cases. The first of these is Schottky noise, which is proportional to the number of ions ($T \gg T_{cr}$). The second is thermal noise ($T \ll T_{cr}$), which is independent of the number of particles and is proportional to temperature. In the case of a well-compensated beam the condition $T \ll T_{cr}$ is always satisfied, indicating in this case thermal noise.

The frequency spectrum of thermal noise will consist of peaks at the frequencies $\omega = uk = un\pi/L$ (where u is the phase speed of longitudinal waves in an ion beam) with a peak width of $\Delta\omega \approx \delta \equiv \nu_{ii} + \omega\gamma_{||}$ [see (2.19)]. From longitudinal oscillation spectrum measurements, we know that for a well-compensated beam the value of δ/ω is of the order 10^{-2}, so that the peaks in the spectrum of thermal noises must be narrow.

Measured spectra of thermal noise were used for calculating the temperature of compensating ions. One can see from (4.4) that fluctuation strength is inversely proportional to ion beam length. So the measurements were done on a short (40 cm) segment of the ion beam [between electrodes 13 and 18 (see Fig. 2)].

Fluctuations in ion charge density were measured by the pick-up electrode with an integrating amplifier. The signal from the amplifier was digitized by the ADC-101 in 2048 (5 μsec intervals of time) and stored in the computer memory. After that the data obtained were subjected to the Vinograd algorithm of Fourier transformations (VAFT) [10], [11] which speeded up the calculations significantly. On the 'Odryonok' computer [19] the rate of VAFT processing was 2.6 times faster then the usual FFT, at 5 sec per measurement cycle (2048 points).* As we were studying the low temperature states of an ion beam and the strength of amplifier noise was comparable with the signal strength studied, the various spectrum measurements were summated. The total number of cycles was from 20–100, which helped reduce statistical error by 5–10 times.

As harmonics of density perturbation are determined by the formula (4.1), in order to obtain the spectrum of noises we had to take into account the fact that the signal from a pick-up of coordinate z_p and length L_p is proportional to:

---

* The Vinograd algorithm of Fourier transformation is useful for computers with a multiply/divide operation time much greater than that of add/subtract operations. If compared with the usual Fast Fourier Transformation the Vinograd Algorithm on such computers gives calculation rates that are 5–6 times faster.

$$f_p = \frac{1}{L_p}\int_{z_p-\frac{L_p}{2}}^{z_p+\frac{L_p}{2}} \cos(k_n x)dx = \cos(k_n z_p)\left[\frac{\sin(k_n L_p/2)}{(k_n L_p/2}\right] . \qquad (4.5)$$

This formula shows that if the pick-up is placed in the centre of the compensated beam region, any odd harmonic of charge density deviation is 'not visible'.

A typical noise spectrum for a beam section 40 cm long is shown in Fig. 16. The second and fourth harmonics are seen very clearly, but the first and third are, in line with (4.5) where $z_p = 21$ cm, suppressed by a factor of approximately 100. The quality of oscillations is clearly high and from the noise spectrum the phase velocity of longitudinal waves can be obtained: for $I_e = 4.8$ mA (Fig. 16) the velocity is $u = 1.6 \times 10^6$ cm/sec.

After integrating the noise spectrum around each harmonic, using (4.4) one can obtain the temperature of the ions. For the spectrum shown in Fig. 16 the ion temperature calculated from the second harmonic is $T_2 = 0.82$ eV and from the fourth harmonic it is $T_4 = 1.14$ eV.

4.2 Thermal noises of transverse oscillations

The amplitude of thermal noise from transverse oscillations is also a key characteristic of beam state. Thermal noise generates fluctuating electric fields which, when amplified, pass down the beam. The mean square of the amplitude of ion oscillations is important from at least two points of view. Firstly, the value can be measured experimentally and used for determining ion beam characteristics. And secondly, such values determine the power of ion heating due to dissipation of natural noise (see below).

Let us estimate the spectral strength of thermal noise in transverse ion oscillations at the end-point of the beam. To do so let us initially ignore its interaction with the electron beam, and cut the beam of length L into segments of length $\ell, a \ll \ell \ll k^{-1}$. By equating the energy stored in the dipole mode of oscillations (taking also into account the energy of the electric field outside the beam) with the ion temperature T_i, we can obtain a mean quadratic deviation of the ion position (on one segment of length ℓ) from the centre of the electron beam:

$$\langle \Delta r^2 \rangle = 2\langle \Delta x^2 \rangle = 2\langle \Delta y^2 \rangle = \frac{T}{\pi^2 n^2 a^2 \ell e^2} = \frac{4r_D^2 L}{N_i \ell} \qquad (4.6)$$

where N_i is the total number of ions in the beam. The strength spectrum of these oscillations is concentrated near the eigen frequency of the ion oscillations (3.10).

Now let us take into consideration their interaction with the electron beam. After passing through one such segment, the electrons will have a displacement of $\Delta\xi_e = i\Omega_d \ell \Delta r / v_0$. At the beam end-point, this displacement will be increased $K(L_i)$ times, producing an ion displacement that is a factor $1/|\varepsilon_\perp|$ larger. As the natural thermal oscillations of different segments are statistically independent, the amplitudes produced by them should be summated quadratically. After performing this operation on the various segments, we obtain:

$$\langle \xi_i^2 \rangle = \sum_j \langle \Delta x^2 \rangle \left(\frac{\Omega_d \ell}{v_0} \right)^2 \frac{1}{|\varepsilon_\perp''|} \exp \left[\frac{2\Omega_d (L - \ell j)}{v_0 |\varepsilon_\perp''|} \right] =$$

$$= \frac{T}{4\pi^2 n^2 a^2 e^2} \frac{\Omega_d}{v_0 |\varepsilon_\perp''|} \exp \left[\frac{2\Omega_d L}{v_0 |\varepsilon_\perp''|} \right] . \qquad (4.7)$$

Then, after summating 'natural thermal' and amplified ion oscillations we have at $\omega_p \gg \Omega_d$ the function of amplitude of transverse ion oscillations on coordinate z along the beam:

$$\langle \xi_i^2 \rangle \approx \frac{2 r_D^2 L}{N_i \ell} + \frac{\sqrt{\pi}}{2} \frac{ec}{v_0 B} \frac{r_D}{a} K^2 , \qquad K = \exp \left[\frac{\Omega_d z}{v_0 |\varepsilon_\perp''|} \right] . \qquad (4.8)$$

Here we have taken into account the fact that the main contribution to dielectric permeability is given by Landau damping as in (3.21). The first term in the formula is inversely proportional to the length of the pick-up electrode segment. This reflects the fact that the oscillations of separate segments (of length ℓ) of the ion beam are statistically independent, and after summing are averaged out. The result is to make the square of the displacement amplitude inversely proportional to the number of separate segments of ions inside the pick-up electrode (the noise amplitude will be independent of the pick-up length). The second term in the formula in case of low enough amplification ($\ln(K_{\max}) < L/(2\ell)$) is independent of pick-up (or segment) length. This is due to the fact that the motion of ions becomes coherent. The ion beam as a whole begins to rotate around the electron beam and the amplitude of the oscillations grows exponentially with length. But if the amplification $\ln(K) > L/(2\ell)$ is great enough, the second term of the spectral strength will also become inversely proportional to the length of the pick-up electrode which is connected with the fact that the length at which oscillations are amplified e times ($e = 2.718..$) is shorter than the pick-up length, i.e. its effective length will be a factor $2\ell/L * \ln(K)$ shorter.

We should note that usually the amplification coefficient is high enough, so the contribution of nonamplified thermal oscillations of ions to spectral strength is relatively small. In this case the additional resonance factor in the amplification coefficient begins to work, so that the spectrum decreases in width and becomes much narrower than that of the nonamplified oscillation spectrum ($\Delta\omega/\omega \sim \gamma_\perp/\omega_\perp$).

Numerical simulations were found to be in good agreement with the estimates given here.

Measurements of the transverse noise spectrum were performed on one of the pick-ups (see Fig. 2) and the SK4-59 spectrum analyser. Each plate of the pick-up was connected to its integrating amplifier. The difference in signal between amplifiers was proportional to the dipole moment of the beam in the pick-up, as measured by the spectrum analyser. Measurement of the natural thermal noise spectrum gave us information on the damping decrement, according to (4.7). Moreover, the same noise spectrum enabled us to check for absence of instability, because where there was instability the amplitude of the noise spectrum increased by a factor 10–100 and, instead of a single peak at the resonance frequency, several peaks would appear at lower frequencies.

Figure 17 shows the spectrum of natural thermal transverse ion oscillations in a well-compensated state and a partially compensated beam above the instability threshold. For the stable-state spectrum the fit is drawn by dotted lines according to (4.8) with $\varepsilon''_\perp = 0.3$.

4.3 Influence of the coherent heating of ions

The thermal motion of ions produces a fluctuating electric field which travels down the beam and is amplified as it goes. Dissipation of this amplified noise leads to additional heating of ions. This system will not yet be in thermodynamic equilibrium so that, to obtain a stable compensation state, ions have to be generated in the electron beam and leave it. Moreover, the temperature rise due to heating by coherent oscillations during the ion lifetime should not exceed the mean temperature of the ions. In line with (A2.10) the dissipation of energy per unit of volume and of time is:

$$Q = \frac{1}{\pi}\sqrt{\frac{2}{\pi}}\,\frac{v_{T_i}}{a}E_0^2 \tag{4.9}$$

Ions are heated only by the coherent part of their transverse thermal oscillations. The electric field can be obtained from (4.7):

$$\langle E_0^2\rangle = 4\pi^2 n_e^2 e^2 \langle \xi_i^2\rangle = \frac{T}{a^2}\,\frac{\Omega_d}{v_0|\varepsilon''_\perp|}K^2 \tag{4.10}$$

and after averaging by the beam length the increase in ion temperature after time interval τ can be obtained from (4.9):

$$\Delta T \sim T\frac{\varepsilon''_\perp \omega_\perp \tau}{4N_i}K^2\ , \tag{4.11}$$

where N_i is the total number of compensating ions in the electron beam, and τ is the compensation time equal to the ion lifetime in the beam. The meaning of the value $\Delta T/T$ is that it cannot be greater than unity, allowing us to write a further limitation to the amplification coefficient:

$$K \le \sqrt{\frac{N_i}{\omega_\perp \tau}}\ , \quad \varepsilon_\perp \le 1\ .$$

For the 'solenoid model' at $\ell = 2.5$ m, $I = 1$ mA, $\tau = 100$ msec we will get $N_i \approx 10^9$, $K < 50$. From this estimate, it can be seen that for a high vacuum in the model (and hence a long ion lifetime in the electron beam), such coherent ion heating can place a limit on obtaining a highly compensated state.

5. METHODS FOR MEASURING THE DEGREE OF COMPENSATION AND CHARGE STATE OF IONS

In Section 2.7 above, measurements of ion charge per unit of length by the fast ion decompensation technique were described. But the integral charge compensation measured in this way is not connected directly with the local space charge compensation because the ion beam radius may not always be equal to the electron beam radius. So in our experiments we also used other techniques, allowing us to measure compensation

by potential (by comparing potential difference between the vacuum chamber wall and the beam centre for compensated and decompensated beams) and for the local charge compensation. We were also able to measure the charge state of ions (Z/M parameter) in the beam.

5.1 The kick-drift technique for measuring space charge compensation

The kick-drift technique is based on the following idea. If the electron beam as a whole can be rapidly displaced from the ion beam centre then the electrons begin to drift in the crossed magnetic and electric fields around the initially motionless ion beam. If we can measure the rotation angle of electrons during such drift we can obtain the electric field of ions and hence the value of compensation. After measurements with different initial displacements r of the electron beam from the ion beam we will obtain the dependence of ion density on radius. Thus, if τ is the time of flight of electrons from the point of displacement to the point where the rotation angle Ψ is recorded, then

$$\Psi(r) = \tau c \frac{E(r)}{rB} , \tag{5.1}$$

but, according to the Maxwell equation:

$$\frac{1}{r} \frac{\partial}{\partial r} (rE(r)) = -4\pi\rho_i(r) , \tag{5.2}$$

where $E(r)$ and $\rho_i(r)$ are the electric field and ion charge density as a function radius. So if we know the $\Psi(r)$ function then we can obtain the ion charge density distribution from the radius:

$$\rho_i(r) = -\frac{B}{4\pi c\tau} \frac{1}{r} \frac{\partial}{\partial r}(r^2\Psi(r)) . \tag{5.3}$$

It should be noted that in the formulas obtained it was assumed that the electron beam would drift round the ion beam as whole—i.e. as a single charge at distance r from the system's axis of symmetry. It is obvious, however, that electrons far from the ions will drift with lower angular velocity than those nearer by. But the effect is small because the value E_r/r (proportional to angular velocity) in regions where r is low ($r < a$) is constant and in regions where the displacement is great ($r > a$) the gradient of the value is proportional to $1/r^3$, and the angles of rotation in this case are also small. These various considerations allow us to use the approximation referred to. In experiments to displace the electron beam we used two pulses from the paraphase pulse generator with the same shape but opposite sign supplying different plates of pick-up electrode 8 (see Fig. 2). The amplitude of pulses V_0 could be varied from 0 to 2000 V, the pulse front's length was almost independent of amplitude and was approximately 40 nsec. We used two pulses of different sign to prevent longitudinal wave excitation in the electron beam and to prevent electron current from locking at high amplitudes V_0.

Electron drift in the electric field of the pick-up electrode results in their horizontal displacement. With further movement in the drift region the electrons will rotate around the initially motionless ions so that at the exit from the system they will have been displaced both horizontally and vertically.

The double displacement was measured on an ADC and two pick-up electrodes. The X- (15) and Y-pick-ups (16) (see Fig. 2) were allocated to the measurement of transverse displacements (i.e the difference in signals induced on opposite plates of each of the pick-ups). The pick-up signals were digitized by the ADC at a time interval of 50 nsec. To reduce statistical errors, the measurements were usually taken 5–10 times.

The result of set of each 5–10 measurements was to show X or Y displacements as a function of time (see upper part of Fig. 18), from which a phase-amplitude picture of oscillations was plotted:

$$\begin{aligned} r * \cos(\Psi) &= X(t) \\ r * \sin(\Psi) &= Y(t) \, . \end{aligned} \tag{5.4}$$

The ions can be considered as motionless only up to a time that is roughly equal to the period of an ion plasma oscillation. This is no less than 100 nsec for electron currents of up to 10 mA, with compensation of about 0.5 and a mean ion mass of 5 u. All these ensure that electrons deflected by the pulse with a front time $\sim$ 40 nsec drifted for at least 100 nsec around ions that were motionless. For this reason the angle Ψ was determined only by the few first points of the $X(t)$ and $Y(t)$ functions. The multiple-turn spiral in the lower part of Fig. 18 corresponds to the transverse oscillations generated in the ion beam as it particpates in the complex movement around the electron beam.

If ion density at the beam centre is considered as being not dependent on radius then (at low r) the following can be obtained:

$$n_i(0) = \frac{\Psi B}{r \pi e c \tau} \, . \tag{5.5}$$

For example, to make the measurement pictured in Fig. 18, the kick amplitude was set at V_0 = 200 V (r= 0.5 mm) so that, from (5.5) and using the measured angle of rotation $\Psi = -1.81$ the compensation value at the beam centre $k = n_i/n_e = 0.29$ could be obtained.

By increasing the kick amplitude, the electron beam can even be displaced outside the ion beam. And the ion density distribution on the radius can then be obtained using (5.2), from measurements of the angle of rotation as against different displacements. The functions of $\Psi(r)$ and $n(r)$ on radius for I_e = 3.3 mA, L = 250 cm, B = 3 kG are shown in Fig. 19. It can be seen that despite the strong magnetic field, the diameter of the ion beam in a non-compensated state is approximately 1.5 times larger than the electron beam diameter.

5.2 Measurement of the mass composition of compensating ions

The mass spectrum of compensating ions is an important characteristic. A special analyser was developed to measure it, based on the principle of a plate electrode 1 (see Fig. 20) being fed by a rectangular voltage pulse at an amplitude of V_0 = 4–12 kV and with τ = 20 ns. All ions will give a transverse momentum advance of $p = \tau Z_i e V_0/d$, where d is the distance between the electrode 1 and a grid. As the momentum is more than 100 times greater than the r.m.s. transverse momentum of thermal movement, ions

will move in an external longitudinal magnetic field B on trajectories, the same radius $R = pc/(Z_i\ eB)$ for all kinds of ion. But the time taken to reach analyser plate 2 (270 degrees) will be different for different ions: $t_i = (3\pi M_i c)/(2Z_i\ eB)$, where B = 3 kG, $t_i = 157 * M_i/Z_i$ (nsec). Studying the current impulse on plate electrode 2 after integrating amplification means that the kind of ion M_i/Z_i can be defined from t_i and the number of such ions determined from the current amplitude.

Ions with a different ratio M_i/Z_i were usually identified from the following table:

M_i/Z_i	1	2	4	6	7	8	10	12	14	16	20
ion	H^+	He^{++}	He^+	C^{++}	N^{++}	O^{++}	Ne^{++}	C^+	N^+	O^+	Ne^+

Electrostatic repulsion (all ions are positively charged) leads to an increase in transverse ion beam size over the initial values of 2–8 times for M_i = 1–20 a.m.u., limiting the accuracy of arrival time t_i to about 10–15% for different types of ion. Longitudinal thermal movements also influence analysis through the finite length of the analyser aperture along the magnetic field (L_a = 10 cm):

$$\frac{\Delta N}{N} \simeq \frac{v_{T_i} t_i}{L_a} = 2\%\sqrt{M_i(\text{a.m.u.})}$$

such that for $M_i = 20$ it gives $\Delta N/N \simeq 10\%$. In a real experiment the thermal movement was one of the main limits to the current efficiency of the analyser, the total number of ions arriving at electrode 2 being $\simeq$ 60% of those discharged by the beam.

Two common views of output current signals from the analyser in showing both good and poor compensation (i.e with instability) are given in Fig. 21.

5.3 Electron cooling method of measuring beam compensation

One method of evaluating compensation is based on measurement of the friction force acting on H^- ions in an electron beam with electron cooling. The friction force depends to a considerable extent on the difference in velocities between H^- ions and electrons. The force is at its greatest when these differences are about equal to the velocity spread in the electron beam, and nullifield if electron and ion velocities are identical. Therefore, when the velocity of H^- ions is known, then measurements of the electron gun cathode* potential for zero friction force can be used to find the difference in potential between the vacuum chamber wall and the centre of the electron beam, and hence compensation by the potential.

The friction force in electron cooling was measured by spectrometer from deviations in H^- ion energy after the ions pass an electron beam [7]. Figure 22 shows the potential φ_n of an electron beam as a function of current for different degrees of compensation (k_φ = 0.0, 0.75, 1.0) for L = 250 cm, B = 3 kG. It can be seen that for a well-compensated

* Note that the cathode's oxide layer resistance, 25–50 ohm, gives a negligible error in compensation measurements ($\simeq$ 5%).

beam φ_n it is not a function of electron current but for zero compensation φ_n it is equal to the potential well of a naked electron beam.

This is a precise method, with an accuracy of the beam potential definition that is no lower than 0.1 V. Good or poor potential compensation indicates only the presence of good or poor charge compensation, but to provide a value of charge compensation from potential measurements is very hard.

We should note that another source of difficulty in defining a beam's potential from measuring the longitudinal friction force is the problem of defining zero. When the gun is in a space charge limitation mode while there is a change of beam current, the energy of electrons is changed by $T_c \ln(I_c/I_e)$ (where T_c is the temperature of the cathode, I_c the current of cathode saturation, and I_e electron current). This value can produce an error of a few tenths of one eV or a few per cent in beam potential definition.

The foregoing technique uses measurement of the longitudinal friction force. Another technique makes it possible to find charge (local) compensation while measuring the decrement in transverse oscillation. To do so, a transverse velocity of cooled ions at the entry to the solenoid was excited by applying alternating voltage to the excitation electrodes. The ions leaving the solenoid were sent to a two-coordinate position-sensitive probe about 5 m from the solenoid. Synchronous detection of the probe signals determined the amplitude of the entire ion beam oscillation horizontally and vertically. Figure 23 shows the dependence of such amplitudes on the energy of the electron beam. When the velocities of electrons and ions are the same, a peculiarity arises in signals that is connected with the damping of transverse oscillations. The relative value of the probe's signals is governed by the decrement of transverse oscillations, the magnetic field and, to a considerable extent, the non-compensating electron beam space charge. Numerical processing of the signals means that not only the decrement but also the degree of compensation can be found. For the example in Fig. 23 (I_e = 1.54 mA, B = 3 kG, L = 250 cm) estimates place the degree of compensation at 65%.

6. EXPERIMENTAL STUDY OF THE STATE OF COMPENSATING IONS AND A DETERMINATION OF THRESHOLD CURRENTS

In this chapter the main results of experimental studies of a compensated electron beam will be described. Various parameters of the system have been measured using different techniques, which has increased the reliability of the results obtained. The main experimental findings fit well enough with those from the theoretical studies described above.

6.1 Location of the well-compensated state

The well-compensated state, as described in Section 3 above, i.e where the charge compensation degree is very close to unity, is confined to a region of change in the beam current and residual gas density. Outside these regions there is an area where the electron beam is partly compensated, and we should note that it is sometimes enough to increase electron currents several times over. For example, in experiments to measure electron cooling friction force at the 'Solenoid Model' [7] most measurements were made with a partly compensated electron beam 250 cm long with a degree of compensation of about

40–70%. This made it possible to run experiments with currents of up to 10 mA, whereas uncompensated beams were successful only up to 3 mA.

The region where compensation is higher than 90% for a 40 cm long electron beam segment in the planes for current and residual gas pressure is shown in Fig. 24. Figure 25 shows changes in the degree of compensation during transition from high to low compensation for various residual gas pressures. Figure 24 shows the existence of lower threshold currents at certain vacuum pressures. Generally speaking, threshold currents were determined in the following manner: at first, the electron current was reduced to zero (locked by the anode), and then the current was increased smoothly for 5–10 seconds. At certain current values the instability started up, and this was monitored by pick-up signals on the oscilloscope and spectrum analyser, and the compensation broke down, which could be checked by direct measurement. The value of this current was taken as the upper threshold. At certain vacuum pressures for weak currents significant noise appeared in the natural oscillation spectra of the beam, leading to the appearance of instability, unless the region was quickly passed through, i.e by raising the current to about 1 mA, so as to reach a stable region. Thereafter, by decreasing the current slowly and recording the onset of instability current threshold could be determined.

For a segment of the electron beam of $L = 250$ cm, the high compensation region of the vacuum was approximately the same as for $L = 40$ cm, but the maximum threshold current was about 1 mA. It was experimentally verified that the upper threshold current was inversely proportional to the compensated length $J_{th} \simeq 1/L$. Figure 26 shows the upper threshold current as a function of electron energy at two values of magnetic field, and shows straight dotted lines constructed from formula (1). Values for threshold currents almost coincide with those predicted by Nezlin's formula (1) in [8] (they are 1.13 times greater), but are about half the size of those derived from (3.13) in Section 3. The possible reasons are discussed below. Thus, experimental data on threshold currents obtained can be represented in the empirical formula as:

$$j_{th} = \frac{Bv_0^2}{3.8Lc} \tag{6.1}$$

where j_{th} is the critical current value for the optimum residual gas pressure.

The lower current threshold is estimated by the condition showing the existence of Landau damping:

$$j_d = \frac{B^2 e v_0}{4\pi \overline{M} c^2} \tag{6.2}$$

For parameters $B = 3$ kG, $\overline{M} = 14$, $v_0 = 1.2 \times 10^9$ cm/s., $a = 1$ mm this formula yields $j_d = 1.2$ mA, which is almost in agreement with experimentally observed data at $L = 40$ cm, but is in conflict with results from the greater compensation length of $L = 250$ cm.

6.2 Behaviour of mass spectra

There are three sources of information about mass spectra of compensating ions. In the first place, the value $\langle Z_i^2/M_i \rangle$ can be calculated from the phase velocity of the longitudinal wave (see (2.16)). The mass spectrum determines the resonance frequency of

forced transverse oscillations in accordance with (3.10). The true mass composition can be measured directly by mass analyser (see Section 5.2 above). Figures 27 and 28 show the average compensating ion mass calculated by the above first two methods mentioned above respectively, as a function of electron beam current assuming that all ions are the same kind and have the charge $Z_i = 1$. One can compare these pictures with Fig. 21 and conclude that on transition to the unstable partially compensated state, the characteristic value of M_i/Z_i^2 significantly increases. This was also proved by mass analyser measurements presented in Fig. 21. Such behaviour on the part of the value of $\langle M_i/Z_i^2 \rangle$ can be explained in the following way: at a state with low compensation the transverse size of the ion column is 1.5–2 times greater than the radius of the electron beam (see Fig. 19), and then the probability of the second ionization is smaller and an average charge $\langle Z_i \rangle$ is smaller than in the well-compensated state and the value $\langle M_i/Z_i^2 \rangle$ is greater.

6.3 Measurement of transverse oscillation damping decrements and the temperature of compensated ions

One of the important parameters of the beam-plasma system is the imaginary part of the dielectric constant $\varepsilon_\perp''$ which determines the damping transverse oscillations and is directly connected with the temperature of compensating ions. The value of $\varepsilon_\perp''$ can be found from different characteristics: from the amplification coefficient, the quality of induced transverse oscillations, and the amplitude of natural thermal transverse oscillations in the ion beam. The values $K_{max}/\varepsilon_\perp''$, the Q-factor of the induced transverse oscillations and amplitude of transverse thermal noise as a function of current and residual gas pressure are shown in Figs. 29–31. The value of $\varepsilon_\perp''$ was calculated from this data using formulae (3.8)–(3.11), (4.1) (see Fig. 32). From this figure it can be seen that in the case of good compensation, $\varepsilon_\perp'' = 0.1$–$0.3$ and slightly varies according to the method of definition.

The temperature of ions calculated from thermal longitudinal noise measurements (as described in Section 4.2 above) is shown in Fig. 33. It can clearly be seen that the temperature calculated from the second harmonic is threshold in nature, with a value of $I_e = 7.7$ mA. Above this value instability appeared and compensation was broken down. The temperature, calculated from the fourth harmonic of longitudinal thermal waves in the ion column, may also be threshold in nature but with a somewhat higher threshold in the electron beam current. We should note that thermodynamic equilibrium really exists at low currents only when temperatures defined from different harmonics have the same values. At higher currents the increase in noise levels, which is not directly connected with the temperature, is a sign of epithermal longitudinal ion oscillations. The threshold dependence of longitudinal oscillations indicates a connection between the low-frequency part of longitudinal ion oscillations and the mechanism that excites the transverse instability.

One of the most precise ways of finding the temperature of ions is to fit the spectra of forced longitudinal oscillations with low amplitudes to formulas of friction and Landau damping (see Sections 2.3 and 2.4 above). But such results also heavily depend on the presence of light ions, such as hydrogen, in the mass spectrum. In Fig. 3.4 decrements of damping are shown and in Fig. 35 temperatures of ions, calculated on the assumption that their mass composition is similar to that given in Fig. 21 for the well-compensated

state, with the lightest element (He) being present at about 5%. The temperatures of ions defined by different techniques are in close agreement with one another.

The clear connection between natural longitudinal oscillations in the ion column and instability excitation is once more demonstrated in Fig. 36, where amplitudes of transverse and longitudinal oscillations are shown as functions of current. As the threshold is approached there is a clear increase in the amplitude of longitudinal oscillations while that of the transverse variety even falls. This behaviour points to the fact that possible feedback for transverse oscillations may take place through longitudinal waves.

6.4 Features of a partly compensated but unstable state

Instability (i.e. generation of axially-nonsymmetric oscillations) takes place if the electron current rises higher than the threshold level. At different residual gas pressure values the degree of compensation can be 50–70%. The amplitude of transverse oscillation with resonance frequency (3.10) is not constant, but rises significantly during bursts of instability before falling again. This behaviour is close to that predicted by (3.5). One burst may last several hundred cycles of the resonant frequency and the burst repetition frequency is 50–1000 Hz, depending on vacuum pressure and electron current values.

Experiments proved that the degree of compensation falls abruptly with bursts of axially-nonsymmetric oscillations. During the bursts, the amplitude of transverse oscillations is ten or more times greater then between the bursts.

Typical oscillograph pictures of transverse oscillations are presented in Fig. 37. The varying patterns of behaviours of these oscillations before and after instability excitation are clearly seen: in addition to the rise in amplitude, bursts appear with 2–10 ms time interval between them. The sum and differential signals from the pick-up electrodes during one burst are shown in Fig. 38. It can be seen that after the burst the average level of the sum signal falls, showing the decrease in number of ions around the electron beam, due to large transverse oscillations.

In spite of the fact that amplitudes of transverse oscillations ($\lesssim 10^{-2}$ cm) are much smaller than electron beam radius spectra in natural transverse oscillations, the spectra may vary significantly at this instability: the resonant frequency decreases and the width of the resonant peak rises up to $\Delta f/f = 0.1$–0.2. The change in resonant frequency can be explained by a fall in the average charge of ions in the column and width of the resonant peak by an absence of electrical neutrality that leads to the appearance of sets of wide intersecting resonant peaks connected with all the different types of ion.

6.5 Measurements of feedback through secondary electrons

As shown in Section 3 above, a significant amount of feedback can limit maximum electron currents in the compensated state. One possible cause of such feedback are secondary electrons repelled from the collector and ionization electrons.

The value of the feedback created by electrons repelled from the collector was measured through the excitation of the wave in secondary electrons. These waves ran counter to the direction of electron beam velocity and were detected at the beginning of the beam on a pick-up electrode by synchronous detection with an excitation signal. These experiments showed a low value for such feedback (below 10^{-4}) if there were the

conditions for restricting repulsion from the collector (+ 600 V at the latter). The feedback coefficient can reach several per cent if the potential of the collector stands at zero or is negative. Thus, significant feedback causes destruction of a stable compensated state if the collector potential is positive.

The influence of ionization electrons was also investigated. These electrons were stored specially by ring electrodes with potential about $-100 \div -400$ V situated close to the collector. They did not interfere with movement of beam electrons but stopped low-energy ionization electrons (the second mirror was the electron gun cathode). The concentration of such electrons was artificially increased at least ten times up to 1–6% but no changes in thresholds or the degree of compensation were observed. This indicates a low coefficient for such feedback.

7. CONCLUSIONS

In an ultra-high vacuum (10^{-8}–10^{-10} torr) device with a strong magnetic field (1–4 kG), an electron beam travelling along the force lines of a magnetic field ionizes atoms of residual gas. The charge of such ions can compensate the electron beam space charge if additional steps for storing them are taken.

Dipole oscillations of the electron beam and the ion column can be excited in the plane perpendicular to the magnetic field in this electron–ion plasma. When such transverse waves are stable the amplitude of the excitation is finite and rises exponentially down the electron beam. If the density of the electron current exceeds the experimentally determined threshold value of:

$$j_{th} = \frac{v_0^2 B}{3.8 L c}$$

(where v_0 is the velocity of electrons, B the magnitude of magnetic field, L the length of the compensated part of the electron beam and c the velocity of light) then the transverse oscillations become unstable and amplitude rises by several orders of magnitude. It leads to a significant increase in the temperature of compensated ions and a fall in their numbers, with the result that the degree of compensation falls to 40–70%.

This instability takes place because of the feedback when the oscillations at the end of the compensated beam act on the beginning. The mechanisms of the feedback may differ: through the link between longitudinal waves in ions and transverse electron–ion oscillations, through electrons repelled from the collector, through ionization electrons, etc. Our experiments confirm the primacy of the first two reasons.

We also discovered the existence of instability in low current thresholds (several times smaller then j_{th}) where the degree of compensation falls to 50%.

Experimental studies of the system in stable state show that the degree of charge compensation differs less than 10% from unity; the temperature of compensating ions is significantly less than the potential difference between the axis and the edge of an uncompensated electron beam; the ion mass spectra are characterized by average values of M_i/Z_i of about 5–7 and a low proportion of ions with high ratio M_i/Z_i in comparison with the unstable situation.

A wide variety of diagnostic techniques, including some that were original, were used during the experimental study of the compensated electron beam. The principal

results are in good agreement with each other, which increases the reliability of the results obtained.

Acknowledgements

The authors thank J. Bosser and S. Maury (CERN/PS), the CERN Translation Service and Desktop Publishing Service for their help in correcting the English version of this paper.

REFERENCES

[1] Bursian V.R., Pavlov V.I. J. Russian Phys.-Chem. Soc., 1923, v. 55, p. 71.

[2] Budker G.I., Atomic Energy, 1956, v. 1 (5), p. 9.

[3] Nezlin M.V., Solntsev A.M., Limiting threshold currents and electron beam oscillations. Sov. ZhETF, 1967, v. 53, p. 437.

[4] Pierce I.R., Limiting Currents in Electron Beam in the Presence of Ions. J. Appl. Phys., 1944, v. 15, p. 721.

[5] Budker G.I., Skinsky A.N., Electron Cooling and New Perspectives in Elementary Particle Physics. Sov. Uspekhi Fiz. Nauk, 1978, v. 124 (4), p. 561.

[6] Kudelain V.I., Parkhomchuk V.V., Pestrikov D.V., Experimental Studies of Stability of Compensated Electron Beam. Sov. ZhTF, 1983, v. 53 (5), p. 870.

[7] Dikanski N.S. et al., Influence of the Sign of an Ion Charge on Friction Force at Electron Cooling. Proc. of EPAC, Rome, 1988, v. 1, p. 529.

[8] Nezlin M.V., Dynamics of Beams in Plasma. Moscow, Energoatomizdat, 1982.

[9] Burov A.V., Stability of Electron Beam for Electron Cooling. Preprint INP 88-124, Novosibirsk, 1988.

[10] Vinograd S., On Computing the DFT. - Mathematical Computation, 1978, v. 32, p. 175.

[11] Nussbaumer G., Fast Fourier Transform and Convolution Algorithms 2nd ed., Springer-Verlag, Berlin, 1982.

[12] Lifshits E.M., Pitaevski L.P., Physical Kinetics. Moscow, Nauka Pub., 1979.

[13] Bogdankevich L.S., Rukhadze A.A., Sov. Uspekhi Fiz. Nauk, 1971, v. 103 (4) p. 609.

[14] Parkhomchuk V.V., Pestrikov D.V., Thermal Noises in an Intense Beam in a Storage Ring. Sov. ZhTF, 1980, v. 50 (7) p. 1411.

[15] Lebedev V.A., Sharapa A.N., Sov. ZhETF, 1987, v. 57 (5) p. 975.

[16] Arapov L.N. et al., Proc. 13 Int. Conf. on High Energy Accelerators, Novosibirsk, 1987, v.1, p. 341.

[17] Kudelainen V.I., Parkhomchuk V.V., Pestrikov D.V., Permanent State of Ions Compensating Electron Beam. Sov. ZhTF, 1983, v. 53 (4) p. 691.

[18] Corn G., Corn T., Mathematics Handbook. Moscow, Nauka Pub., 1978, p. 238.

[19] Piskunov G.S., Tararishkin S.V., 24-bit Computer in CAMAC. Sov. Autometria, 1986 (4) p. 23.

APPENDIX 1

TRANSVERSE OSCILLATIONS OF ION COLUMN

Let us find the solution to equation system (3.4), which depends on an initial value for ion amplitudes of $\xi_i(z)|_{t=0}$. Let us assume that all ions are of the same kind and that at $t = 0$ for $z > 0$ displacements are constant $\xi_i(z)|_{t=0} = \xi_{i0}, \partial\xi_i/\partial t|_{t=0} = 0$. Then after a Laplace transform of (3.4):

$$i\omega\xi_e + v_0\frac{\partial\xi_e}{\partial z} = -\frac{i\omega_p^2}{2\Omega_i}(\xi_i - \xi_e) ,$$

$$-\omega^2\xi_i - i\omega\xi_{i0} = -\frac{\omega_p^2}{2}(\xi_i - \xi_e) + i\Omega_i(i\omega\xi_i - \xi_{i0}) , \qquad (A1-1)$$

where we did not take damping into account. Hence the equation for ξ_e:

$$\frac{\partial\xi_e}{\partial z} = -\frac{i}{v_o}\left[\omega + \frac{\omega_p^2}{2\Omega_i}\frac{(\Omega_i - \omega)\omega}{\left(\omega^2 - \omega\Omega_i - \frac{\omega_p^2}{2}\right)}\right]\xi_e + \frac{(\Omega_i - \omega)\xi_{i0}}{\left(\omega^2 - \omega\Omega_i - \frac{\omega_p^2}{2}\right)}\frac{\omega_p^2}{2\Omega_i v_0} . \qquad (A1-2)$$

The solution, satisfying the condition $\xi_e(z = 0) = 0$, is:

$$\xi_e = \frac{e^{i\kappa z} - 1}{i\kappa}\frac{(\Omega_i - \omega)}{\left(\omega^2 - \omega\Omega_i - \frac{\omega_p^2}{2}\right)}\frac{\omega_p^2}{2\Omega_i v_0}\xi_{i0} , \qquad (A1-3)$$

where

$$\kappa = -\frac{\omega^2}{v_0}\frac{(\omega - \omega_1)}{(\omega - \omega_2)(\omega - \omega_3)} , \quad \omega_1 = \Omega_i + \frac{\omega_p^2}{2\Omega_i} ,$$

$$\frac{\omega_p^2}{2} = \frac{2\pi n e^2}{M} , \quad \omega_{2,3} = \frac{\Omega_i}{2} \pm \sqrt{\frac{\Omega_i^2}{4} + \frac{\omega_p^2}{2}} .$$

An inverse Laplace transform gives the dependence of the amplitude of electron oscillations on time:

$$\xi_e(t) = \frac{\xi_{i0}\omega_p^2}{2\pi i\Omega_i^2}\int_{-\infty}^{\infty} e^{i\omega t}\frac{(e^{i\kappa z} - 1)(\Omega - \omega)}{\omega^2(\omega - \omega_1)}d\omega . \qquad (A1-4)$$

The greatest contribution to the integral I the right hand of (A1-4) is from special points at which the denomination of the exponential curve becomes zero. In the asymptotic $t \to \infty$ this therefore gives:

$$I \simeq \frac{(\Omega - \omega_2)e^{i\omega_2 t}}{\omega_2^2(\omega_2 - \omega_1)}\int \exp\left(i\omega t + \frac{i\kappa_2 z}{\omega}\right)d\omega +$$
$$+ \frac{(\Omega - \omega_3)e^{i\omega_3 t}}{\omega_3^2(\omega_3 - \omega_1)}\int \exp\left(i\omega t + \frac{i\kappa_3 z}{\omega}\right)d\omega , \qquad (A1-5)$$

where

$$\kappa_{2,3} = -\frac{\omega_{2,3}^2}{v_0}\frac{(\omega_{2,3} - \omega_1)}{(\omega_{2,3} - \omega_{3,2})} .$$

Since using the Laplace transform table [18] we obtain:

$$\int \exp\left(i\omega t + \frac{i\kappa_2 z}{\omega}\right) d\omega =$$

$$= \int \exp\left(ts - \frac{x_2 z}{s}\right) \frac{ds}{s^2} \frac{i\kappa_2 z}{t} \rightarrow \sqrt{\frac{\kappa_2 z}{t}} J_1(2\sqrt{\kappa_2 z t}) \ . \qquad (A1-6)$$

While the asymptotic of the Bessel function is:

$$J_1(x) \simeq \sqrt{\frac{2}{\pi x}} \cos\left(x - \frac{\pi}{4}\right) \ , \quad \text{if } x \rightarrow \infty \ , \qquad (A1-7)$$

then if $t \rightarrow \infty$, the main contribution to the integral will give the component with $J_1(2\sqrt{\kappa_3 z t})$ because $\kappa_3 < 0$:

$$\xi_e(t) = \frac{\xi_{i0}\omega_p^2}{8\pi^{3/2}\Omega_i} \frac{(\Omega_i - \omega_3)e^{i\omega_3 t}}{\omega_3^2(\omega_3 - \omega_1)} \frac{(|\kappa_3|z)^{1/4}}{t^{3/4}} \exp(2\sqrt{|\kappa_3| z t}) \ . \qquad (A1-8)$$

According to the result, after a deflection amplitude of ion-electron oscillations grows infinitely if there is no dissipation. The dissipation can be taken into account in the oscillationg exponent $e^{i\omega_3 t}$. Then (A1.8) will be changed as:

$$\xi_e(t) \propto \exp\left(-\frac{\gamma_\perp t}{2}\left(1 - \frac{\Omega_i}{2\sqrt{\frac{\Omega_i^2}{4} + \frac{\omega_p^2}{2}}}\right) + 2\sqrt{|\kappa_3| z t}\right) \qquad (A1-9)$$

i.e. with the dissipation the amplitude is finite. The maximum amplitude of oscillations takes place after a time of:

$$t_{max} \simeq \frac{4|\kappa_3|z}{\gamma_\perp^2\left(1 - \frac{\Omega}{2\sqrt{\frac{\Omega^2}{4} + \frac{\omega_p^2}{2}}}\right)^2} \ , \qquad (A1-10)$$

and the maximum amplitude at this moment

$$\xi_{max} \sim \exp\left[\frac{z\omega_p^2}{2\gamma_\perp v_0 \Omega_i}\left(\frac{\Omega_i}{2} + \sqrt{\frac{\Omega_i^2}{4} + \frac{\omega_p^2}{2}}\right)\right] \ . \qquad (A1-11)$$

APPENDIX 2

LANDAU DAMPING OF THE TRANSVERSE WAVES

A technique for calculating the Landau damping of transverse oscillations in the compensated electron beam was suggested in [9].

The model investigated below is two-dimensional (2-D), the electron beam is cylindrical with radius a and the density n_0 is constant over the cross-section, the mass of compensated ions is M, their charge is Ze. The ions are weakly magnetized $\omega_p \gg \Omega_i = \mathrm{ZeB}/Mc$ and the resonance frequency of transverse oscillations is equal to [see (3.10)]:

$$\omega_\perp = \frac{\omega_p}{\sqrt{2}} = \sqrt{\frac{2\pi n_0 e^2 Z_Z}{M}} \ . \qquad (A2-1)$$

The electric field of the wave that arises is uniform inside the beam and similar to the field of the dipole outside.

The movement of ions undisturbed by the electric field is in a straight line and at constant velocity from one collision with the beam wall to the next. After every collision the direction of the ion velocity changes by an angle of φ (different for different particles). The size of the region where the velocity of ion changes is about the Debye radius r_D, and while the condition of high compensation needs $r_D \ll a$ (a being the radius of the beam) this interaction can be easily approximated as the interaction with an elastic rigid wall.

In 2-D geometry it is very convenient to use the complex values $v = v_x + iv_y$, $E = E_x + iE_y = E_0 e^{i\omega t + \delta t}$. A small decrement δ is taken as providing the condition $E \to 0$ for $t \to -\infty$. Let the velocity distribution of the ions be Maxwellian in the absence of a wave field:

$$f_0 \sim \exp\left(-\frac{v^2}{2v_T^2}\right) \ . \qquad (A2-2)$$

The kinetic equation determines the disturbance of the distribution function by the electric field of the wave:

$$\frac{d\tilde{f}}{dt} = -\frac{Z_Z e}{M}\left(E, \frac{\partial f_0}{\partial v}\right) \ .$$

from which

$$\tilde{f} = \frac{Z_Z e}{M}\left[\int_{-\infty}^{t} (E(t'),\ v(t'))dt'\right]\frac{\partial f_0}{\partial(v^2/2)} \ . \qquad (A2-3)$$

The transition of the wave energy to ions is (in unit of time):

$$Q = \int d\Gamma \overline{\tilde{f}(Ze\,E, v)} = -\frac{Z_Z^2 e^2}{M}\int d\Gamma \frac{\partial f_0}{\partial(v^2/2)}\mathrm{Re}(Ev^*)\mathrm{Re}\int_{-\infty}^{t} dt'\ Ev^* \ , \qquad (A2-4)$$

here, $d\Gamma$ is the phase space element. While between collisions the direction of ion velocity changes by angle φ after time T, then:

$$v(t+T) = v(t)e^{i\varphi} \ .$$

One can apply a Fourier transform to the periodic function $u(t) = v(t)\exp(-i\varphi t/\tau)$:

$$u_n = \frac{1}{T}\int_{-T/2}^{T/2} \exp\left(2\pi i n\frac{t}{T}\right)|v|\exp\left(-i\varphi\frac{t}{T}\right)$$
$$= |v|\frac{\sin(\pi n-\varphi/2)}{\pi n-\varphi/2} = -|v|(-1)^n\frac{\sin(\varphi/2)}{\pi n-\varphi/2}\ ,$$

then

$$v(t) = \sum_{n=-\infty}^{+\infty} u_n \exp\left(i(\varphi-2\pi n)\frac{t-\tau}{T}\right)\ . \qquad (A2-5)$$

Here τ is the time before the first interaction with the boundary (the initial condition for every particle). Then, taking into account (A2-5), the formula (A2-4) changes by:

$$Q = -\frac{Z^2e^2}{2M}\,E_0^2\int d\Gamma\,\frac{\partial f_0}{\partial(v^2/2)}\times$$
$$\mathrm{Re}\sum_{m,n}\frac{u_m u_n\exp(-i(2\varphi-2\pi n-2\pi m)(t-\tau)/T+2i\omega t)+u_m u_n^*\exp(-2\pi i(n-m)(t-\tau)/T)}{\delta+i(\omega+(2\pi m-\varphi)/T)} \qquad (A2-6)$$

After averaging over the initial conditions (τ changes from 0 to T), we will have

$$Q = -\frac{Z^2e^2}{2M}\,E_0^2\int d\Gamma\,\frac{\partial f_0}{\partial(v^2/2)}\times$$
$$\times\ \mathrm{Re}\left\{\sum_{m,n}\frac{u_m u_n\exp(-i(2\varphi-2\pi n-2\pi m)t/T+2i\omega t)}{\delta+i(\omega+(2\pi m-\varphi)/T)}\,\frac{\sin(\varphi-\pi n-\pi m)}{(\varphi-\pi n-\pi m)}\ +\right.$$
$$\left.+\sum_n\frac{u_n u_n^*}{\delta+i(\omega+(2\pi m-\varphi)/T)}\right\} \qquad (A2-7)$$

It can be seen that the first term of (A2-7) is $1/\omega T$ times less than the second. Within the assumption that there are many oscillations of the wave between two collisions with a board, the condition $\omega T \gg 1$ is valid. For particles that are characterized by the angle φ:

$$T = \frac{2a}{v}\sin\frac{\varphi}{2} = \frac{2a}{v}\cos\psi\ ,\quad \psi = \frac{\pi-\varphi}{2}\ ;\quad -\frac{\pi}{2}\le\psi\le\frac{\pi}{2}\ .$$

Therefore:

$$Q = -\frac{Z_Z^2e^2E_0^2}{2M}\sum_n\int d\Gamma\frac{\partial f_0}{\partial v^2/2}\,\mathrm{Re}\,\frac{|u_n|^2}{\delta+i\left(\omega+\frac{\pi(n-\frac{1}{2})+\psi}{a\cos\psi}v\right)}\ . \qquad (A2-8)$$

It is easy to prove that in the case of equal probability for all ion velocity directions the distribution of the angle will be proportional to $\cos^2\psi$. Therefore:

$$f_0 d\Gamma = \frac{2n_i}{\pi v_{Ti}^2}\exp\left(-\frac{v^2}{2v_{Ti}^2}\right)v\,dv\,dV\,\cos^2\psi d\psi\ .$$

(dV being the volume element).

The condition of compensation connects the electron and ion densities $Zn_i = n_0$. Integration over velocity in (A2–8) can be done following the rule:

$$\frac{1}{z - i0} = P.V.\frac{1}{z} + i\pi\delta(z) .$$

Finally after simple calculations that replace the sum by the integral (which is valid if $a\omega/v_T \gg 1$):

$$Q = \frac{2^{1/2} v_T}{\pi^{3/2} a} E_0^2 V , \quad v_{Ti} = \sqrt{T/M} . \qquad (A2-9)$$

The total wave energy contains the energy of the field inside and outside the beam and the kinetic energy of particles:

$$W = V\frac{E_0^2}{2\pi} . \qquad (A2-10)$$

Hence, the damping decrement of the wave will be:

$$\gamma_\perp = \frac{Q}{2W} = \frac{2^{1/2} v_T}{\pi^{1/2} a} . \qquad (A2-11)$$

Figure captions

Fig. 1 Set-up of 'Solenoid Model'.
1) H^- ion source; 2) electrostatic accelerator; 3) vapour-magnesium target; 4) electron gun; 5) solenoid; 6) electron collector; 7) spectrometer; 8) auxiliary solenoid; 9) ion beam position detector.

Fig. 2 Distribution of electrodes inside solenoid.
1) ion beam; 2) electron gun anode; 3) cathode; 4) electrode alongside cathode; 5) electron beam; 6), 7), 12), 13), 17), 18) split ring confinement electrodes; 8), 15), 16) pickup electrodes; 9), 10), 11) 'oblique' confinement electrodes; 14) ion composition analyser; 19) collector; 20) confinement electrode on collector. Explanations given in text.

Fig. 3 Characteristic shape of longitudinal wave spectrum: B = 3 kG; I_e= 0.9 mA; $P = 7 \times 10^{-8}$ Pa, L = 40 cm.

Fig. 4 Value of non-linear dispersion of longitudinal oscillations Δ_f as a function of the harmonic number N.
Points: experiment, curve calculated according to the formula $\Delta_f = \pi^2(16 \ln R/a)\,(R^2/L^3)\,(uN^3)$; L = 40 cm, $u = 1.15 \times 10^6$ cm/sec.

Fig. 5 Signal from summation pick-up on being excited by longitudinal waves of great amplitude in an ion column with an impulse of: $(\Delta n/n_0)_{max} = +7.2 \times 10^{-2}(a), +16.3 \times 10^{-2}(b), -6.5 \times 10^{-2}(c)$, L = 40 cm, $P = 2.7 \times 10^{-7}$ Pa., I_e = 2.97 mA.

Fig. 6 Dependence on time of ion charge in pick-up (1) and its derivative in time (2) taken following excitation of ion density. Excitation took place at time t = 0. From the derivative it is seen that the length of the excitation at the first pass across the pick-up was $\sim$ 3 cm ($u = 10^6$ cm/sec).

Fig. 7 Dependence of the decrement of damping $\gamma_\perp (k = \gamma_\perp \cdot L/u$ on a compensation region of L = 40 cm, $u = 1.196 \times 10^6$ cm/sec) on excitation amplitude $\delta n/n$.

Fig. 8 Behaviour of ion density and velocity vs z/tu in a decompensation wave where $t < L/u$.

Fig. 9 Decompensation wave. Ion density as a function of time and coordinates.

Fig. 10 Signal from pick-up when extraction method is being used to determine compensation (the entire picture covers 2 ms).

Fig. 11 Results of numerical modelling of decompensation in an electron beam 75 cm long.

Fig. 12 Phase velocity of longitudinal waves in an electron beam as a function of current.

Fig. 13 Amplitude of fast and slow components of longitudinal wave in electrons as a function of current. Continuous lines drawn using expressions (2.32) and (2.35).

Fig. 14 Frequency spectrum of longitudinal waves in an electron beam (from 0 to 20 MHz). $I_e = 2.7$ mA.
Above: cosine part, below: sine part.

Fig. 15 Value of $K/\varepsilon_\perp$ in transverse waves as a function of frequency. $I_e = 4.8$ mA; $P = 1.5 \times 10^{-7}$ Pa, $B = 3$ kG; $L = 20$ cm. Theoretical curve based on formula (3.6) where $\gamma = 86$ kG ($\varepsilon''_\perp \approx 0.179$).

Fig. 16 Spectrum of longitudinal thermal ion noise. $I_e = 4.8$ mA; $u = 1.6 \times 10^6$ cm/sec; $L = 40$ cm; $T_2 = 0.82$ eV; $T_4 = 1.14$ eV.

Fig. 17 Spectrum of natural transverse ion oscillations in a well-compensated state (1) and during instability (2). Values of curve (2) are a factor of 10 smaller. The dotted line is drawn in accordance with formula (4.8) with $I_e = 3.5$ mA; $L = 40$ cm; $\varepsilon'' = 0.3$. The bandwidth of the spectrum analyser was $\Delta\omega/(2\pi)$ =10 kHz.

Fig. 18 Electron beam motion vs time (the axis Z is parallel to the magnetic field). Total time is 2 μsec. Maximum displacement is $0.5a$.

Fig. 19 Compensating ion density as a function of radius (solid line). $B = 3$ kG, $L = 265$ cm, $I_e = 3.33$ mA. The rotating angle (in relative units) as a function of radius is shown by the dotted line.

Fig. 20 Diagram of detector for measuring composition of compensating ions.
1) knock-on plate; 2) measurement plate; 3) electron beam; 4) trajectory of ion movement.

Fig. 21 Mass spectrum of compensating ions (upper part) obtained by differentiation of ion charge on receiver plate (lower part).
$I_e = 2.57$ mA; $L = 40$ cm; $P = 2.4 \times 10^{-7}$ Pa, a - unstable state, b - stable state.

Fig. 22 Potential of beam, as a function of current for states with varying degrees of compensation. Measurement by electron cooling.

Fig. 23 Signal (in relative units) from synchronous detectors X and Y with measurement of transverse friction force using electron cooling.

Fig. 24 Stable region for the compensated state of an electron beam in the current-residual gas pressure plane. $B = 3$ kG, $L = 40$ cm, $\tau_k = 1/n\sigma v_e$ – beam compensation time from residual gas atoms.

Fig. 25 Charge compensation as a function of current over a 40 cm length at different residual gas pressures. Measurements were made by ion extraction (cf. section 2.7).

Fig. 26 Longitudinal and transverse instability threshold currents as a function of electron beam energy. Beam radius $a = 1$ mm; $P = 6 \times 10^{-8}$ Pa: $\cdot$ – $B = 3$ kG; $\times$ – $B = 1.5$ kG. Dotted lines from expression (1), continuous lines from (6.1).

Fig. 27 Mass of compensating ions, determined from longitudinal spectra.

Fig. 28 Mass of compensating ions, determined from transverse forced oscillation spectra.

Fig. 29 $K/\varepsilon''_{\perp}$ as a function of current for various vacuums. $L = 40$ cm.

Fig. 30 Spectral quality of forced transverse oscillations (width at half-height). $L = 40$ cm.

Fig. 31 Amplitude of natural thermal ion oscillations. $L = 40$ cm. $A_{\perp} \equiv \sqrt{A^2 w \Delta\omega}$. 1 mV of signal corresponds to an ion repulsion quotient of $10^{-3}/I_e$ (mA) cm.

Fig. 32 Decrement of transverse oscillations $\gamma_{\perp}$ as related to the frequency $\omega_{\perp}(\varepsilon''_{\perp} = 2\gamma_{\perp}/\omega_{\perp})$: o - calculations by width of the peak; × - by coefficient of amplification; Δ - by temperature. $L = 40$ cm, $P = 6 \times 10^{-7}$ Pa.

Fig. 33 Ion temperature determined from the strength of longitudinal thermal noise as a function of current. $L = 40$ cm; n-harmonic number for determining temperature.

Fig. 34 Decrement of longitudinal ion oscillations, determined as an addition to phase velocity $u(1 + i\gamma_{||})$ (pressure in Pa).

Fig. 35 Compensating ion temperature obtained from decrements of longitudinal oscillation damping.

Fig. 36 Dependence on current during approach to instability threshold (5 mA) of natural longitudinal $A_{||}$ and transverse oscillation amplitudes $A_{\perp\,\mathrm{therm}}$ and the forced transverse oscillation threshold amplitude $A_{\perp}$. $L = 40$ cm.

Fig. 37 Transverse electron–ion oscillations measured by pick-up electrode in the following states: a) stable, b) unstable. $I_e = 1.2$ mA; $B = 3$ kG; $P_{\mathrm{res}} = 3 \times 10^{-7}$ Pa.

Fig. 38 Signals from pick-up electrode during a single burst of transverse oscillations: a) summation signal, b) difference signal. Time of measurement 1 ms. Measurement units: relative.

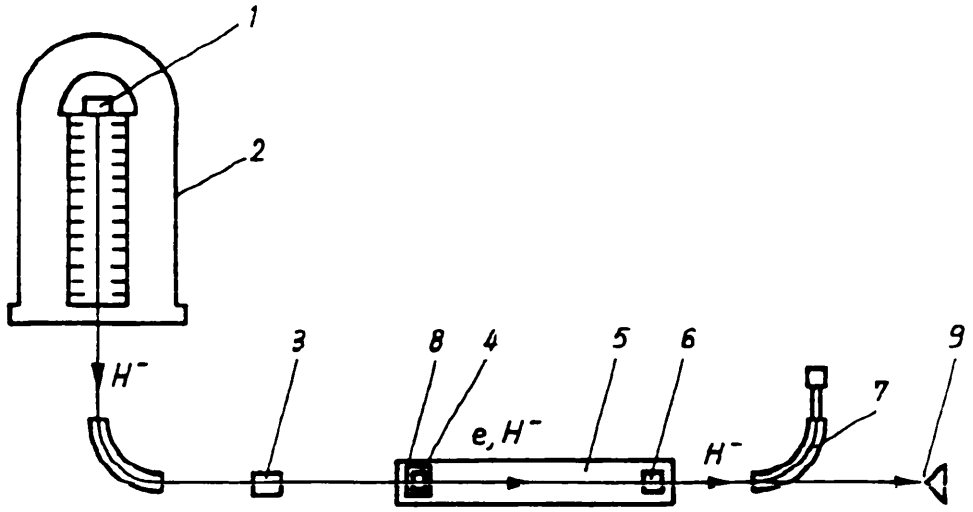

Figure 1

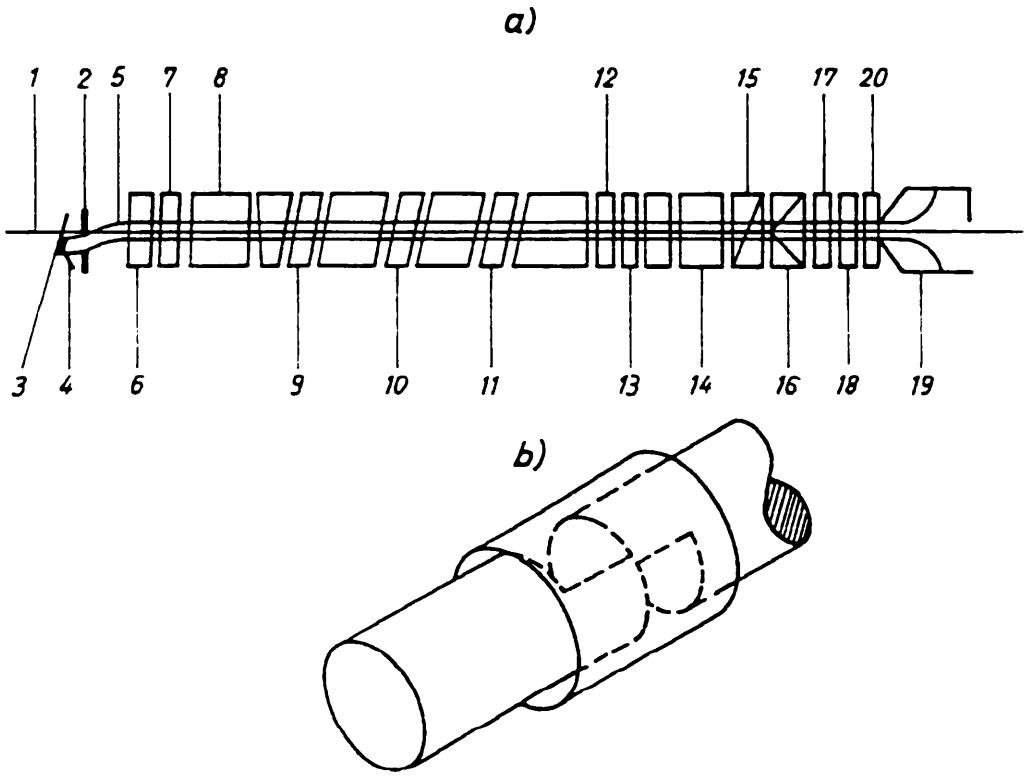

Figure 2

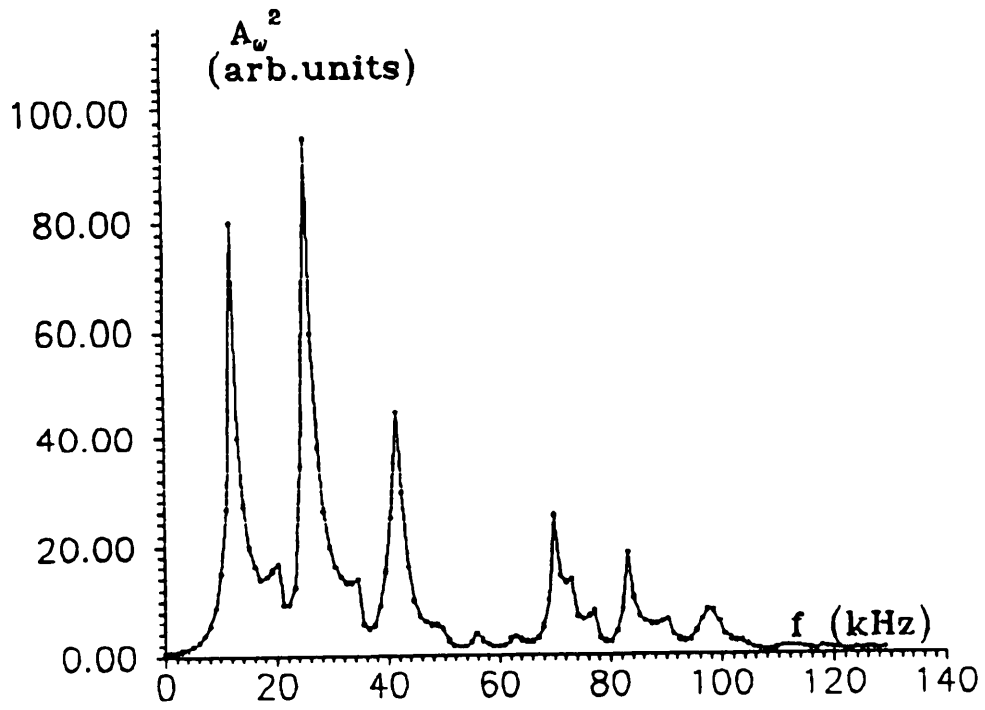

Figure 3

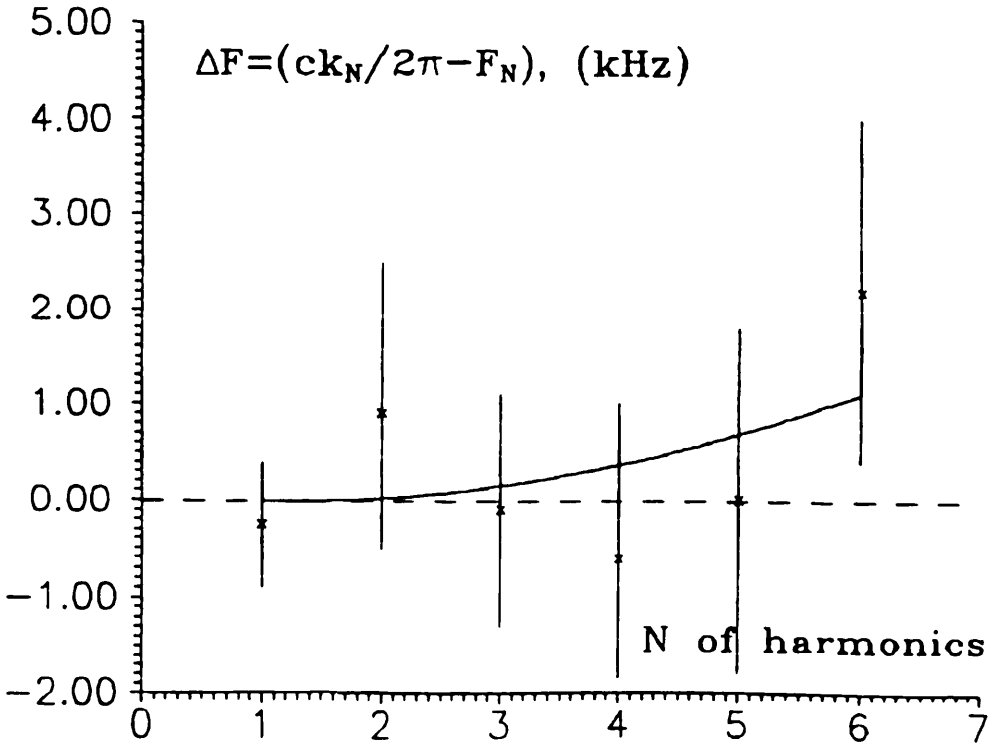

Figure 4

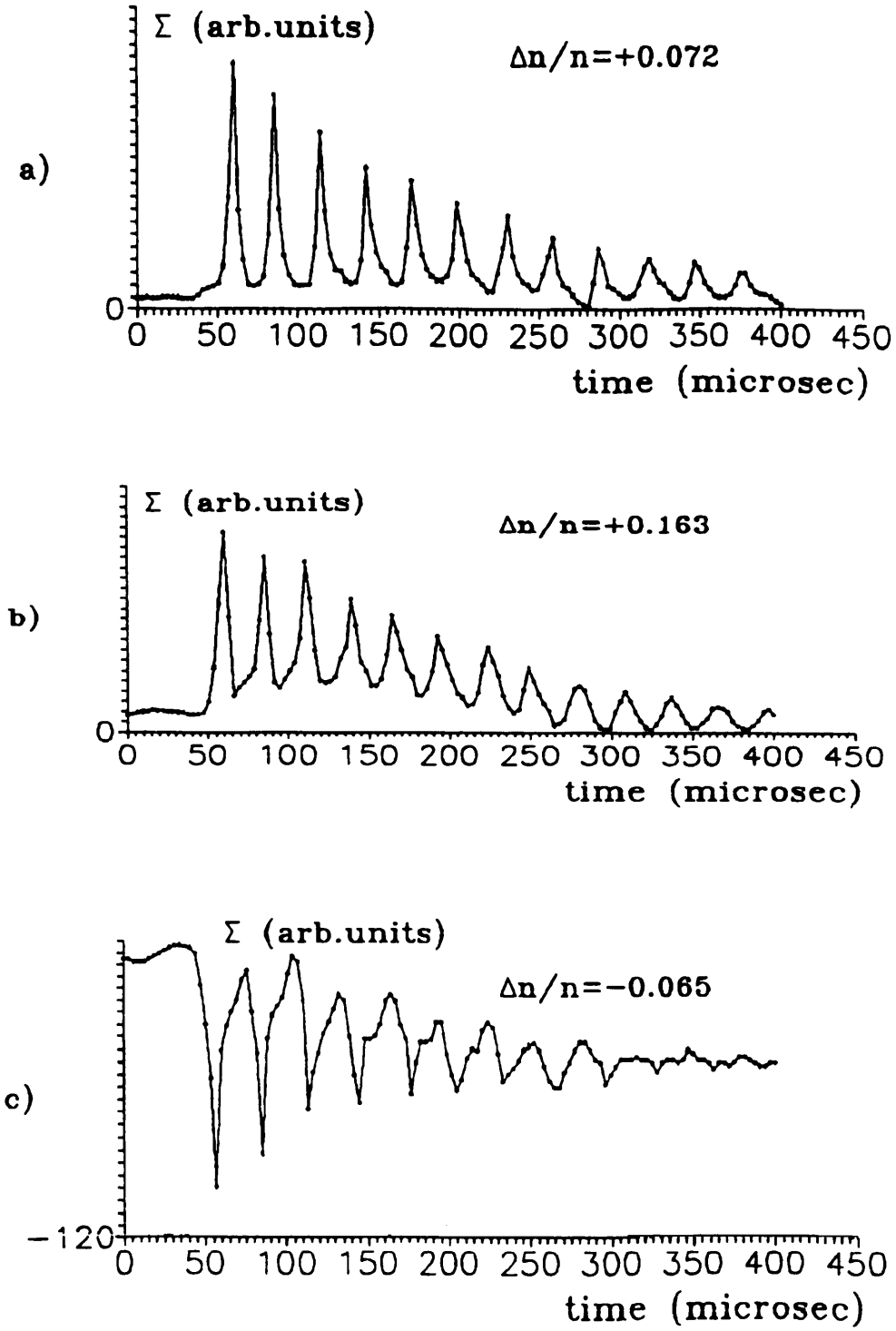
a)
Σ (arb.units)
Δn/n=+0.072
0
0 50 100 150 200 250 300 350 400 450
time (microsec)
b)
Σ (arb.units)
Δn/n=+0.163
0
0 50 100 150 200 250 300 350 400 450
time (microsec)
c)
Σ (arb.units)
Δn/n=−0.065
−120
0 50 100 150 200 250 300 350 400 450
time (microsec)

Figure 5

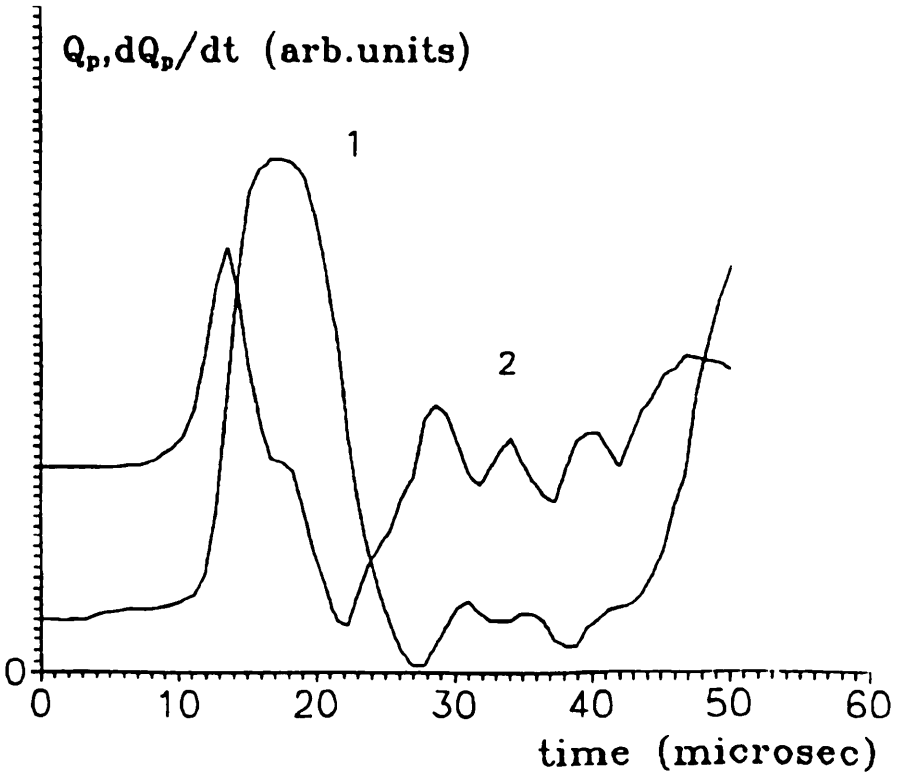

Figure 6

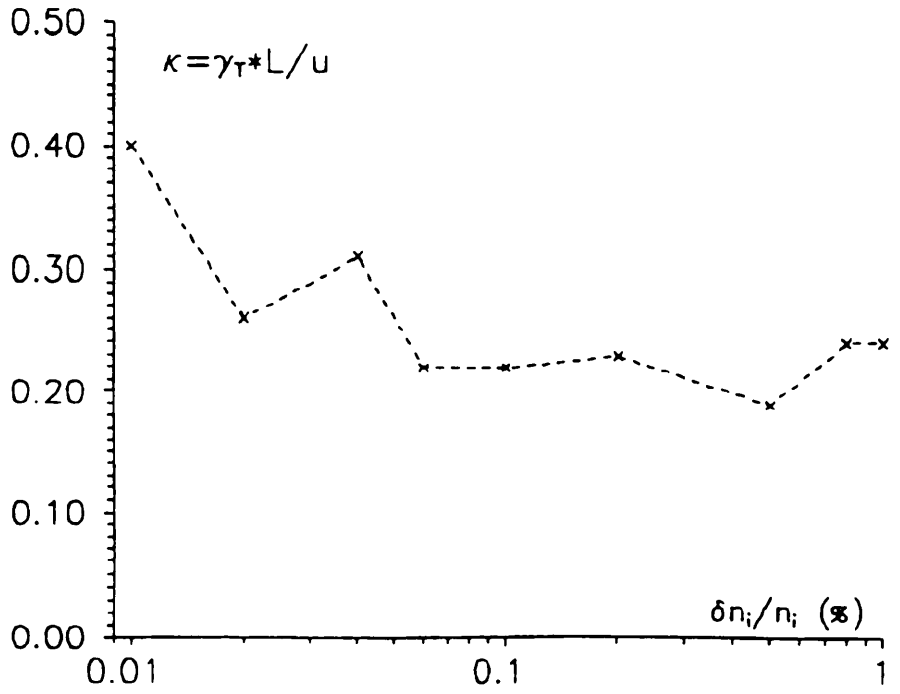

Figure 7

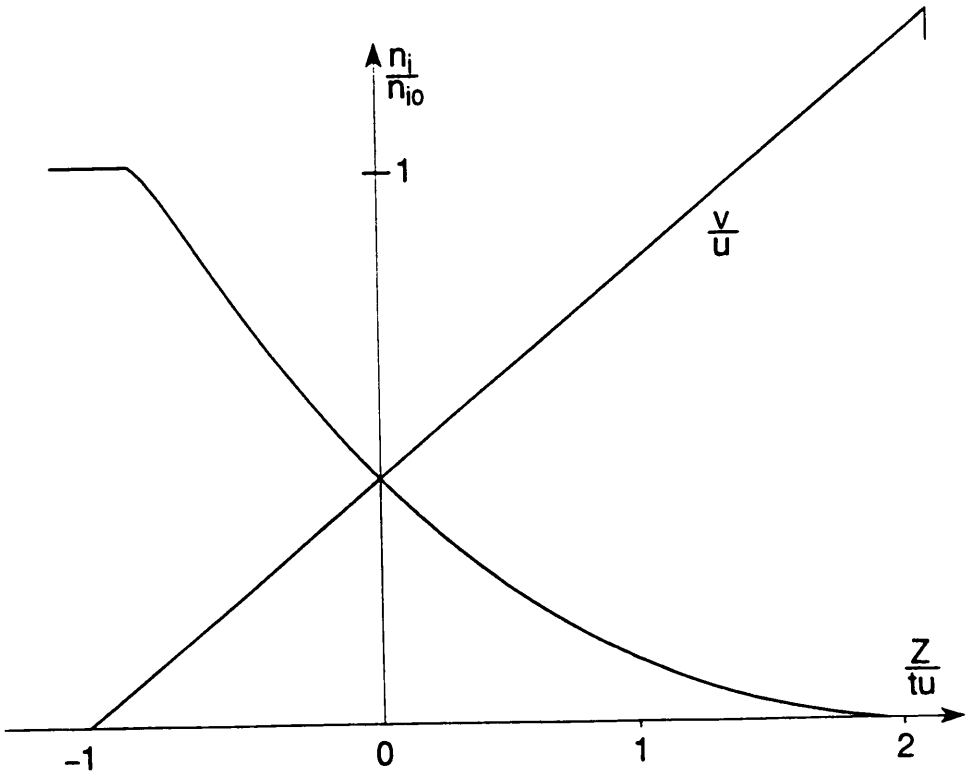

Figure 8

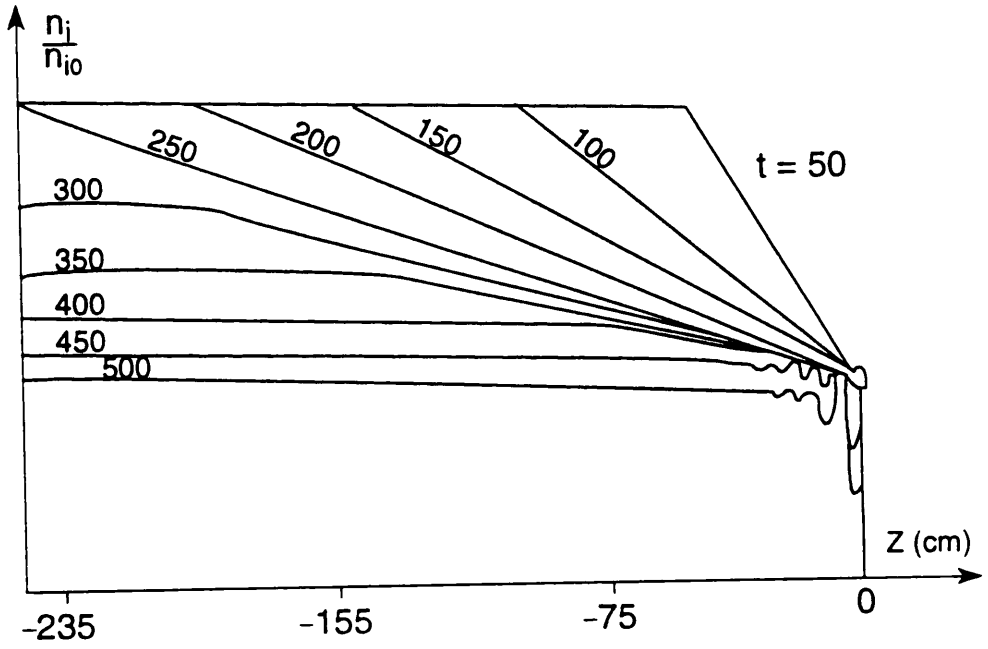

Figure 9

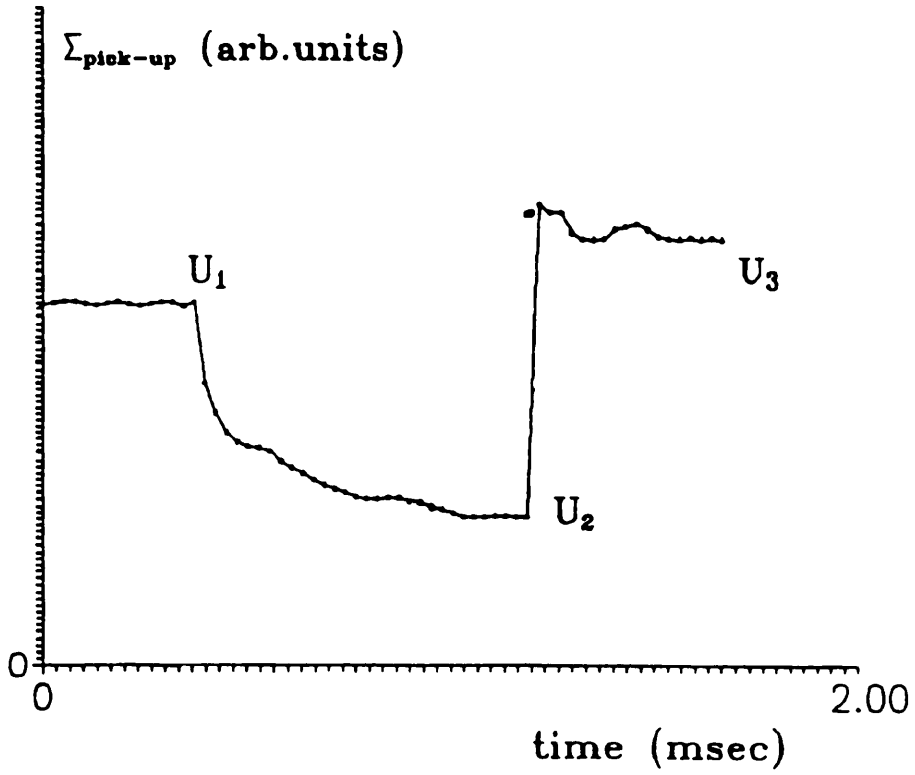

Figure 10

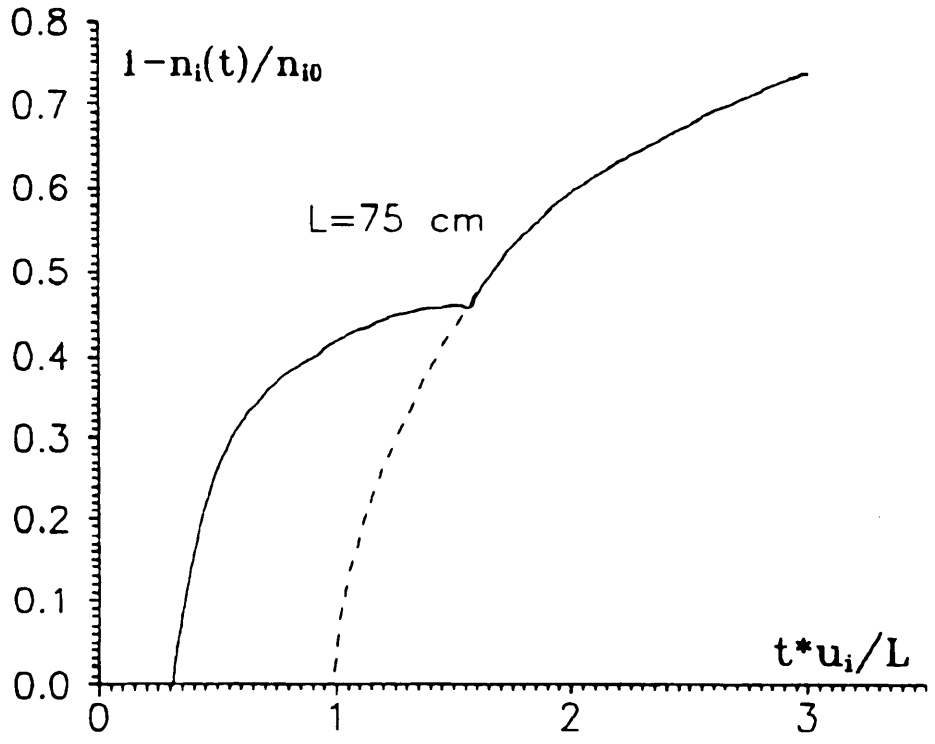

Figure 11

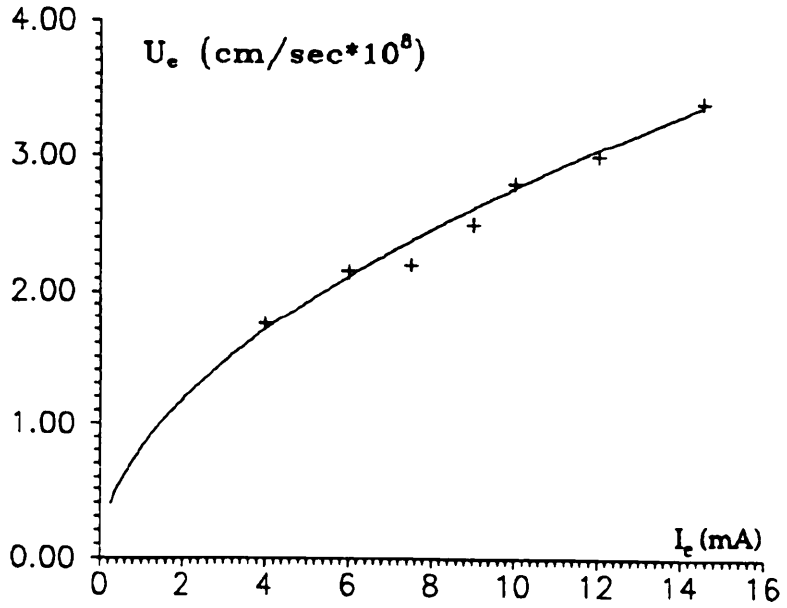

Figure 12

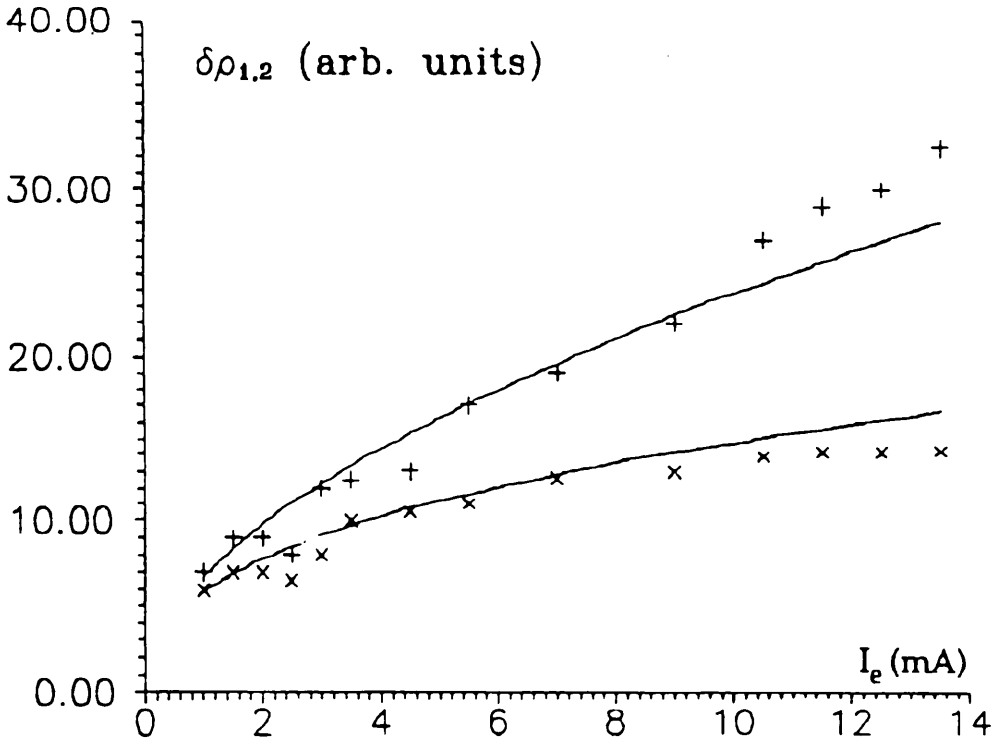

Figure 13

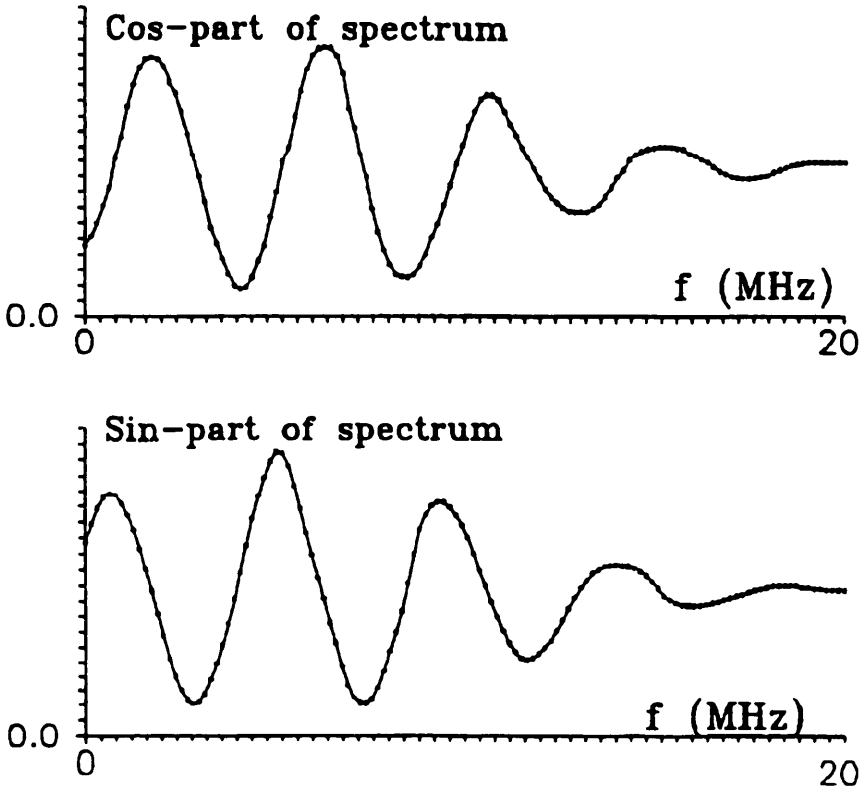

Figure 14

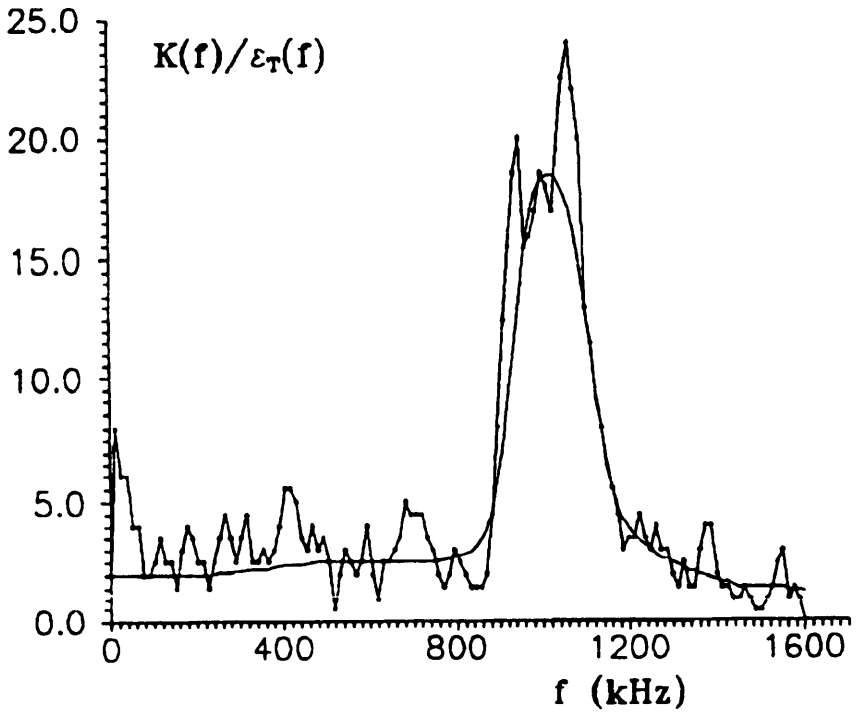

Figure 15

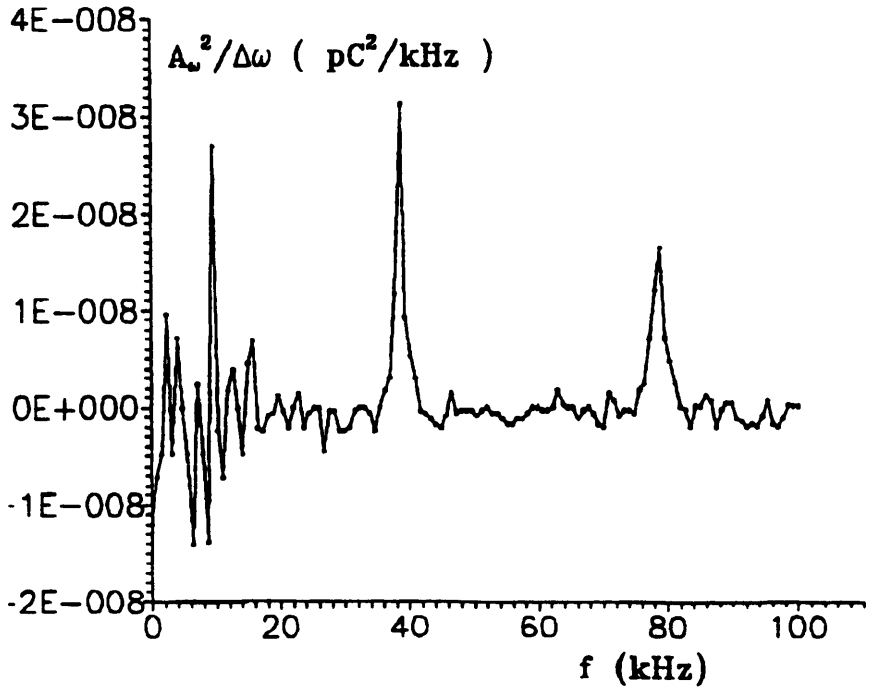

Figure 16

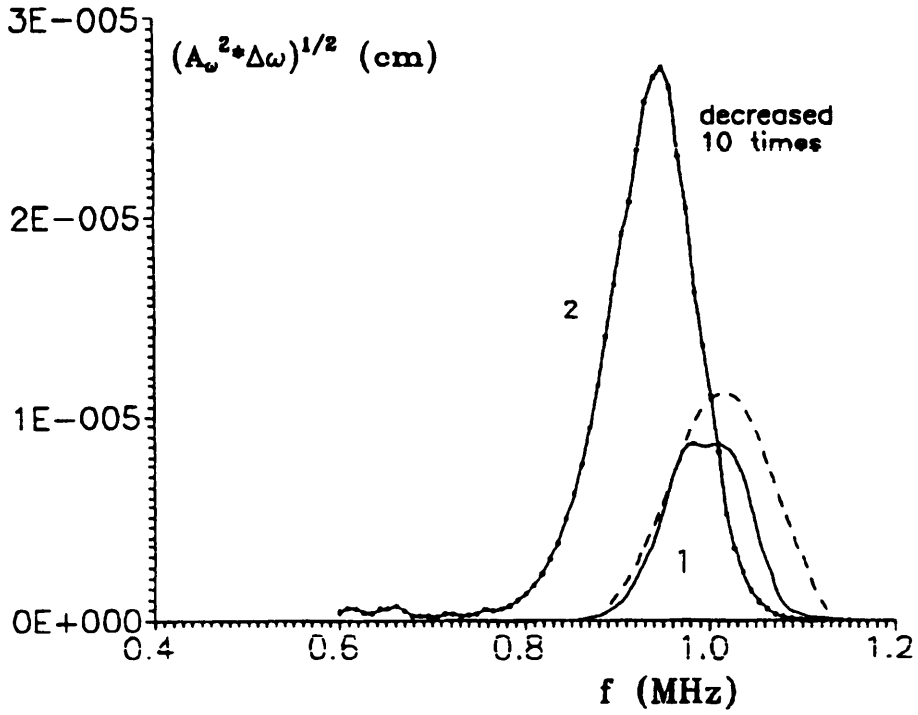

Figure 17

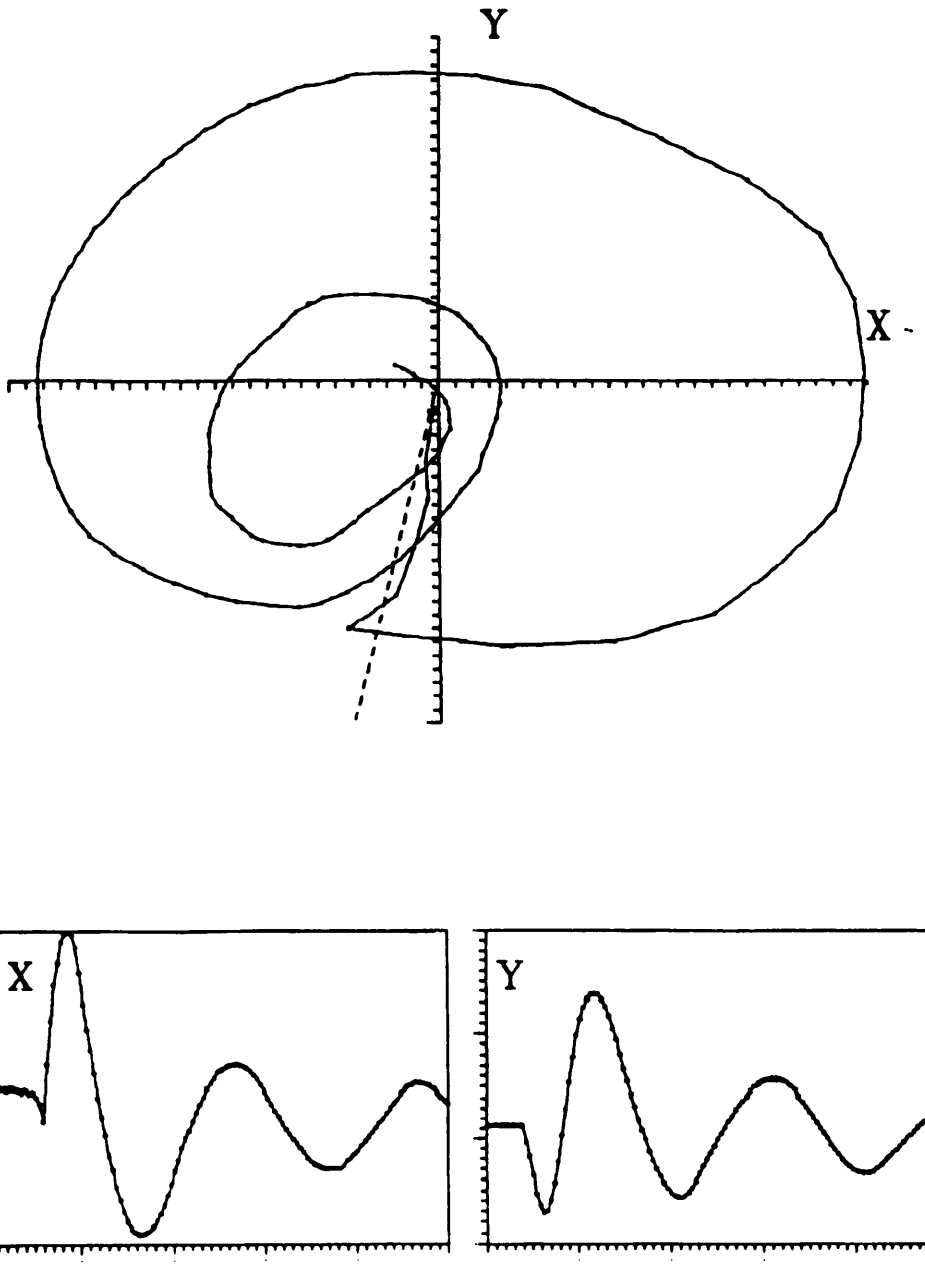

Figure 18

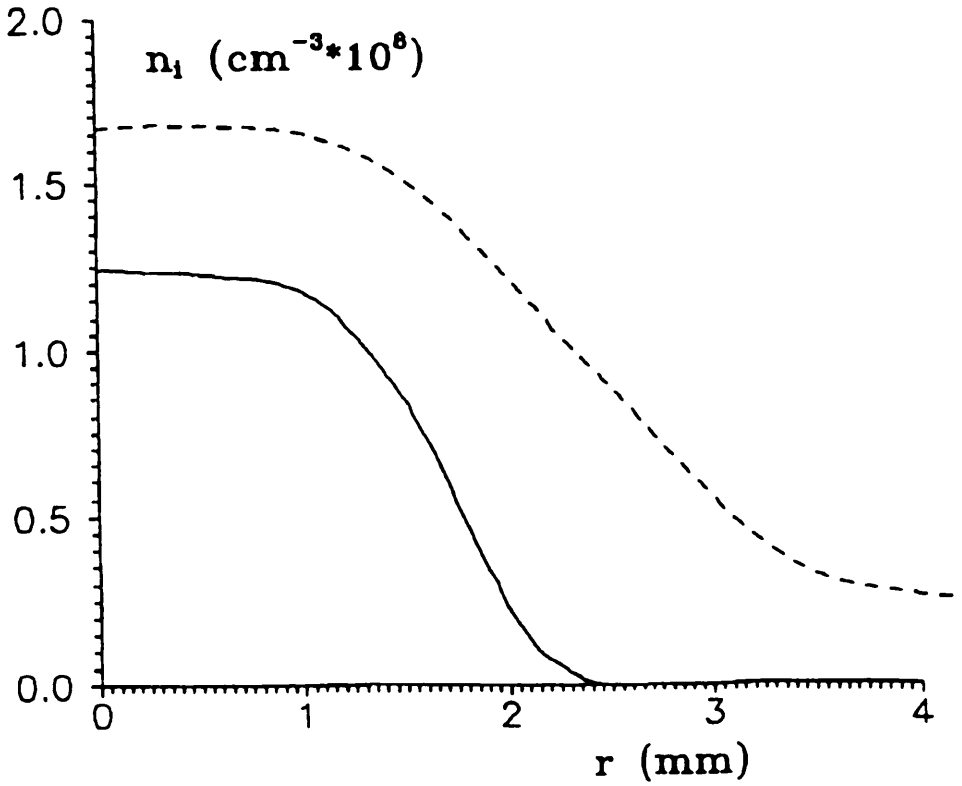

Figure 19

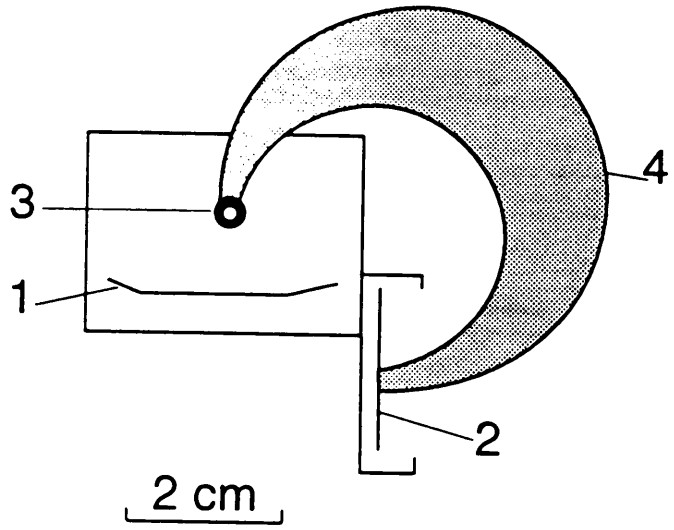

Figure 20

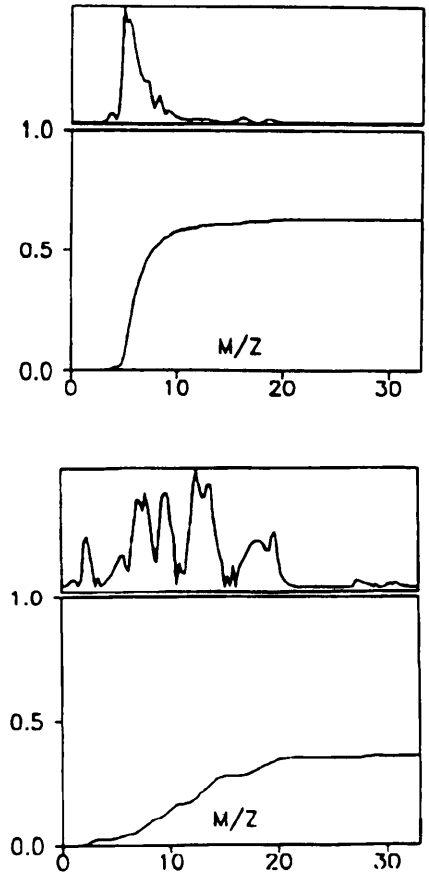

Figure 21

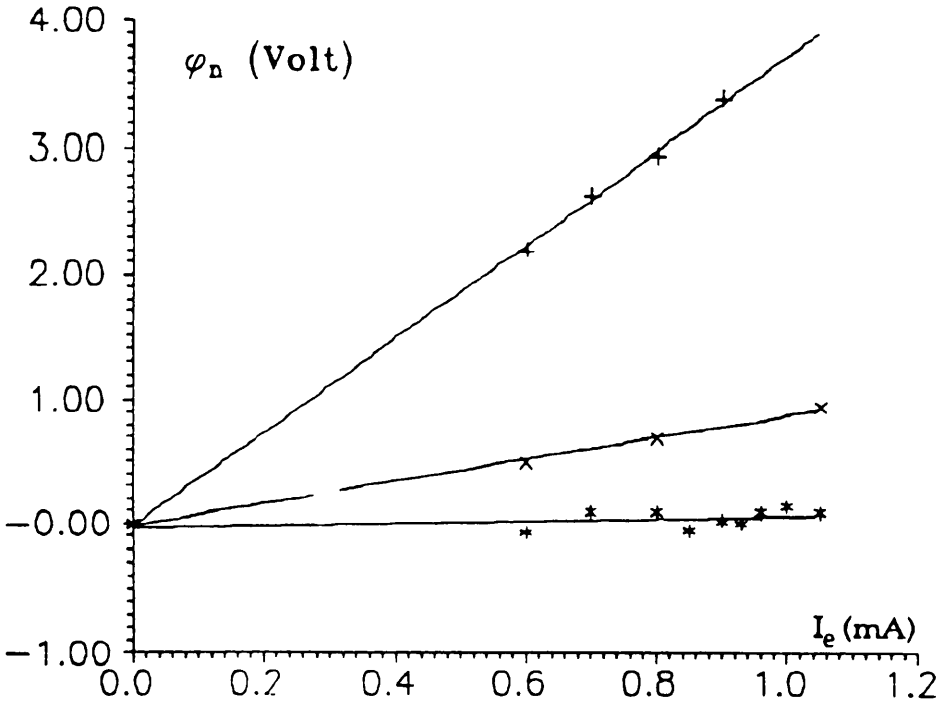

Figure 22

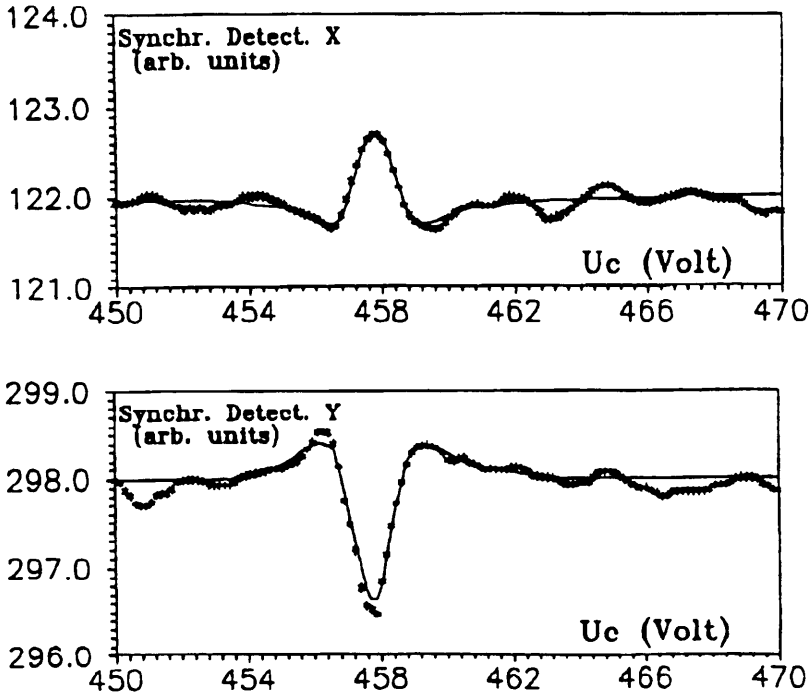

Figure 23

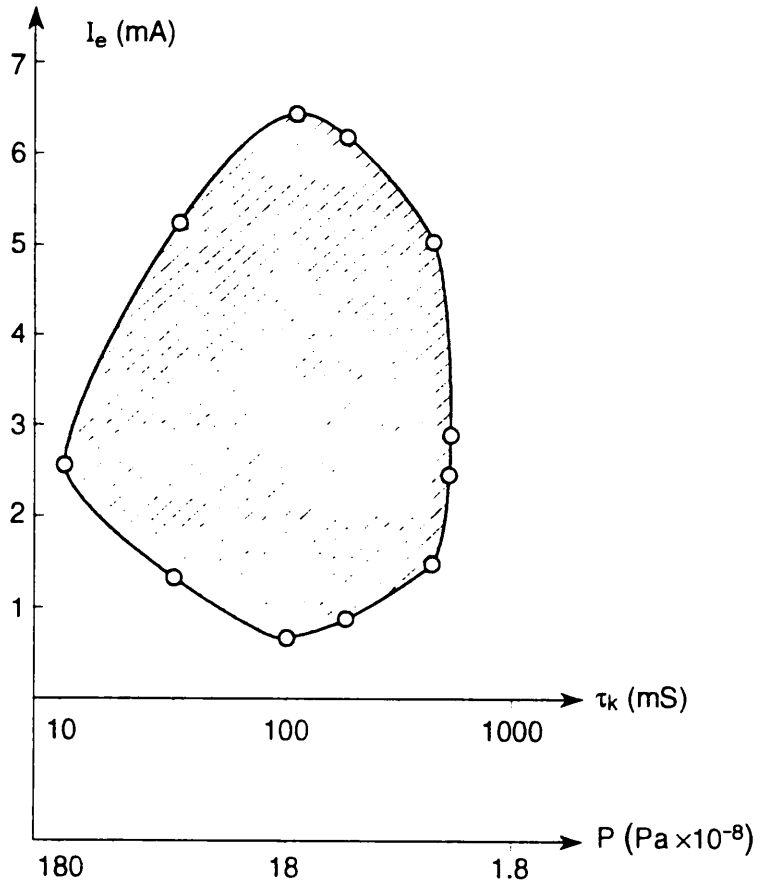

Figure 24

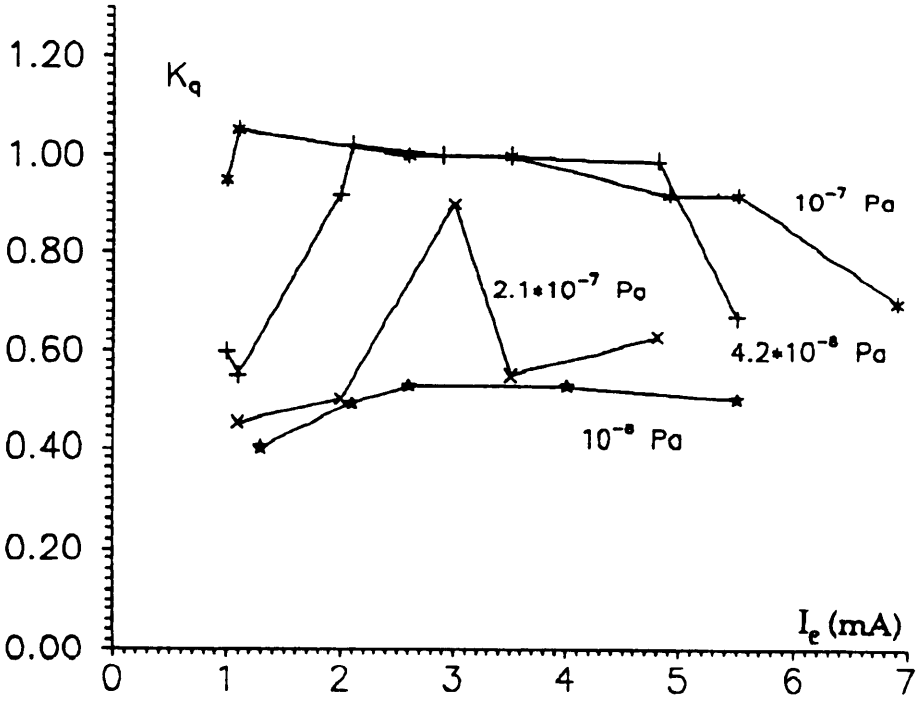

Figure 25

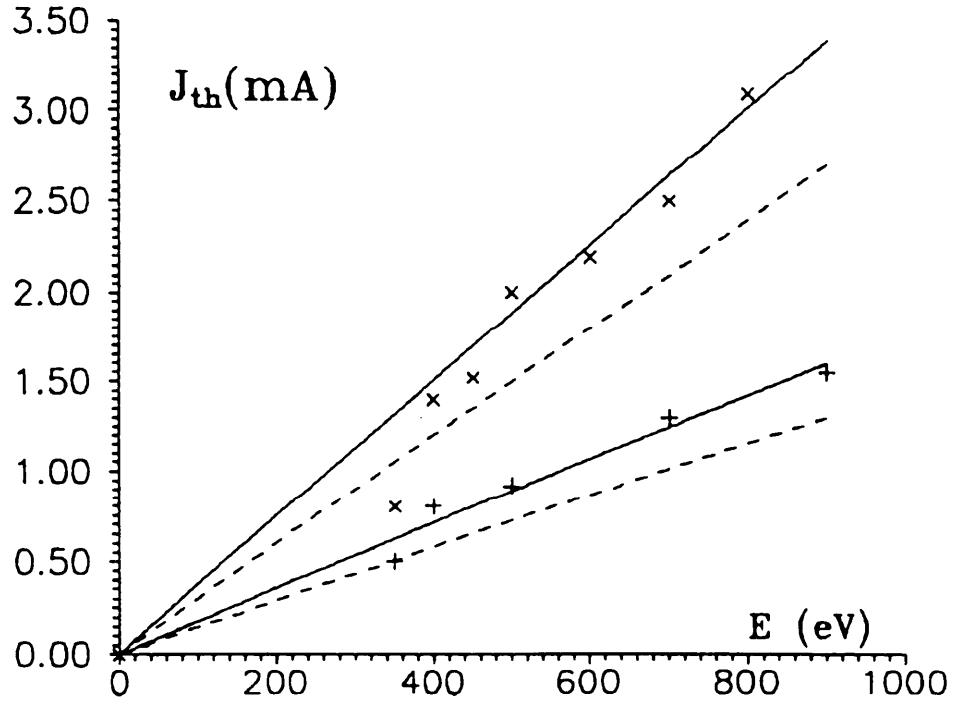

Figure 26

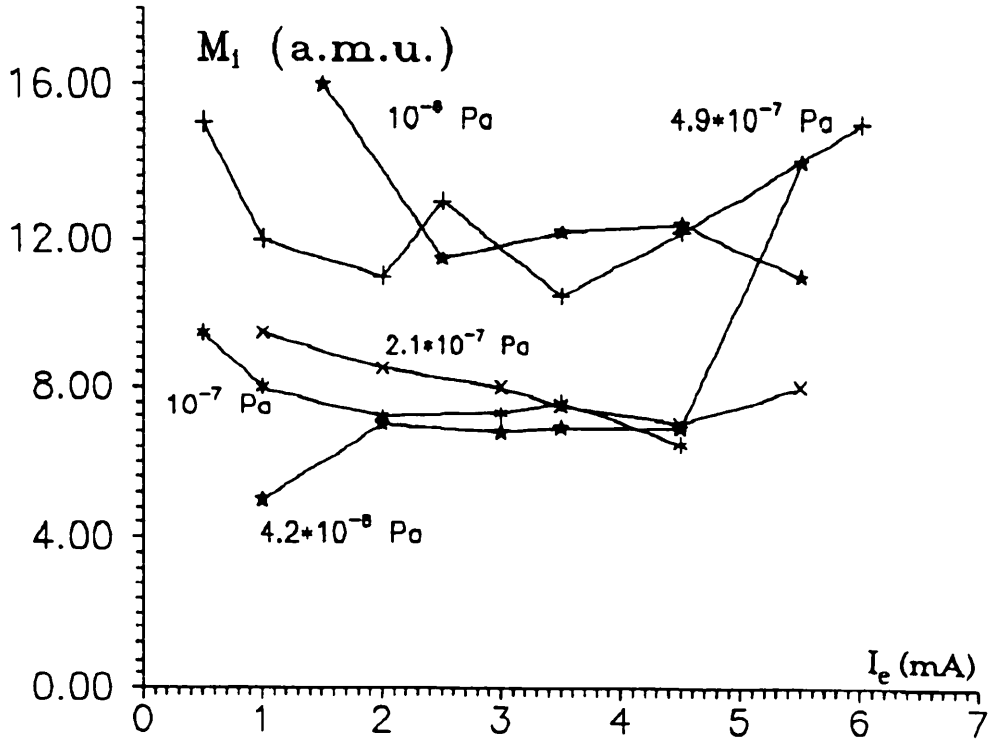

Figure 27

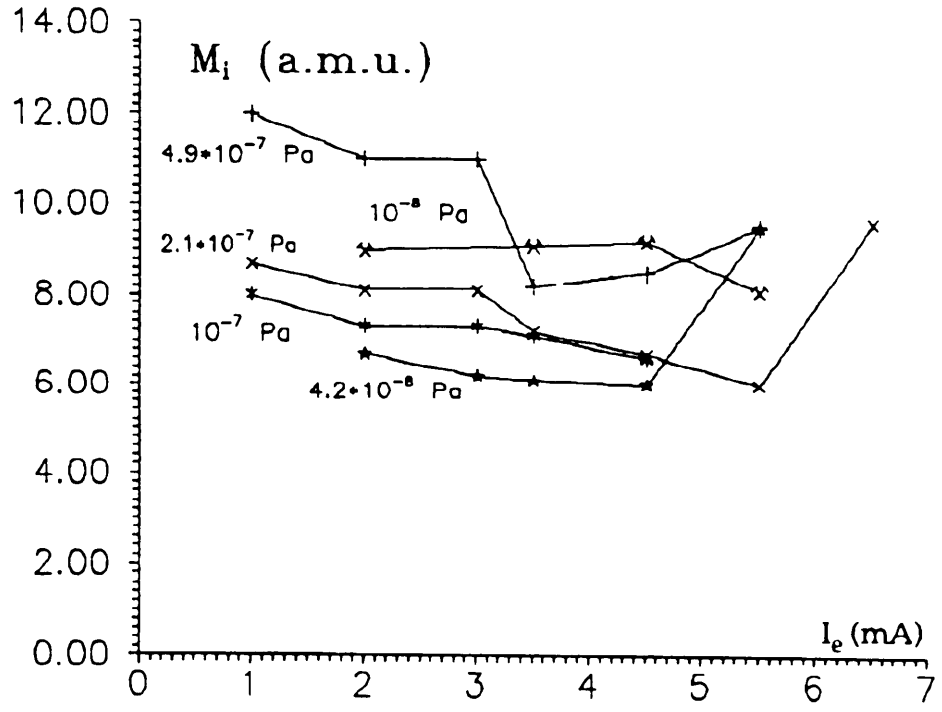

Figure 28

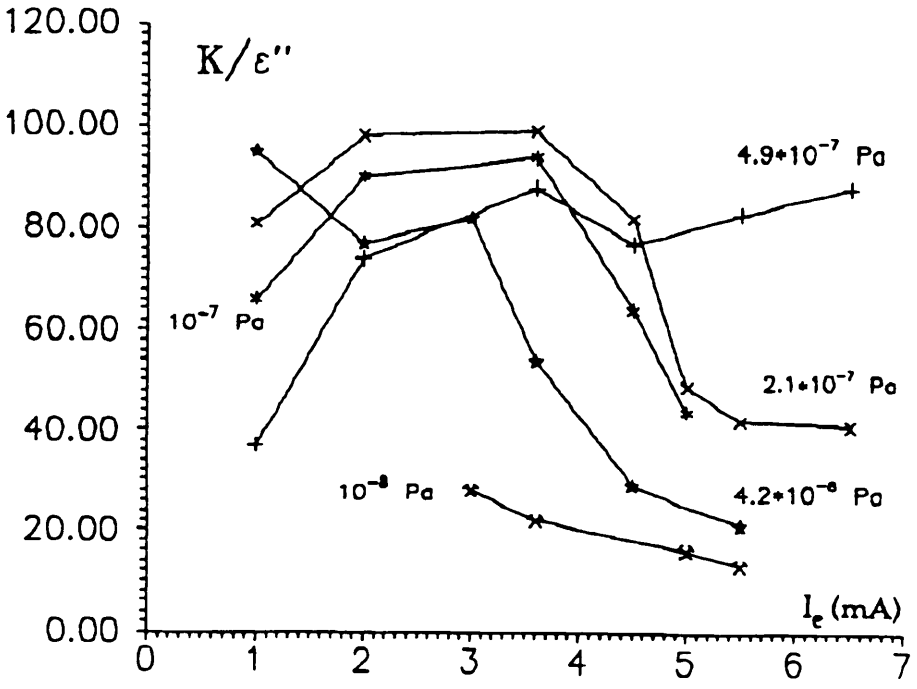

Figure 29

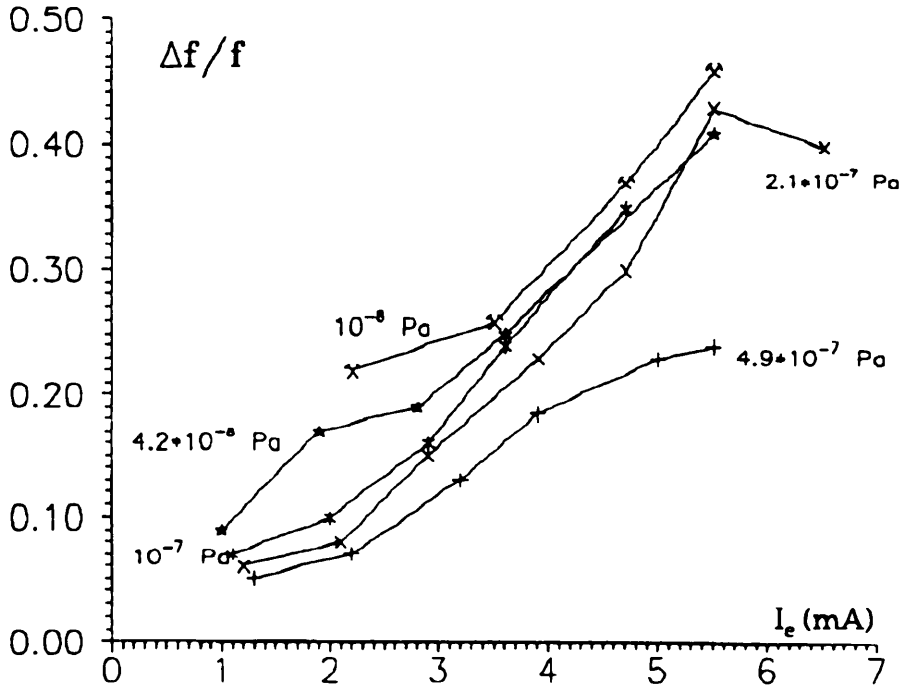

Figure 30

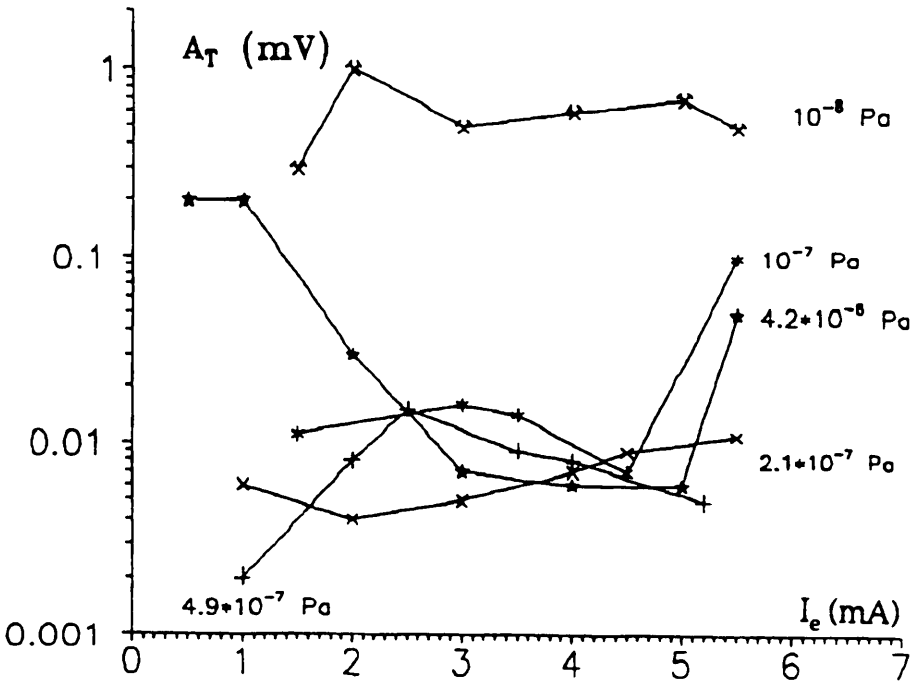

Figure 31

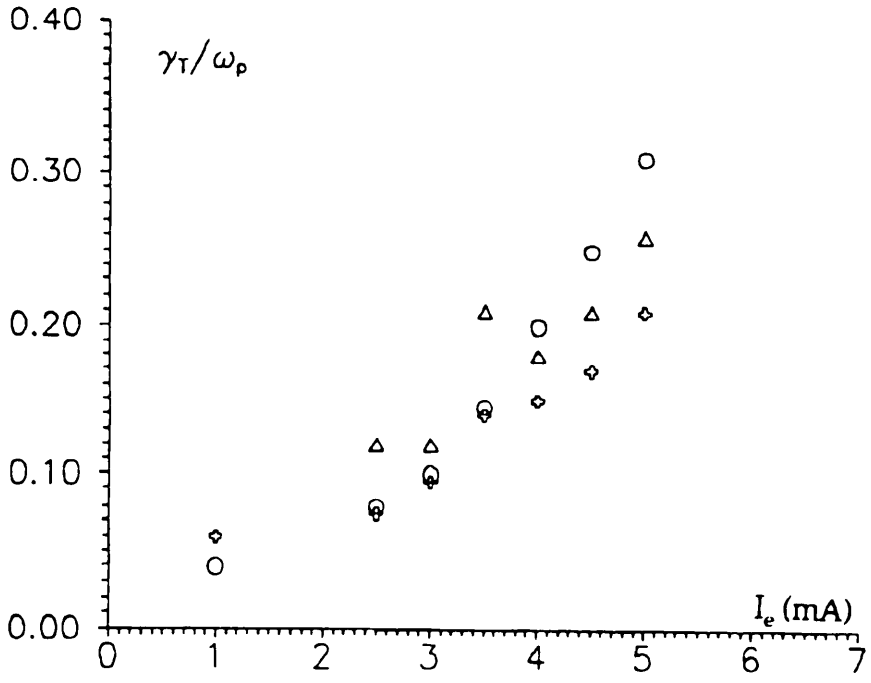

Figure 32

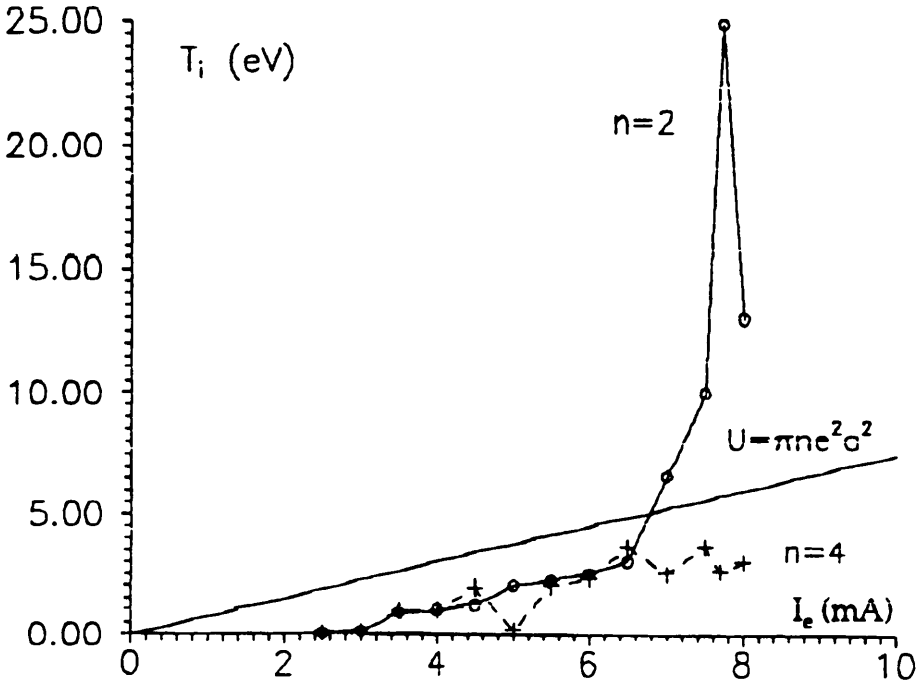

Figure 33

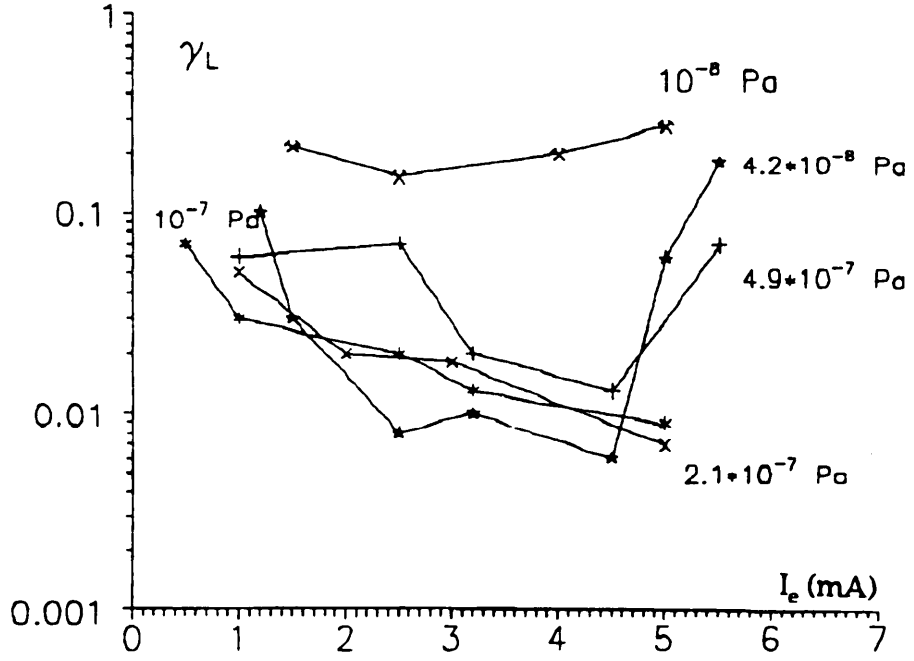

Figure 34

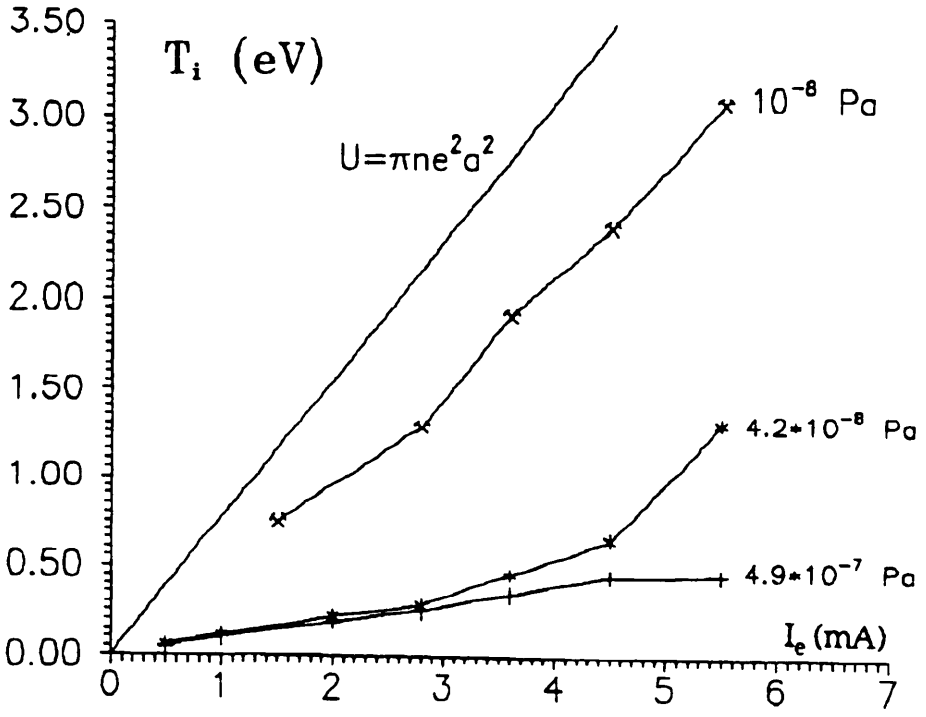

Figure 35

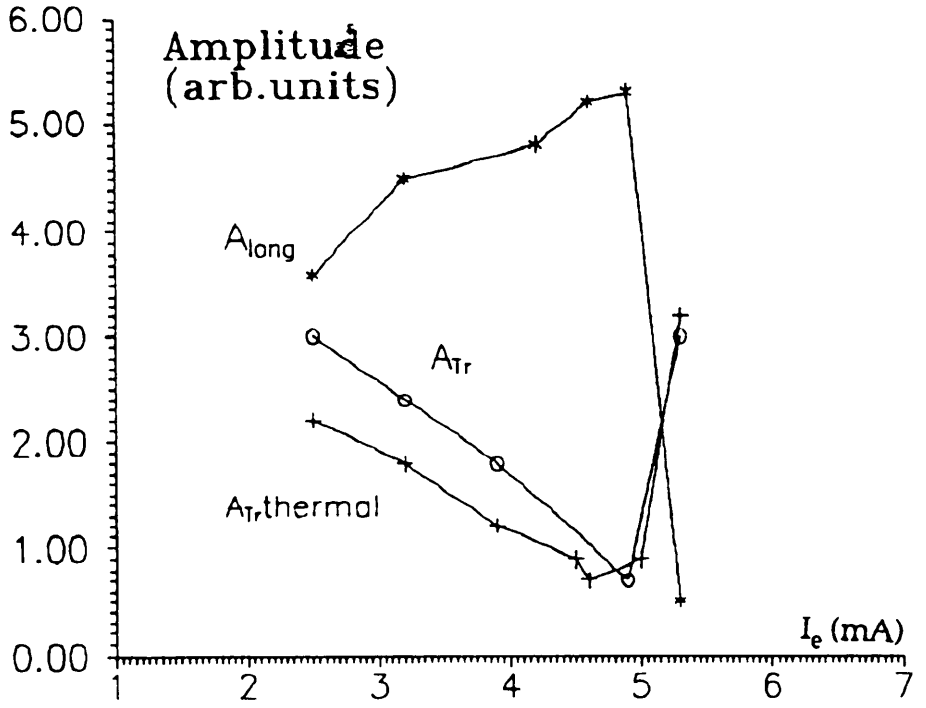

Figure 36

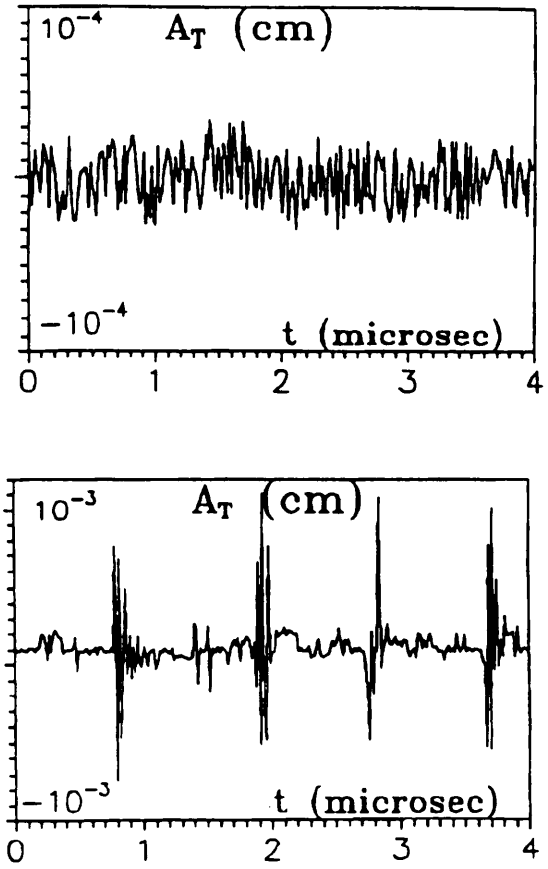

Figure 37

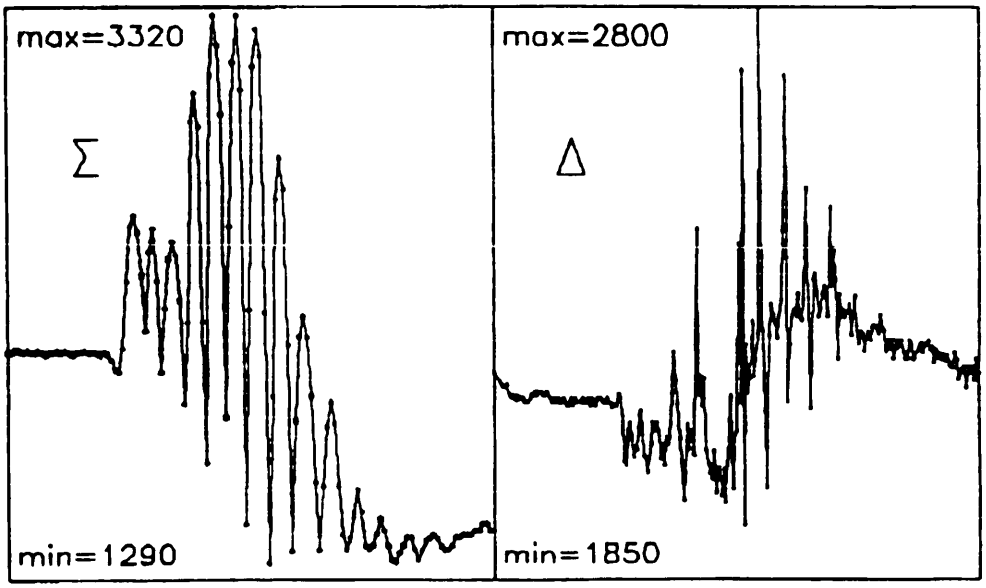

Figure 38